MONTHLY NOTICES

OF THE

ROYAL ASTRONOMICAL SOCIETY

Vol. 94 No. 6

MEETING OF 1934 APRIL 13

Prof. F. J. M. Stratton, President, in the Chair.

The election by the Council of the following Fellows was duly confirmed :—

Ernest Archibald Chamberlain, Royal Observatory, Greenwich, London, S.E. 10 ;

Laurence E. Lefèvre, M.A., D.Phil., Eton College, Windsor ; and

Joseph Tetley, 10 Cumberland Road, Headingley, Leeds, 6.

The following candidates were proposed for election as Fellows of the Society, the names of the proposers from personal knowledge being appended :—

George William Evans-Cross, M.A., D.Sc., Avenue House, 20 Grand Avenue, Bournemouth East (proposed by R. Langton-Jones) ; and

Alfred Percy Freeman, Sunnylands, High Road, Hutton, Brentwood, Essex (proposed by W. A. Parr).

The President announced that the following had been elected by the Council as Associates of the Society :—

Count F. M. da Costa Lobo, Professor of Astronomy in the University of Coimbra, Portugal, and Director of the University Observatory ; and

Dr. Frank E. Ross, Yerkes Observatory, Williams Bay, Wis., U.S.A.

One hundred and three presents were announced as having been received since the last meeting.

THE ZERO POINT OF THE GREENWICH COLOUR TEMPERATURE SYSTEM.

W. M. H. Greaves, C. Davidson and E. Martin.

(Communicated by the Astronomer Royal)

1. In 1932 a Greenwich publication was issued * which gave details of colour temperature observations during the years 1926 to 1932. In this work individual stars were compared with one or more of a system of standard stars whose relative spectrophotometric gradients had been derived by a comprehensive set of intercomparisons. The gradients of the stars relative to the zero of the system were thus obtained, and in order to derive absolute colour temperatures it was necessary to determine the colour temperature corresponding to the zero point of the system (which was defined as the mean of 9 stars of type Ao). This determination had to be effected by comparisons between stars and a laboratory source of light of known colour temperature. The source of light used in 1931 was an Eastman Kodak Standard Acetylene Burner, burnt under certain prescribed conditions.† The result obtained for the zero point was

$$\phi_0 = 1{\cdot}16 \pm 0{\cdot}05,$$

where

$$\phi_0 = \frac{c_2}{T_0}\Big/(1 - e^{-2c_2/T_0}),$$

T_0 being the colour temperature of the zero point and c_2 the well-known constant ($= 14320$ microns degrees) in Planck's formula. The value of T_0 corresponding to this value of ϕ_0 is 14300°.

The acetylene burner had been calibrated at the National Physical Laboratory, but subsequent to the publication of the Greenwich volume a communication was received from the National Physical Laboratory to the effect that the laboratory colour temperature standards in the vicinity of 2360° K. had been revised, and that values previously given would have to be increased by 35°. This means a diminution in ϕ of 0·09, and the result accordingly becomes

$$\phi_0 = 1{\cdot}07,$$

corresponding to

$$T_0 = 16100°.$$

The determination of ϕ_0 is difficult, and in the previous work some trouble was experienced in connection with the burner. It was, in fact, found that the colour temperature of the flame varied with the pressure of the gas in the containing cylinder, thereby introducing some uncertainty. It was therefore decided to repeat the determination, using an electric vacuum tungsten lamp,

* *Observations of Colour Temperatures of Stars*, 1926–1932. H.M. Stationery Office.

† *Loc. cit.*, pp. 20, 21.

suitably calibrated, as comparison standard, and a series of observations were secured during the summer of 1933. The results are given in the present paper.

2. Except as specified below, the notation and methods used are those described in the Greenwich volume. They are here summarised briefly.

The spectrophotometric comparison of any two sources of light yields the quantity

$$\frac{d}{d(1/\lambda)} \cdot \log_e (I_{1\lambda}/I_{2\lambda}),$$

where $I_{1\lambda}$ and $I_{2\lambda}$ are the light intensities at wave-length λ. It is convenient to use the stellar magnitude as the unit of light difference, and the above expression then becomes

$$0{\cdot}921 \frac{d}{d(1/\lambda)} \cdot \Delta m_\lambda,$$

where

$$\Delta m = \tfrac{5}{2} \Delta (\log_{10} I).$$

It is to be noted that the magnitude differences Δm are here reckoned positively in the sense bright minus faint.

From Planck's formula it follows that

$$-\frac{d}{d(1/\lambda)} \log_e (I_{1\lambda}/I_{2\lambda}) = \phi_1 - \phi_2 = \Delta\phi,$$

where

$$\phi = \frac{c_2}{T} \Big/ (1 - e^{-c_2/\lambda T}),$$

T being the colour temperature. The variation of $\Delta\phi$ with λ is slight, and in practice $\Delta\phi$ is derived from a series of measures of Δm over a considerable range of wave-length. If λ_m be the mean wave-length of the spectral range used, λ_m is to be substituted for λ in the formula for ϕ. In the case of the Greenwich work it is sufficient to adopt $\lambda_m = 0{\cdot}5$ microns. We thus have

$$\left.\begin{aligned} \Delta\phi &= -0{\cdot}921 \frac{d \,.\, \Delta m_\lambda}{d(1/\lambda)} \\ \text{where} \qquad & \\ \phi &= \frac{c_2}{T} \Big/ (1 - e^{-2c_2/T}). \end{aligned}\right\}$$

The quantities Δm_λ are derived from the measures of optical density on the plates. Each plate has to be calibrated by photographing a scale on it, and this was effected by the use of a spectrograph with multiple slit, as described on pp. 13 to 15 of the Greenwich volume.

The intercomparisons of the standard stars gave for each of them the gradient G defined by

$$G = \phi - \phi_0,$$

where ϕ_0 is the value of ϕ corresponding to the zero of the system. The gradients of other stars were obtained by comparisons with the standard stars.

3. In the 1931 observations the acetylene burner was mounted on the roof of the Octagonal Building, as described on p. 21 of the Greenwich volume. The plates had each to be exposed on the stars and on the burner. This involved the re-focussing of the 30-inch reflector, and, as it proved impracticable to complete the comparison on the same night, at least 24 hours elapsed between the exposures. This interval is a possible source of error, and the danger of prolonging it unduly often led to the photographing of the acetylene spectrum on nights when the visibility conditions were poor, and the corrections for horizontal reddening unduly large.

Adopting a different plan in 1933, an electric filament lamp was used as the comparison source. The spectrum of a standard star was photographed with the telescope, and on the same plate the lamp spectrum was subsequently photographed with the laboratory spectrograph used for the photography of the scales (p. 13 of the Greenwich volume). The value of $\Delta\phi$ for lamp *minus* star, derived from the measurement of the plate, has to be corrected for the differences in the transmissions of the two optical trains at the wave-lengths used. The acetylene burner was used to determine these differences. On nights chosen for fair visibility, the burner was mounted on the roof of the Octagonal Building, as before, and its spectrum photographed with the telescope. It was then taken to the laboratory and its spectrum photographed with the scale spectrograph. The plate was then scaled and measured in the usual way, and gave the correction for optical train difference for the date of comparison. These comparisons were carried out at frequent intervals during the observing programme, and, as will be seen, the results exhibit very clearly the deterioration of the telescope mirrors over the period covered by the observations.

It should be observed that the difficulty experienced in 1931, owing to the change of the colour temperature of the acetylene burner with the pressure of the gas in the containing cylinder, does not now arise. In 1931 the burner was employed as an absolute standard of colour temperature, and the secular change which it underwent throughout the life of each cylinder was detrimental. In the 1933 programme it is merely required that on each occasion there should be no appreciable colour difference as between the use of the burner on the roof and in the laboratory, and, in fact, each comparison for optical train difference is carried through at the same epoch in the life of the containing cylinder.

4. As before, all the spectra were measured at 20 wave-lengths, arranged in five groups of 4 wave-lengths each. The actual wave-lengths used differed slightly from those employed in 1931 and are given in Table I.

Within each group the measures were meaned prior to reduction. Consequently each comparison yielded five values of Δm_λ corresponding to the five mean values of $1/\lambda$.

5. The electric filament lamp used was of the type known as an "Osram" Uni-Planar Tungsten Filament Vacuum Lamp. The calibration, which was carried out at the National Physical Laboratory, consisted in determining the voltage which had to be applied in order to give a colour temperature of 2360° K. At Greenwich the source of supply was a direct current generator,

and the voltage was adjusted by means of an adjustable resistance in series with the lamp. It was maintained at the prescribed value with the aid of a volt box and potentiometer, the reduced voltage being balanced against a Weston normal cell in the usual way.

TABLE I

Group	λ (in microns)	$1/\lambda$	Mean
I	0·4429	2·258	2·237
	0·4460	2·242	
	0·4485	2·230	
	0·4509	2·217	
II	0·4746	2·107	2·090
	0·4779	2·092	
	0·4798	2·084	
	0·4820	2·075	
III	0·5234	1·911	1·884
	0·5284	1·893	
	0·5334	1·875	
	0·5384	1·858	
IV	0·5720	1·748	1·730
	0·5760	1·736	
	0·5800	1·724	
	0·5840	1·712	
V	0·6364	1·571	1·557
	0·6395	1·564	
	0·6443	1·552	
	0·6486	1·542	

The lamp was mounted 39 inches behind the diffusing screen of the scale spectrograph (see section 8 of the Greenwich volume). A lens of focal length 12 inches was placed immediately behind the diffusing screen. When the spectrograph was employed for the photography of the acetylene flame the burner was placed 7 inches behind the screen and lens. Under these conditions the lamp and the burner gave spectra of comparable density with the same exposure time, and in each case the angles of incidence of the rays on the diffusing screen are small.

Three standard lamps of the uni-planar type were obtained and were calibrated at the National Physical Laboratory. The voltages corresponding to a colour temperature of 2360° K. were given by the National Physical Laboratory as 101·9, 103·5 and 102·3 volts for the three lamps which were designated A, B and C respectively.

The lamps were run at these voltages throughout. As a safeguard against deterioration with use, all the comparisons with stars were carried out against lamp B, and this lamp was compared with the other two on four occasions during the programme. Assuming a colour temperature of 2360° K. for A and C when run at their prescribed voltages, the colour temperatures of B given by these comparisons are as follows :—

Date 1933	Comparison with A	C
May 23	2366	2365
July 1	2375	2351
Aug. 14	2359	2360
Sept. 21	2346	2359

The total amount of use of lamps A and C is thus small, and it may safely be assumed that in their case no deterioration has taken place. The above figures show that no appreciable deterioration set in for lamp B, which was used more heavily.

As a further check, the three lamps were returned to the National Physical Laboratory after the conclusion of the observing programme. The voltages for 2360° K. were there determined afresh, the results being 102·0, 103·3 and 102·3 volts for A, B and C respectively.

In as much as a change of colour temperature of 10° corresponds to about one volt, these values are sensibly the same as those given by the previous calibration.

The stars, as has been said, were always compared with lamp B. This lamp was run throughout at 103·5 volts and its colour temperature taken as 2360°. The voltage was controlled to an accuracy of a tenth of a volt.

6. In the measurement of large colour differences it is very desirable (see section 3 of the Greenwich colour temperature volume) to reduce the colours of the light sources to approximate equality by the use of colour filters. The transmissions of these at the wave-lengths used must then be determined with laboratory instruments under rigorous photometric conditions, including equality of exposure time.

In the 1933 programme two colour filters were employed. For the photography, with the laboratory spectrograph, of the standard lamp and of the acetylene burner a Wratten 78 filter was inserted in the beam. For the photography of the burner with the telescope, a combination of a Wratten 78 and a Wratten 78 A filter was employed. The comparisons of the stars with the lamp are thus affected by the transmissions of the Wratten 78 filter, and the comparisons of the two optical trains are affected by the transmissions of the Wratten 78 A filter.

The filters used were not those employed in the previous work, but new ones purchased for the occasion, the filters previously in use having shown signs of deterioration.

The absorptions of these filters at the wave-lengths used were determined with the scale spectrograph in the same way as previously (Greenwich volume, p. 22). For the measurement of the absorptions of the Wratten 78 filter, the spectrum of the scale lamp was photographed first through the filter and then through a blackened gauze screen of approximately the same mean absorption. In the case of the Wratten 78 A filter, photographs were taken, first using the Wratten 78 and then the combination of the two filters 78 and 78 A.

The results for the five wave-length groups are given in Tables II and III.

The values given for each plate are the relative absorptions in magnitudes, that is, the total absorptions with a constant subtracted so as to make the mean for the five groups zero. The determinations were spread over the period of the observing programme.

TABLE II

Relative Absorptions for Filter 78

Plate	Groups				
	I	II	III	IV	V
1	−1·12	−·90	+·07	+·70	+1·26
2	−1·10	−·87	+·06	+·67	+1·26
3	−1·13	−·92	+·07	+·68	+1·32
4	−1·15	−·87	+·03	+·68	+1·29
5	−1·10	−·88	+·05	+·67	+1·25
6	−1·11	−·88	+·05	+·66	+1·28
7	−1·13	−·91	+·06	+·69	+1·28
8	−1·15	−·93	+·05	+·72	+1·32
9	−1·10	−·88	+·04	+·68	+1·24
10	−1·12	−·91	+·05	+·65	+1·33
Mean	−1·121	−·895	+·053	+·680	+1·283

TABLE III

Relative Absorptions for Filter 78 A

Plate	Groups				
	I	II	III	IV	V
1	−·49	−·40	−·01	+·32	+·57
2	−·46	−·39	·00	+·30	+·54
3	−·45	−·39	·00	+·29	+·54
4	−·44	−·41	+·01	+·30	+·52
5	−·49	−·41	+·02	+·32	+·58
6	−·44	−·42	+·04	+·33	+·52
7	−·46	−·45	+·03	+·31	+·59
8	−·47	−·39	+·01	+·31	+·55
9	−·41	−·38	+·01	+·29	+·48
10	−·45	−·40	·00	+·29	+·57
11	−·45	−·40	·00	+·30	+·56
Mean	−·455	−·404	+·010	+·305	+·547

7. At this stage it will be convenient to consider two possible sources of error. In the first place, in the determination of the absorptions of the Wratten 78 filter it has been assumed that the absorption of the blackened gauze was non-selective. Again, the acetylene burner, when photographed with the scale spectrograph in the laboratory, was not placed in the same position as that used for the standard lamp (see section 5 above).

To determine these errors, special observations were undertaken. The spectrum of a small 30 watt motor-car headlamp was photographed with and without the gauze. Next, the same lamp was photographed in the positions

occupied by the standard lamp and burner. In these experiments exposure times were kept constant, equality of density being secured by means of the gauze, the full and half apertures and the three slits (Greenwich colour temperature volume, section 14). The results are given in Tables IV and V, a constant being applied to the measured magnitude differences so as to make the mean of the five groups zero.

TABLE IV

Relative Absorptions of Gauze

Plate	Groups				
	I	II	III	IV	V
1	+·002	+·001	−·001	+·009	−·010
2	−·001	+·026	−·014	−·012	+·002
3	+·001	+·011	−·002	−·005	−·007
4	+·001	+·006	+·003	−·014	+·004
5	−·014	+·003	−·021	+·006	+·025
6	−·003	+·014	−·011	−·016	+·017
Mean	−·002	+·010	−·008	−·005	+·005

TABLE V

Lamp. Near Position minus *Far Position*

Plate	Groups				
	I	II	III	IV	V
1	+·015	+·015	−·005	+·004	−·028
2	+·014	+·010	+·010	−·004	−·029
3	+·029	+·013	−·017	−·011	−·015
4	+·016	+·013	−·004	−·007	−·017
5	+·004	+·003	+·016	+·003	−·027
6	+·023	+·003	−·002	−·016	−·007
Mean	+·017	+·009	·000	−·005	−·020

The mean results for the gauze were not applied. Those for the near *minus* far comparisons were added to the mean results for the Wratten 78 A filter, and the totals thus obtained were applied to the values of Δm measured on the plates taken for the comparison of the optical trains.

8. The star and acetylene plates were scaled, as in the previous work, by exposures with the scale spectrograph, using full and half apertures and the multiple slit. This method gives on each plate a set of three pairs of exposures, the magnitude difference for each pair being $0^{m}\cdot75$, corresponding to a light ratio of 2 to 1. From the density measures of the resulting spectra a calibration curve can be constructed giving γ (the slope of the curve of density against log intensity) as a function of density.

But the direct calibration of each plate by the method of full and half apertures introduces accidental errors arising from small errors in timing and small fluctuations in the voltage of the scale lamp. The use of the 2 to 1 light ratios provided by this method was accordingly restricted to the

determination, from each plate, of the relative amounts of light passing through the three slits.

Denoting the slits, as previously, by a, b and c, let $I_a : I_b : I_c$ be the light ratios when a single exposure is made. Denote by $(b-a)$ and $(c-b)$ the magnitude differences corresponding to the light ratios $I_b : I_a$ and $I_c : I_b$. That is :

$$(b-a) = \tfrac{5}{2} \log_{10} (I_b/I_a),$$
$$(c-b) = \tfrac{5}{2} \log_{10} (I_c/I_b).$$

For each plate a calibration curve was constructed from the exposures with full and half aperture, and was used for the measurement of the slit differences $(b-a)$ and $(c-b)$. In the plates taken for the determination of filter absorptions, each exposure was made with full and half apertures, and gave a determination of $(b-a)$ and $(c-b)$. In this way the whole series of plates was utilised to obtain definitive values of the slit differences, and these values were then used for the construction of fresh calibration curves for each plate. From these curves values of γ were read and applied to the reduction of the measures.

The results for the slit differences from 87 determinations were

$$b-a = 0^{m}.840,$$
$$c-b = 0^{m}.772.$$

The probable errors of a single determination of slit difference were $\pm\ 0^{m}.038$ and $\pm\ 0^{m}.026$ for $(b-a)$ and $(c-b)$ respectively. In the case of $c-b$ the individual determinations are symmetrically distributed about the mean value $0^{m}.772$, and the probable error of the mean $\pm\ 0.003$ may be taken as a fair representation of the accuracy of the result. But the determinations of $(b-a)$ were not so good. The distribution is asymmetrical, there being a tendency for large values to occur (4 determinations exceeded $1^{m}.0$). The mean of the 87 determinations was $0^{m}.854$ and the peak of the frequency curve was at $0^{m}.825$. The value $0^{m}.84$ was adopted, thereby giving diminished weight to the large positive residuals.

The values of Δm derived from the calibration curves based on the above values of the slit differences may be taken as being systematically correct to within $\pm$ one per cent.

9. In section 3 of the Greenwich colour temperature volume it was pointed out that there is a possibility of error if scales derived from exposures with a given exposure time are applied to the reduction of comparisons taken with a different exposure time. In the cases of the filter and gauze determinations and of the plates taken for distance effect (section 7), each exposure was made with the multiple slit of the scale spectrograph, and thus carried its own scale. Furthermore, the same exposure time was used throughout each plate, so that no error can arise from this cause.

But in the application of scales obtained with the laboratory spectrograph to the star and acetylene plates, it becomes necessary to consider the possibilities of error.

The plates used throughout were Imperial Panchromatic B (backed), and

were developed for ten minutes in dilute pyro-soda at 60° Fahrenheit. All scales were taken with the scale spectrograph, using an exposure of 120 seconds. For plates taken with the telescope the spectra were broadened by trailing the image on the plate, and the equivalent exposure time is roughly one-fifth of the actual time spent in making the exposure. But even if the equivalent time were the same as the exposure time for the scales, there still remains a difference in the conditions in as much as the telescope exposures are intermittent.

The average exposure times are as follows. For telescope exposures the times given are equivalent times, *i.e.* one-fifth of the actual times of exposure.

Star Plates		Acetylene Plates	
Stars (Telescope)	36^s	Telescope	25^s
Standard Lamp (Laboratory)	20^m	Laboratory	20^m
Scales	120^s	Scales	120^s

Owing to the employment of filters, the magnitude differences to be measured on these plates were all small, and the effect of scale error is consequently quite trivial. Nevertheless, it seemed advisable to determine corrections whereby the values of γ derived from the laboratory scale could be reduced to values appropriate to the telescope exposures and to the 20-minute exposures with the scale spectrograph.

On some of the occasions when the acetylene flame was being photographed with the telescope, exposures were made with full and half apertures, semicircular discs being employed which could be fitted on the telescope tube. In this way a light ratio of 2 : 1, *i.e.* a magnitude difference of $0^m{\cdot}75$ was photographed with the telescope. An equivalent exposure time of 30^s was used. This magnitude difference of $0^m{\cdot}75$ was then measured, using calibration curves given by the scale exposures. The mean result from 15 determinations was

$$0^m{\cdot}746 \pm 0^m{\cdot}009.$$

This agrees, within the limits of error, with the true value $0^m{\cdot}75$. It thus appears that values of γ derived from the laboratory scales may be applied without correction to the exposures made with the telescope.

The standard lamp and the acetylene burner were photographed in the laboratory with an exposure time of 20 minutes. They were photographed with the multiple slit, and the values of the slit difference $(c - b)$ were measured for these exposures, using the calibration curves obtained from the 2-minute scale exposures. The mean result from 40 plates is

$$(c - b) = 0^m{\cdot}850 \pm 0^m{\cdot}004.$$

But the true value of $(c - b)$ is $0^m{\cdot}772$ (see above), so that the values of γ derived from the scale exposures need increasing by 10 per cent. before they can be applied to measures from exposures of 20 minutes. This increase of γ with exposure time is in accordance with expectation, and can be ascribed to the falling off in the Schwarzschild index, p (*i.e.* to the increasing failure of the reciprocity law), for feeble light fluxes.*

* See section 3 of the Greenwich colour temperature volume.

Actually star and acetylene exposures taken with the telescope, and requiring no scale correction, are compared with 20-minute exposures in the laboratory which need a 10 per cent. correction. The values of γ given by the scales were accordingly increased by 5 per cent. before being used for the reduction of these comparisons. But the final effect of this correction is trivial. As a consequence of the employment of the filters the colour differences between the stars and the standard lamp are very nearly the same as the colour differences between the acetylene as photographed with the telescope and with the laboratory spectrograph, a circumstance which in itself practically leads to the complete elimination of scale error.

In addition to the stars photographed near the zenith for comparison with the standard lamp, each plate contains the spectra of stars photographed at a low altitude, which, when compared with the spectra of the high stars, give determinations of atmospheric reddening. The average equivalent exposure on the low stars was 46 seconds. The values of γ derived from the scales were applied without correction to these comparisons.

10. As has been stated in section 4 above, all spectra were measured at 20 selected wave-lengths. The micro-photometer described in section 10 of the Greenwich volume was used. For the spectra of the stars the screw readings corresponding to the wave-lengths were inferred (by the Hartmann-Cornu formula) from the measured positions of the Balmer lines. When the acetylene flame was photographed with the telescope, two exposures per plate were made on an arc, and the wave-length settings inferred from the measured positions of the arc lines. In the case of exposures with the laboratory spectrograph the same device was adopted as previously. A wire is placed just in front of the plate, and its silhouette gives a convenient reference mark. The image of a hydrogen discharge is thrown on the slit, and from its spectrum the scale of the dispersion and the wave-length corresponding to the silhouette of the wire are determined.

The effect of small errors in wave-length is enhanced by the colour curve of a panchromatic plate. The first and fourth wave-length groups used lie on slopes of increasing density with increasing wave-length, and the second and fifth groups lie on slopes of decreasing density. Consequently, if a particular spectrum is measured at wave-lengths which are, say, slightly in excess of the correct ones, the measured densities will be too large for Groups I and IV and too small for Groups II and V.

In the 1933 work, errors of this kind were eliminated by suitable weighting of the groups. The density slopes of the first two groups are roughly equal, and the downward slope of Group V is roughly twice as large as the upward slope of Group IV. Consequently, it is necessary to combine the first two groups with equal weight and the last two with relative weights of 2 to 1.

Thus, if for a particular comparison Δm_1, Δm_2, etc. be the measured magnitude differences for the groups, and if the respective mean reciprocal wave-lengths be denoted by $1/\lambda_1$, $1/\lambda_2$, etc., then the gradient difference $\Delta\phi$ is obtained from the formula

$$\Delta\phi = \frac{\frac{1}{3}(2\Delta m_4 + \Delta m_5) - \frac{1}{2}(\Delta m_1 + \Delta m_2)}{\frac{1}{3}(2/\lambda_4 + 1/\lambda_5) - \frac{1}{2}(1/\lambda_1 + 1/\lambda_2)} \times 0{\cdot}921.$$

All the reductions were carried out in this way. It will be noticed that the third group plays no part in the derivation of gradient differences.

11. Plates were exposed on stars on 12 nights selected for good, and apparently uniform, transparency. On 12 other nights, selected for fair visibility conditions, plates were taken, with the telescope, of the spectrum of the acetylene flame mounted 600 feet away on the roof of the Octagonal Building.

The star plates were placed in the scale spectrograph and exposed to the standard lamp on the mornings following each night's work. They were then scaled and subsequently developed. In the same way, the acetylene plates were placed in the scale spectrograph, re-exposed to the acetylene flame, scaled, and developed on the mornings subsequent to the photographing of the acetylene flame with the telescope.

There is thus symmetry in the treatment of the two sets of plates, and this circumstance provides a safeguard against photographic and other errors.

On each star plate there is photographed the spectra of

(1) A standard star near the zenith.
(2) Two standard stars at zenith distances 50° to 60°. These are photographed before and after the zenith star and in different azimuths.
(3) The standard lamp.
(4) The photometric scale.

The gradient difference A for atmospheric reddening at the zenith is determined by comparisons between the zenith stars and the low stars. The value of $\Delta\phi$ for each such comparison is corrected by the real difference of gradient between the two stars in question, and, if $\Delta\phi'$ be the corrected value, we have

$$A\,(\sec z_2 - \sec z_1) = \Delta\phi',$$

where z_1 and z_2 are the zenith distances. It is essential that the comparisons between high and low stars should be carried out at the same wave-lengths, and reduced in the same way, as the comparisons between zenith stars and standard lamp. For further details see section 15 of the Greenwich volume.

The quantity A having been determined, the measured value of $\Delta\phi$ for standard lamp *minus* zenith star has to be increased by the quantity

$$A \sec z,$$

where z is the zenith distance of the star.

Further, the measured value of $\Delta\phi$ for acetylene (laboratory) *minus* acetylene (telescope) has to be increased by a quantity A', which represents the reddening of the light during its passage through the 600 feet of air between the 30-inch reflector and the Octagonal Building. It was found previously (see Greenwich volume, section 16) that the horizontal reddening

A' was a function of the visibility, values for which are estimated, as a matter of routine, by the meteorological department of the observatory. In the 1933 observations, the requisite values of A' were read off, using the routine visibility observations, from the curve given in the Greenwich colour temperature volume.

12. The results of the determinations of the gradient difference A for atmospheric reddening at the zenith are given in Table VI. The successive columns give the date, the zenith star and its zenith distance z_1, the two low stars and their zenith distances and azimuths. The column $\Delta\phi$ gives the observed gradient differences in the sense *low* minus *high* corrected for the real gradient differences of the stars, the corrections being taken from the results for the standard stars given on p. 20 of the Greenwich volume. The last column gives the deduced value of A, the gradient difference for atmospheric reddening at the zenith. It is obtained by dividing $\Delta\phi$ by sec z_2 – sec z_1.

Table VII gives the values of A when grouped according to the azimuth of the low star. The mean values for the groups are also given.

The range in the mean values for the four groups is not satisfactory. It must, however, be recognised that Greenwich is not a really suitable site for *absolute* colour temperature work of the highest precision. To the north side of the observatory lies an industrial area, and in fact haze and smoke can often be seen from the observatory to extend to an altitude of about 25 degrees above the northerly horizon. Even on the nights selected for the present work, there would be a danger of interference in the case of the low stars on the north side, and the application of values of A derived from the observation of such stars to the reduction of zenith observations would be of doubtful validity.

The mean values of A derived from the comparison of zenith stars with low stars on the south (Groups I and II) and north (Groups III and IV) sides are

$$\text{From south stars} \quad A = 0{\cdot}31 \pm {\cdot}01,$$
$$\text{From north stars} \quad A = 0{\cdot}38 \pm {\cdot}04.$$

These figures do not in themselves establish a systematic difference in the atmospheric transmissions north and south. It will be observed, however, that the scatter of the observations is considerably greater for the north stars, and in view of this, and of the danger of interference which is known to exist in the northern portion of the sky, the value $A = 0{\cdot}31$ has been adopted.

This value has been applied to the reduction of all comparisons between the standard lamp and standard stars photographed in the zenith. Doubtless, the value of A varies from night to night, but such variations are of the same order as the accidental errors of observation.

13. Table VIII gives the results of the comparisons between the standard lamp and the standard stars photographed in the zenith. The successive columns give the date, and the time t in days from 1933 April 27, which is the date of the first comparison of optical trains (see below), and has been chosen as zero epoch. Then follow the zenith star, its zenith distance z and the

TABLE VI

Determinations of Atmospheric Reddening

Date	Zenith Stars		Low Stars			$\Delta\phi$ Low—High corrected for difference of Gradient	A
	Name	Z.D. z_1	Name	Z.D. z_2	Azimuth		
		°		°			
June 1	η U Maj	12·9	δ Leon	53·0	W *b* S	+·208	·32
			ζ Aqil	57·8	E S E	+·387	·46
June 3	η U Maj	15·0	δ Leon	54·0	W *b* S	+·160	·24
			ζ Aqil	55·9	E S E	+·285	·38
June 7	γ U Min	21·9	α Aqil	60·9	E S E	+·258	·26
			δ Cass	60·3	N N E	+·486	·52
	γ U Min	24·5	δ Cass	59·6	N N E	+·288	·33
			β U Maj	54·2	NW *b* N	+·352	·58
June 28	α Ceph	21·3	β U Maj	59·9	NW *b* N	+·445	·48
			α Andr	57·3	E	+·335	·43
July 2	γ U Min	23·9	α Aqil	55·5	SE *b* E	+·227	·34
			β U Maj	52·4	NW *b* N	+·269	·49
	γ U Min	26·7	δ Cass	57·2	NE *b* N	+·234	·32
			β U Maj	57·9	NW *b* N	+·292	·38
July 12	γ U Min	29·3	δ Cass	54·2	NE *b* N	+·140	·25
			β U Maj	60·4	NW *b* N	+·246	·28
July 25	α Ceph	19·3	α Pegs	59·1	E S E	+·247	·28
			η U Maj	52·0	N W	+·144	·26
	α Ceph	15·7	η U Maj	52·8	N W	+·021	·03
			γ Pegs	59·9	E S E	+·333	·35
Aug. 1	α Ceph	18·3	α Pegs	58·7	E S E	+·349	·40
			η U Maj	52·8	N W	+·287	·48
	α Ceph	14·7	η U Maj	53·4	N W	+·178	·28
			γ Pegs	58·4	E S E	+·238	·27
Aug. 8	α Ceph	10·7	α Ophi	57·2	W S W	+·310	·37
			β Aris	59·4	E *b* S	+·314	·33
Aug. 23	α Ceph	12·1	γ Pegs	58·4	E S E	+·253	·29
			η U Maj	60·9	N W	+·343	·33
	α Ceph	10·7	α Ophi	57·3	W S W	+·166	·20
			β Aris	58·7	E *b* S	+·185	·20
Aug. 26	α Ceph	12·6	γ Pegs	59·3	E S E	+·268	·29
			η U Maj	60·5	N W	+·483	·48
	α Ceph	10·7	α Ophi	56·9	W S W	+·093	·11
			β Aris	57·9	E *b* S	+·354	·41
Sept. 8	δ Cass	20·8	α Aqil	56·4	SW *b* W	+·247	·33
			β Auri	58·4	NE *b* E	+·543	·65

TABLE VII

	I			II		
June 1	E S E	·46		W *b* S	·32	
June 3	E S E	·38		W *b* S	·24	
June 7	E S E	·26		W S W	·37	·26
June 28	E	·43		W S W	·20	
July 2	SE *b* E	·34		W S W	·11	
July 25	E S E	·28		SW *b* W	·33	
July 25	E S E	·35				
Aug. 1	E S E	·40	·33			
Aug. 1	E S E	·27				
Aug. 8	E *b* S	·33				
Aug. 23	E S E	·29				
Aug. 23	E *b* S	·20				
Aug. 26	E S E	·29				
Aug. 26	E *b* S	·41				

	III			IV		
June 7	N N E	·52		NW *b* N	·58	
June 7	N N E	·33		NW *b* N	·48	
July 2	NE *b* N	·32	·41	NW *b* N	·49	
July 12	NE *b* N	·25		NW *b* N	·38	
Sept. 8	NE *b* N	·65		NW *b* N	·28	
				N W	·26	·37
				N W	·03	
				N W	·48	
				N W	·28	
				N W	·33	
				N W	·48	

TABLE VIII

Results of Lamp and Star Comparisons

Date 1933	t	Stars: Name	Stars: Z.D. z	$\Delta\phi$ Lamp − star +0·31 sec z	Gradient of Star	$\Delta\phi_1$	R_1
			°				
June 1	35	η U Maj	12·9	+4·836	−·232	+4·60	+·01
June 3	37	η U Maj	15·0	4·773	−·232	4·54	−·04
June 7	41	γ U Min	21·9	4·272	+·193	4·46	−·10
June 7	41	γ U Min	24·5	4·308	+·193	4·50	−·06
June 28	62	α Ceph	21·3	3·789	+·435	4·22	−·21
July 2	66	γ U Min	23·9	4·123	+·193	4·32	−·09
July 2	66	γ U Min	26·7	4·136	+·193	4·33	−·08
July 12	76	γ U Min	29·3	4·131	+·193	4·32	−·03
July 25	89	α Ceph	19·3	3·923	+·435	4·36	+·09
July 25	89	α Ceph	15·7	3·951	+·435	4·39	+·12
Aug. 1	96	α Ceph	18·3	3·854	+·435	4·29	+·06
Aug. 1	96	α Ceph	14·7	3·819	+·435	4·25	+·02
Aug. 8	103	α Ceph	10·7	3·779	+·435	4·21	+·02
Aug. 23	118	α Ceph	12·1	3·758	+·435	4·19	+·09
Aug. 23	118	α Ceph	10·7	3·837	+·435	4·27	+·17
Aug. 26	121	α Ceph	12·6	3·626	+·435	4·06	−·03
Aug. 26	121	α Ceph	10·7	3·702	+·435	4·14	+·05
Sept. 8	134	δ Cass	20·8	+3·789	+·248	+4·04	+·03

observed gradient difference $\Delta\phi$ between it and the standard lamp. The values given in this column are in the sense lamp *minus* star, and they are the gradient differences derived from the measures of Δm on the plates, to which the values given in Table II for filter 78 were added. Further, the values of $\Delta\phi$ given in Table VIII are corrected for atmospheric reddening, the quantity 0·31 sec z having been added to the derived gradient differences. The next column gives the gradient of the star relative to the zero of the standard system, taken from the Greenwich colour temperature volume. The column $\Delta\phi_1$ is the sum of the previous two, and is accordingly the gradient difference, uncorrected for optical train, between the standard lamp and the zero of the standard system of stars. The last column, headed R_1, gives the residuals from the final least square solution (see p. 503).

TABLE IX

Results of comparison of Optical Trains

Date 1933	t	$\Delta\phi$ Lab. – Tel.	Horizontal Reddening A'	$\Delta\phi_2$	R_2
April 27	0	−0·39	+0·12	−0·27	+·09
April 27	0	−0·43		−0·31	+·05
April 28	1	−0·33	+0·12	−0·21	+·16
April 28	1	−0·48		−0·36	+·01
June 12	46	−0·77	+0·04	−0·73	−·10
June 15	49	−0·78	+0·16	−0·62	+·03
June 15	49	−0·78		−0·62	+·03
July 4	68	−0·94		−0·82	−·06
July 4	68	−0·81	+0·12	−0·69	+·07
July 4	68	−0·81		−0·69	+·07
July 17	81	−0·86	+0·07	−0·79	+·05
July 26	90	−1·04	+0·12	−0·92	−·03
Aug. 4	99	−1·08		−1·03	−·09
Aug. 4	99	−1·07	+0·05	−1·02	−·08
Aug. 4	99	−1·09		−1·04	−·10
Aug. 25	120	−1·07		−1·00	+·07
Aug. 25	120	−1·09	+0·07	−1·02	+·05
Aug. 25	120	−1·09		−1·02	+·05
Aug. 29	124	−1·13		−1·07	+·02
Aug. 29	124	−1·16	+0·06	−1·10	−·01
Aug. 29	124	−1·07		−1·01	+·08
Sept. 11	137	−1·35		−1·28	−·11
Sept. 11	137	−1·40	+0·07	−1·33	−·16
Sept. 11	137	−1·38		−1·31	−·14
Sept. 14	140	−1·31		−1·19	·00
Sept. 14	140	−1·33	+0·12	−1·21	−·02
Sept. 14	140	−1·29		−1·17	+·02

The results of the plates taken for the comparison of the two optical trains are given in Table IX. The first two columns give the date and the corresponding time t reckoned, as before, from 1933 April 27. The column $\Delta\phi$

gives the gradient differences for the acetylene burner photographed with the laboratory spectrograph *minus* the same burner photographed with the telescope. In forming these gradient differences, the totals obtained by adding the mean results given in Tables III and V were subtracted from the values of Δm derived from the measures of the plates. The values of $\Delta\phi$ so obtained have to be corrected by the addition of the horizontal reddening A' (see section 11 above), given in the fourth column of the table. The column $\Delta\phi_2$ gives the values of $\Delta\phi + A'$. The last column gives the residuals R_2 obtained from the final least square solution.

A preliminary plot of $\Delta\phi_2$ against t showed that the change with time of the gradient difference between the two optical systems can be represented satisfactorily by a straight line. The quantities in Tables VIII and IX accordingly give the following equations of condition :—

$$\Delta\phi_0 + \alpha t + \beta = \Delta\phi_1,$$
$$\alpha t + \beta = \Delta\phi_2,$$

where $\Delta\phi_0$ denotes the true difference of gradient between the standard lamp and the zero point of the system of standard stars.

In forming the equations the mean result for the plates on each night was taken. When only one plate was secured on a particular night, the corresponding equation of condition was given half weight. Full weight thus corresponds to the mean of two or three plates. A least square solution was then carried through and there resulted :—

$$\Delta\phi_0 = 5{\cdot}16 \pm {\cdot}02,$$
$$\alpha = -{\cdot}0059 \pm {\cdot}0003,$$
$$\beta = -{\cdot}36 \pm {\cdot}03.$$

The residuals given in the last columns of Tables VIII and IX were computed from this solution.

In the accompanying diagram, the night means of $\Delta\phi_1$ and $\Delta\phi_2$ are plotted against the time t. In each case the straight line given by the least square solution is shown, and the slope of this line represents the progressive change in the relative performance of the two systems. The change is due in the main to the deterioration in the silvered surfaces of the 30-inch and cassegrain mirrors.

It will be observed that the residuals R_1 tend to be negative for the earlier and positive for the later plates. This systematic tendency is an unsatisfactory feature.

14. If ϕ_0 and ϕ_L denote the respective values of ϕ for the zero point of the standard system of stars and for the standard lamp, then

$$\phi_L - \phi_0 = \Delta\phi_0.$$

The least square solution gave $\pm$ ·02 as the probable error of $\Delta\phi_0$. From the results given in Tables II, III and V it is found that the total contribution to the final probable error from the measurements of the filter transmissions and of the distance effect is $\pm$ ·02. As regards the atmospheric reddening A the probable error of the value $A = 0{\cdot}31$ given by the south stars only was $\pm$ ·01, but in view of the range in the mean values for the four azimuth

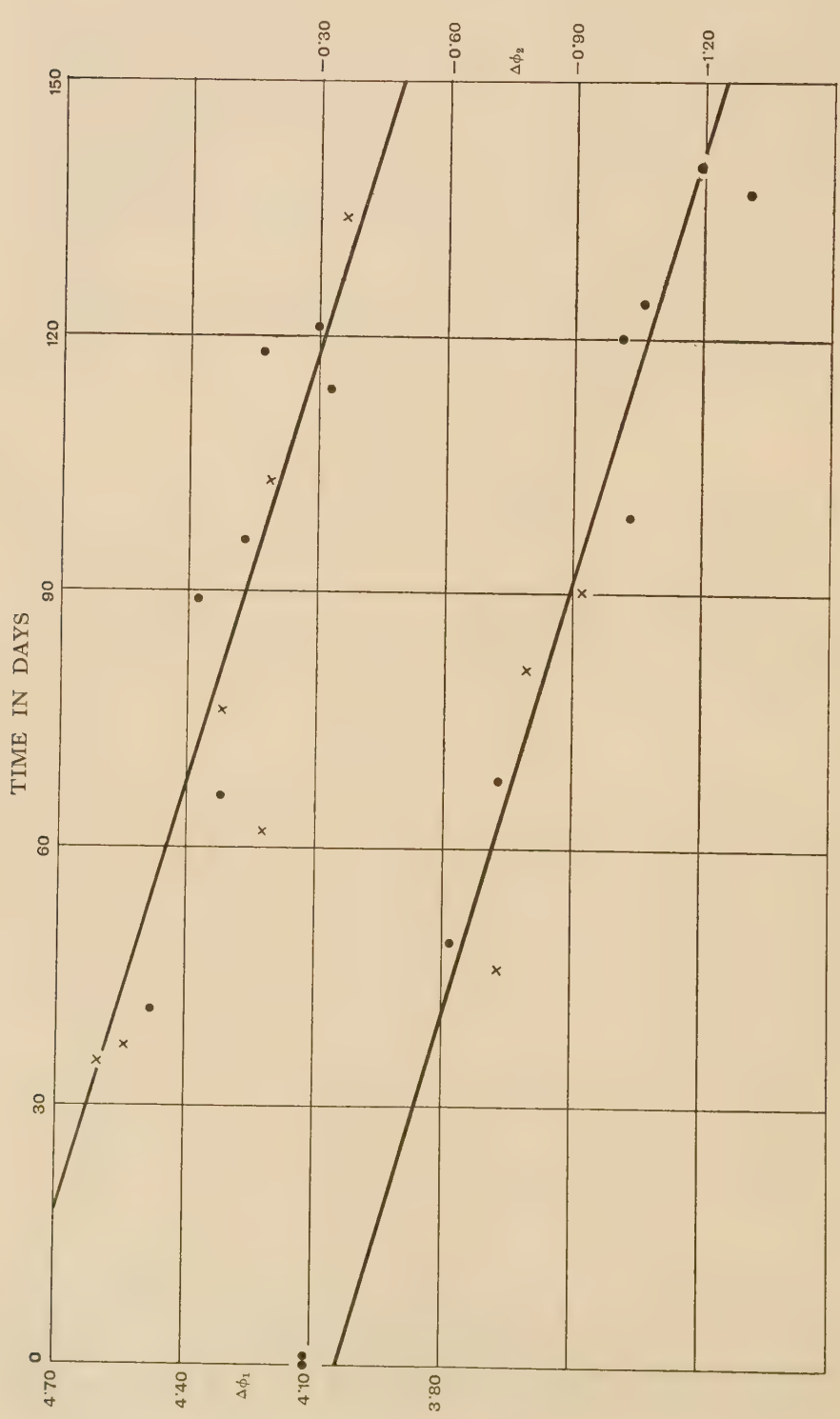

The upper part of the diagram refers to star and lamp comparisons, and the lower to acetylene comparisons.

groups (see Table VII) it is felt that this does not adequately represent the uncertainty introduced. It has accordingly been written up to ± ·03. Furthermore, the probable error of the photometric scale based on the adopted values of the slit differences (see section 8 above) may be taken as ± 0·5 per cent., which contributes ± ·025 towards the probable error of $\Delta\phi_0$. The final probable error is thus ± ·05, and we have

$$\phi_L - \phi_0 = 5{\cdot}16 \pm {\cdot}05.$$

For the standard lamp,

$$T = 2360^\circ \text{ K.},$$

corresponding to

$$\phi_L = 6{\cdot}07.$$

Hence there results

$$\phi_0 = 0{\cdot}91 \pm {\cdot}05.$$

Using the revised values of the laboratory standards (see section 1) the previous result becomes

$$\phi_0 = 1{\cdot}07 \pm {\cdot}05.$$

The mean gives $\phi_0 = 0{\cdot}99$, corresponding to $T_0 = 18100^\circ$.

Both series of observations are liable to systematic error arising from the uncertainty in the laboratory colour temperature scale at 2360° K. The National Physical Laboratory, in their calibration of the standard lamps, estimated this uncertainty to be ± 20° K., corresponding to ± 0·05 in ϕ.

To one decimal place the final result is

$$\phi_0 = 1{\cdot}0.$$

The total error, from all causes, of this result can hardly be as much as 0·15.

15. As stated in section 10 above, all gradient differences in the present work have been derived from measures at the wave-lengths listed in Groups I, II, IV and V of Table I. The first two groups were combined with equal weight, and the last two with relative weights of two to one. The effect of this procedure is to eliminate the effect of small errors in wave-length.

The existence of such errors is, in point of fact, suggested by the figures given in Table X, which exhibits for all five groups the mean residuals from the linear gradients obtained as described. The successive columns give the residuals for the comparisons between the standard lamp and the zenith stars, between the acetylene flame photographed with the two optical trains and between the stars at high and low zenith distances for the determination of atmospheric reddening. In the last case, the mean residuals in the sense low star *minus* high have been divided by the mean value of $\sec z_2 - \sec z_1$, so as to reduce them to the zenith. The numerical value of this factor was 0·80.

It will be observed that in the first two columns the residuals for Groups IV and V are in each case opposite in sign. For these groups the slopes of density against wave-length are comparatively large, and there is thus a suggestion that small wave-length errors are present in the comparison of

spectra photographed with the telescope and with the laboratory spectrograph.

TABLE X

Mean Residuals for Wave-Length Groups

Group	ρ_1 Lamp − star	ρ_2 Lab. − Tel.	ρ_3 Atmosphere at Zenith
	m	m	m
I	+·009	+·014	−·013
II	−·010	−·015	+·014
III	−·012	−·059	+·040
IV	+·033	+·047	−·004
V	−·069	−·095	+·008

The gradient differences do not involve the measures for Group III, and so the residuals for this group can be used to discuss how far the observations depart from a linear fit. The residual ρ_1 for lamp *minus* star is affected by the difference of optical train and by the atmospheric reddening. If ρ denotes the real residual for lamp *minus* star then

$$\rho = \rho_1 - (\rho_2 + \tfrac{9}{31}\rho_3) + 1{\cdot}06\rho_3.$$

The factor 9/31 arises from the fact that the observations for optical train difference are affected by the 600 feet of air between the telescope and the roof of the Octagonal Building. The mean values of A, the atmospheric reddening at the zenith, and A', the horizontal reddening over the 600 feet, are ·31 and ·09, and it has accordingly been assumed that the effect is $\frac{9}{31}\rho_3$.

The factor 1·06 is the mean value of sec z where z denotes the zenith distance at which a star was photographed for comparison with the lamp.

From the internal evidence the probable errors of ρ_1, ρ_2 and ρ_3 for the third group come out to be $\pm$ m·005, $\pm$ m·007 and $\pm$ m·005. The first two of these include the contributions from the filter and distance effect determinations.

There thus results for the third group

$$\rho = 0{\cdot}078 \pm 0^{m}{\cdot}010.$$

It is necessary to compare this with the theoretical residual computed for black bodies at 2360° K. and 18000° K. This was computed and found to be $+0^{m}{\cdot}008$. Subtracting it from ρ there results

$$\rho' = +0^{m}{\cdot}070 \pm 0^{m}{\cdot}010,$$

where ρ' is the corrected residual corresponding to departures from Planck's law. A positive value of ρ' implies an excess of radiation at λ 5300 for the lamp, or a deficiency for the stars, as compared with a black-body curve fitted to the actual radiations at λ 4600 and λ 6000.

As regards the lamp, Forsythe has found for tungsten an excess in the green of the order of 1 per cent. as compared with a black-body curve fitted to the red and blue.* The above value of ρ' thus gives a deficiency of 6 per cent. for the stars.

* *J.O.S.A.* and *R.S.I.*, 7, 1115, 1923.

The previous observations gave a residual in the third group of the order of 0·01 of a magnitude for the stars compared with the acetylene flame. In one respect, the present results are more satisfactory. The positive value of ρ_3 found in Group III is in accordance with expectation. It indicates an increasing value of the atmospheric reddening A for the shorter wave-lengths.

16. The Greenwich observations have given for the zero of the standard system of stars

$$\phi_0 = 1{\cdot}0,$$

corresponding to $T_0 = 18000°$ K.* Apart from the possibility of a systematic error, which has so far escaped detection, it is very improbable that this value can be as much as 0·15 in error. The zero of the system is effectively the mean of the Ao stars, and it seems that the colour temperatures of such stars are considerably in excess of 11000°, a value which is often quoted. The value of ϕ corresponding to $T = 11000°$ is 1·40, so that a colour temperature as low as this is definitely excluded by the observations.

It may, perhaps, be of interest to refer briefly to the results for the stars of type Go. The Greenwich colour temperature volume gives gradients for nine of these. Two, namely α Aurigæ and ϵ Leonis, are giant stars with comparatively low colour temperatures. The mean gradient for the remaining seven is $+1{\cdot}14$. Using $\phi_0 = 1{\cdot}0$, this gives $\phi = 2{\cdot}14$ for the mean of these stars, corresponding to $T = 6820°$ K. The extreme observational uncertainty in ϕ_0 is $\pm$ 0·15, so that the extreme permissible values for the mean dwarf Go star are $\phi = 1{\cdot}99$ and $\phi = 2{\cdot}29$, corresponding to $T = 7340°$ and $T = 6340°$. These figures may be compared with the results found for the Sun by H. H. Plaskett.† For the *centre* of the disc he obtains a colour temperature of 6700° to 7000°, the extreme limits of uncertainty being given as 6300° and 7500°. The values for the integrated disc may be taken as about 400° smaller. Both the Victoria and Greenwich observations are based on measures at wave-lengths chosen so as to be as free as possible from the effect of absorption lines.

Absolute colour temperature work is difficult, and it seems probable that a more precise value for ϕ_0 can only be obtained as a result of observations at several observatories working under good climatic conditions. It is not proposed to undertake further absolute observations at Greenwich. The future colour temperature programme will consist of relative observations for gradient, the stars under observation being compared with suitably chosen stars from the standard list. Experience has shown that gradients, relative to the zero point of the standard system, can be obtained with a satisfactorily small probable error, but it seems likely that for some time to come the uncertainty in the value of ϕ_0 will remain relatively large.

* A table for the conversion of ϕ into T and *vice versa* is given at the end of the Greenwich colour temperature volume.

† *Pub. D.A.O.*, 2, No. 12, 1923.

SOME NEW MEMBERS OF THE HYADES CLUSTER.

P. J. van Rhijn and J. J. Raimond, Jun.

1. *Introduction and Summary*

In 1924 some proper motion plates of the Hyades cluster were measured at the Kapteyn Laboratory. The results are published in the *Publications of the Kapteyn Astronomical Laboratory*, No. 35. The photographic magnitude of the faintest members of the cluster found in that paper is about 11. In order to extend this investigation to fainter stars we asked M. Picart, the director of the Bordeaux Observatory, to repeat some of the chart plates of the *Carte du Ciel*, and to send them together with the early plates to Groningen for measurement.

M. Picart kindly assented to our request, and the result of the investigation is given in the present paper. The centres of the plates are in Table I. The field measured for each plate is a circle with a radius of 65′. With the exception of the stars too bright for measurement the members of the cluster in this field are given in Table VII, down to a limiting photographic magnitude which for the various plates varies between 12 and 14.

The photographic magnitudes of the members of the cluster have been derived at this laboratory from plates kindly taken by Mr. Wood with the Franklin-Adams refractor at the Union Observatory, Johannesburg. The spectral classes of the stars were furnished by Professor Schwassmann of the Hamburger Sternwarte, classified on plates especially taken for the purpose. The luminosity curves of the members of the cluster of each spectral class are discussed in this paper.

We want to express our thanks to M. Picart and to Mr. Wood for the plates kindly put at our disposal, to Professor Schwassmann for the spectral classification of the members of the Hyades cluster, and to Mr. H. J. Smith and Mr. W. Ebels, computers at the Kapteyn Laboratory, for their efficient help in the measurement and reduction.

2. *The Plates*

As stated in the introduction, the plates were taken with the *Carte du Ciel* instrument at the Bordeaux Observatory. Each plate contains three exposures of equal length. A list of the plates is in Table I.

3. *The Measurements*

The plates have been measured by Mr. W. Ebels, computer at the Kapteyn Laboratory. He made first of all a Durchmusterung for each of the regions of Table I, containing the rectangular co-ordinates to 0·1 mm. of all stars occurring on the plate, and an estimate of the diameter of the star image on an arbitrary scale by comparison with the constant distance

TABLE I

List of the Plates

Plate Number	Centre		Date	Hour Angle
	α 1900	δ 1900		
	h m s	° ′		m
1531	4 15 56	+14 3·5	1911 Jan. 26	+ 4·6
2155			1924 Dec. 22	−48·6
1527	4 24 1	+14 2·6	1911 Jan. 24	+ 5·6
2156			1924 Dec. 22	+17·4
1749	4 31 59	+14 3·0	1912 Dec. 11	− 8·8
2160			1925 Jan. 16	+14·5
1486	4 16 0	+16 3·6	1909 Dec. 30	−20·0
2157			1924 Dec. 24	−47·6
683	4 24 0	+16 3·6	1902 Dec. 23	−30·5
2159			1925 Jan. 16	−49·5
682	4 32 0	+16 3·5	1902 Dec. 22	+ 0·5
2158			1924 Dec. 24	+ 7·4

of 2″ between two wires of the micrometer. The Durchmusterung for each region has always been made on the plate containing the largest number of stars. The early and new plates have been measured in four positions differing by 90°. The machine is of the usual *Carte du Ciel* type. The position of the star on both plates has been determined with respect to the same division line of the scale (see *Groningen Publications*, No. 28, p. 3). We have measured the stars inside a circle with a radius of 65′. Only some bright stars for which the images of the three exposures overlapped and a few stars for which all three images coincided with a réseau line have not been measured. For a certain number of stars only one or two images have been measured, the others being immeasurable by the coincidence with a réseau line. The stability of the machine has been tested by remeasuring every day two standard stars before and after the regular measurements. Further, the run of the screw has been investigated by measuring every day the distance between the same divisions of the scale.

The position of each star image on the early and new plates have been measured relatively to the same division line of the scale. The difference of both measurements is taken and the average of these differences for the three images of each star measured in two positions of the plate is formed. These average quantities denoted by m_x and m_y for the direction of the right ascension and declination respectively are reduced to proper motions in two steps. In the preliminary solution we take

$$m_x = a + bx + cy,$$
$$m_y = a' + b'x + c'y,$$

where x and y are the rectangular co-ordinates of the star image and a, b, c, a', b', c' are constants.

The values of the constants are computed by means of some 16 stars, 4 in each quadrant of the plate. The differences,

$$p_x = m_x - a - bx - c'y,$$
$$p_y = m_y - a' - b'x - c'y,$$

represent preliminary relative proper motions. In the final solution these p_x and p_y have been taken equal to

$$\left.\begin{aligned} p_x &= a + bx + cy + dx^2 + cxy + fy^2, \\ p_y &= a' + b'x + c'y + d'x^2 + c'xy + f'y^2, \end{aligned}\right\} \qquad (1)$$

and the values of the constants have been determined by a least squares solution, using the stars which fulfil the following conditions :—

1. The distance of the star from the centre of the plate does not exceed 1°.
2. The preliminary proper motion does not exceed a certain limit, which for the various plates lies between 0″·025 and 0″·050.
3. The estimated diameters are between given limits. The corresponding photographic magnitudes differ from plate to plate, but are always confined between 12·0 and 15·0.

The number of stars used in the solution of the equations of condition varies for the different plates from 70 to 150.

The final values of the relative proper motions are derived from equations (1).

4. *Probable Error*

The probable error of the proper motions has been found by comparison of the values found in the present paper with *Groningen Publications*, No. 35. The probable error of the latter being derived in the quoted publication, we easily find the following probable errors of the proper motion in either co-ordinate derived in the present paper :—

$r = \pm \dfrac{0''\cdot 16}{T}$ for stars with a distance from the centre $< 60'$, where T is the epoch difference between the plates.

The value $\pm$ 0″·16 agrees pretty well with the average found in *M.N.*, **93**, 646, 1933.

5. *Photographic Magnitudes*

The photographic magnitudes of the members of the cluster listed in Tables VII and VIII have been found by means of four plates taken with the Franklin-Adams telescope at the Union Observatory (1 mm. = 3′·05 ; aperture 25 cm.). Each plate contains three exposures of equal length ; two exposures on the Hyades and a third one on either of the Harvard Standard Regions C_2 and C_3 for which the photographic magnitudes are known.* A list of the plates is in Table II.

* *Harvard Annals*, **71**, 271, 1917.

TABLE II

List of the Magnitude Plates

H.S.R. = Harvard Standard Region

Plate Number	Object	Exposure Time
8018	Hyades	8 min.
	H.S.R. C_2	,,
	Hyades	,,
8019	Hyades	30 min.
	H.S.R. C_2	,,
	Hyades	,,
8020	Hyades	6 min.
	H.S.R. C_3	,,
	Hyades	,,
8025	Hyades	30 min.
	H.S.R. C_3	,,
	Hyades	,,

The plates being pressed against a piece of plate-glass are measured with a thermopile and galvanometer.* It appeared that the plates Nos. 8018 and 8019 were all right; but for Nos. 8020 and 8025 it was impossible to get the right focus over the whole surface of the plate. We therefore have measured the plates Nos. 8020 and 8025 in a different way. The diameters of the images of the brighter stars were measured with a micrometer; for the fainter ones the diameter changes little with the magnitude, and we therefore estimated the opacity of the stellar images by comparison with a scale of opacities. This scale contains eight images of increasing opacity marked on a small area of a Franklin-Adams plate taken for another purpose.

The opacities were estimated in the stereocomparator, the scale being put in the left-hand part of the machine and the plate to be measured in the right-hand part. The difference between two consecutive images of the scale is about 0·5 magnitude; a tenth of this interval has been estimated.

The magnitudes of the Harvard Standard Regions reduced to the international photographic scale † have been plotted against the galvanometer readings, measured diameters and estimated opacities respectively. The magnitudes of the Hyades are easily found by means of this curve.

These magnitudes have been compared with Hertzsprung's results ‡ (see Table III).

The magnitudes given by Hertzsprung are denoted by m_H, the magnitudes of the present paper by m_G. The differences between the two sets of magnitudes are in the column $\bar{m}_H - \bar{m}_G$ uncorrected. At least part of the differences are probably due to an error in the magnitudes of the present

* *Groningen Publications*, No. 32, 1924.

† *Harvard Bulletin* 781, 1923.

‡ *Astronomische Nachrichten*, **209**, 115, 1919. We have compared only the magnitudes brighter than 9·5 because Hertzsprung's results for the fainter stars depend on the observations of a single plate only.

TABLE III

Comparison of the Magnitudes of the Present Paper and Hertzsprung's Magnitudes for the Stars brighter than $m = 9{\cdot}5$

Limits, m_H	$\bar{m}_H$	$\bar{m}_H - \bar{m}_G$		Number
		Uncorr.	Corr.	
8·47 to 8·50	8·49	+·11	−·01	6
8·50 ,, 8·72	8·66	+·18	+·08	7
8·72 ,, 8·96	8·83	+·07	·00	9
8·96 ,, 9·31	9·15	+·12	−·01	7

paper depending on the distance from the centre of the plate. The differences $m_H - m_G$ have been tabulated in Table IV according to the distance from the centre of the plate.

TABLE IV

Differences $m_H - m_G$ for the Stars brighter than $m = 9{\cdot}5$ according to Distance from the Centre of the Plate

r	$\bar{m}_H - \bar{m}_G$	Number
′		
56	·00	6
105	+·03	5
120	+·04	5
157	+·24	6
221	+·23	7

A correction for distance is indicated.

The correction for distance from the centre of the plate for the fainter stars has been derived from the observations of Chapman and Melotte.* The authors give the position-corrections to the centre of the plate for the logarithms of the densities at a distance of 180′, which, by means of the data of *Groningen Publications*, No. 43, table vii, are easily reduced to corrections for the magnitudes. The values of the division of the comparison scale μ for which the corrections are valid are reduced to magnitudes by means of the numbers of stars brighter than the scale division μ given in the papers quoted and the data of *Groningen Publications*, No. 43, table vii. The limiting magnitudes of our plates being 2·2 brighter than in Chapman's and Melotte's investigations, we have taken the correction on our plates for the magnitude $m - 2{\cdot}2$ to be equal to the correction for the magnitude m on the Greenwich plates. We thus find that for the magnitudes 12 to 15 the correction amounts to $-0^{m}{\cdot}17$ at the distance of 180′. We have adopted the following corrections :—

* *Memoirs of the Royal Astronomical Society*, **60**, part iv, table i, 1914; and *M.N.*, **78**, 73, table D, 1917.

Adopted Corrections to our Magnitudes for Distance from the Centre of the Plate

r \ m	<9·5	9·5 to 11·5	>11·5
<130′	0·00	0·00	$-\frac{0\cdot17}{180}r$ (r = distance expressed in minutes of arc).
>130′	+0·20	0·00	

After applying these corrections to the magnitudes of the present paper, we find the differences in the fourth column of Table III which are sufficiently small.

The magnitudes of this paper have been derived partly from galvanometer readings with the thermopile, and partly from estimates of the density of the images by comparison with a scale of increasing densities. It is by no means certain that the corrections for distance will be the same in both cases. We have, however, applied the same corrections in both cases because the differences between both sets of magnitudes show no dependence on the distance from the centre of the plate.

6. *Reduction to Absolute Proper Motion. The Magnitude Error of the Proper Motions*

The relative proper motions derived from the photographic plates have been reduced to absolute values according to the method described in *Groningen Publications*, No. 45, § 8. The stars are grouped according to apparent magnitude and the mean values of the relative proper motion $\bar{\mu}_x$ and $\bar{\mu}_y$ are formed for each group ; the members of the group and stars at a distance from the centre of the plate exceeding 60′ have been excluded. The differences between the parallactic motion in the x and y direction for the mean magnitude of the group and the mean values of $\bar{\mu}_x$ and $\bar{\mu}_y$ are taken to represent the reduction to absolute proper motion. If the differences depend on the apparent magnitude the proper motions of the plate probably contain a magnitude error. The values of the parallactic motion have been computed by means of table viii of *Groningen Publications*, No. 45. The reduction of the mean photographic magnitudes found in this paper to the Harvard visual scale used in *Groningen Publications*, No. 45, has been performed by means of *Mount Wilson Contribution*, No. 287, p. 13, and No. 288, pp. 4 and 5.

The proper motions appear to be free from magnitude error with the exception of the pair at $\alpha = 4^h\ 24^m$, $\delta = +14°$ in the x direction.

The reductions to absolute proper motion are in the following table :—

TABLE V

Reduction to Absolute Proper Motion

α_0	δ_0	$\Delta\bar{\mu}_x$	$\Delta\bar{\mu}_y$
h m	°	″	
4 16	+14	−0·002	0·000
4 24	+14	+ ·003	·000
4 32	+14	− ·001	+ ·003
4 16	+16	+ ·001	·000
4 24	+16	+ ·001	− ·003
4 32	+16	·000	− ·001

A correction for magnitude error amounting to $-0''.008\,(m-12)$ has been applied to the μ_x of the plate $\alpha = 4^h\ 24^m$, $\delta = +14°$ for the stars brighter than the magnitude 12.

7. *Limit of Completeness of the Plates*

The proper motion is found from the comparison of the early and the new plate. The Durchmusterung for each region being made on either of the two plates which contains the larger number of stars, it is certainly complete to a fainter limit of brightness than the faintest stars with measurable proper motion. We therefore easily find the faintest diameter estimate (see section 2) for which the proper motions of all stars could be measured. These diameters have been reduced to photographic magnitudes by means of some stars for which the magnitude is found as described in section 5. The results are in the following table, which also contains the limit of completeness on the bright side. The measured area is a circle with a radius of 60′.

TABLE VI

Limit of Completeness of the Proper Motion Plates of Table I

Number	Centre of Plate		Limits of Completeness for Radius 60′	
	α	δ	Bright	Faint
	h m	°	m	m
1	4 16	+14	7·5	14·0
2	4 24	+14	10·1	13·9
3	4 32	+14	8·0	13·5
4	4 16	+16	10·0	14·2
5	4 24	+16	9·7	12·4
6	4 32	+16	10·0	11·9

The stars with a distance from the centre exceeding 60′ have been marked in the catalogue.

8. *The Members of the Hyades Cluster*

We have found the following members of the Hyades cluster on the plates measured in this paper. Only stars at a distance from the plate centre not exceeding 65′ are given in tables VII and VIII; stars at a distance between 60′ and 65′ are marked with an asterisk in the declination column. The stars which according to *Groningen Publications*, No. 35, belong to the cluster have been reprinted, and the mean of the values of the proper motion found here and in *Groningen Publications*, No. 35, is adopted. The weights are taken inversely proportional to the squares of the probable errors.

The photographic magnitudes given in Table VIII have been discussed in section 5. The magnitudes with an asterisk have been taken from Hertzsprung's paper.* The spectral class Berg. is from an unpublished investigation by Schwassmann; the spectral class Harv. from the Henry Draper Catalogue. The $\Delta\mu_x$ and $\Delta\mu_y$ are equal to the differences between the group motion for the star under consideration and the adopted value of the

* *Astronomische Nachrichten*, **209**, 115, 1919.

TABLE VII

Members of the Hyades Cluster, the Proper Motion of which is Measured in this Paper

No.	α_{1900}	δ_{1900}	m	Spectral Class		This Paper		*G.P.* 35		Adopted		$\Delta\mu_x$	$\Delta\mu_y$
				Berg.	Harv.	μ_x	μ_y	μ_x	μ_y	μ_x	μ_y		
	h m s	° ′				″	″	″	″	″	″	″	″
1	4 13 41	+14 4·4	14·07	too faint		+0·112	−0·014	...	...	+0·112	−0·014	−0·002	−0·009
2	4 17 3	14 49·3	7·55*	F9	Go	+ ·099	− ·017	+0·103	−0·013	+ ·102	− ·014	+ ·003	− ·014
3	4 17 6	14 1·0	10·48	G4	...	+ ·073	− ·037	+ ·108	− ·012	+ ·090	− ·024	+ ·013	·000
4	4 17 43	15 31·8	11·48	K4	...	+ ·124	− ·019	+ ·134	− ·043	+ ·129	− ·031	− ·024	+ ·001
5	4 17 52	14 26·3	9·62	G4	G5	+ ·112	− ·017	+ ·122	− ·009	+ ·117	− ·013	− ·014	− ·013
6	4 18 9	14 41·3	14·71	K	...	+ ·123	− ·022	...	...	+ ·123	− ·022	− ·017	− ·004
7	4 18 12	16 7·4	14·26	Go	...	+ ·103	− ·017	...	...	+ ·103	− ·017	+ ·001	− ·015
8	4 18 15	16 29·4	13·78	K2	...	+ ·119	− ·012	...	...	+ ·119	− ·012	− ·015	− ·022
9	4 18 16	13 49·4	11·93	K4	...	+ ·114	− ·007	...	...	+ ·114	− ·007	− ·011	− ·017
10	4 18 32	14 31·6	8·15*	F8	Go	+ ·061	− ·030	+ ·118	+ ·012	+ ·090	− ·009	+ ·016	− ·017
11	4 19 6	15 38·6	12·95	Ko	...	+ ·116	− ·011	...	...	+ ·116	− ·011	− ·012	− ·021
12	4 21 47	14 2·4	11·43	K3	...	+ ·091	− ·013	+ ·113	− ·046	+ ·105	− ·035	− ·006	+ ·010
13	4 22 8	14 11·7	10·27	K1	...	+ ·090	− ·019	+ ·100	− ·022	+ ·097	− ·021	+ ·002	− ·005
14	4 22 25	16 14·7	12·28	K8	...	+ ·099	− ·029	+ ·120	− ·002	+ ·110	− ·015	− ·009	− ·018
15	4 22 27	13 38·7	9·75	G5	G5	+ ·100	− ·016	...	...	+ ·100	− ·016	− ·001	− ·009
16	4 22 54	16 44·8	14·26	F–G	...	+ ·093	− ·015	...	...	+ ·093	− ·015	+ ·007	− ·020
17	4 23 7	16 3·9	11·88	K6	...	+ ·086	− ·015	+ ·083	− ·014	+ ·084	− ·014	+ ·017	− ·019
18	4 23 10	15 45·6	13·12	K5	...	+ ·089	− ·018	...	...	+ ·089	− ·018	+ ·012	− ·015
19	4 23 32	15 3·3*	13·65	K3	...	+ ·101	− ·033	...	...	+ ·101	− ·033	− ·003	+ ·003
20	4 23 47	16 1·5	11·49	K3	...	+ ·099	− ·020	+ ·091	− ·011	+ ·093	− ·013	+ ·008	− ·020
21	4 24 13	16 27·4	9·83	G8	Ko	+ ·103	− ·016	+ ·108	− ·013	+ ·106	− ·014	− ·006	− ·021
22	4 24 52	15 31·0	9·78	G6	Ko	+ ·083	− ·015	+ ·090	− ·015	+ ·089	− ·015	+ ·008	− ·017
23	4 26 3	15 24·9	13·24	K2	...	+ ·092	− ·012	...	...	+ ·092	− ·012	+ ·005	− ·020
24	4 26 4	14 49·5	13·63	K5	...	+ ·091	− ·033	...	...	+ ·091	− ·033	+ ·007	+ ·003
25	4 26 11	15 17·1	12·44	K3	...	+ ·097	− ·023	+ ·118	− ·013	+ ·108	− ·018	− ·011	− ·014
26	4 26 16	14 27·9	11·94	G6	...	+ ·090	− ·031	+ ·067	− ·023	+ ·080	− ·027	+ ·018	− ·001
27	4 27 7	15 47·8	9·79	G5	Ko	+ ·095	− ·005	+ ·107	− ·032	+ ·105	− ·027	− ·009	− ·006
28	4 28 50	15 37·2	10·59	G8	Ko	+ ·090	− ·009	+ ·091	− ·012	+ ·091	− ·011	+ ·003	− ·021
29	4 30 16	16 20·2	11·93	K4	...	+ ·082	− ·017	+ ·094	− ·011	+ ·091	− ·012	+ ·001	− ·023
30	4 30 23	15 28·8	10·31	G9	Ko	+ ·093	− ·013	+ ·105	− ·013	+ ·102	− ·013	− ·008	− ·019
31	4 33 18	13 54·4	8·59*	G5	...	+ ·074	− ·026	...	...	+ ·074	− ·026	+ ·011	·000
32	4 34 41	16 19·1	10·46	K3	Ko	+ ·079	− ·020	+ ·113	− ·030	+ ·096	− ·025	− ·007	− ·009

TABLE VIII

Doubtful Members of the Hyades the Proper Motion of which is Measured in this Paper

No.	α	δ	m	Spectral Class Berge-dorf	This Paper		*G.P.* 35		Adopted		$\Delta\mu_x$	$\Delta\mu$
					μ_x	μ_y	μ_x	μ_y	μ_x	μ_y		
	h m s	° ′			″	″	″	″	″	″	″	″
33	4 12 37	15 50·7	10·30	G8	+0·109	−0·018	+0·131	+0·015	+0·120	−0·001	−0·012	−0·0
34	4 13 42	15 49·0	>14·8	...	+ ·065	− ·035	...	...	+ ·065	− ·035	+ ·043	+ ·0
35	4 15 54	14 35·8	10·43	G3	+ ·125	− ·067	+ ·132	− ·041	+ ·130	− ·050	− ·024	+ ·0
36	4 17 52	16 10·7	12·90	G1	+ ·072	− ·035	...	...	+ ·072	− ·035	+ ·032	+ ·0
37	4 19 16	16 45·3*	11·21	K2	+ ·064	− ·009	+ ·088	·000	+ ·080	− ·003	+ ·023	− ·0
38	4 21 8	13 36·6	14·40	G	+ ·082	+ ·007	...	...	+ ·082	+ ·007	+ ·017	− ·0
39	4 21 52	15 8·5*	11·63	G5	+ ·081	− ·010	+ ·072	− ·021	+ ·074	− ·018	+ ·028	− ·0
40	4 27 22	14 29·1	14·22	G−K	+ ·077	− ·003	...	...	+ ·077	− ·003	+ ·021	− ·0
41	4 32 36	15 15·8	10·44	G5	+ ·067	+ ·008	+ ·079	+ ·010	+ ·073	+ ·009	+ ·021	− ·0

proper motion. The group motion is equal to $\mu_x = 0''\cdot218 \sin\lambda \sin\phi$ and $\mu_y = 0''\cdot218 \sin\lambda \cos\phi$, where λ is the angular distance between the star and the convergent of the motion $\alpha = 6^h\ 13^m$, $\delta = +7°\cdot0$,* and ϕ the position angle at the star of the direction towards the convergent. The value of the total motion $0''\cdot218$ for $\lambda = 90°$ has been found from the data on pp. 10 and 11 of *Groningen Publications*, No. 35.

The numbers 4, 10, 12 and 26 were doubtful members of the group in *Groningen Publications*, No. 35. They have now been taken to belong to the cluster.

No. 37 was a cluster star in *Groningen Publications*, No. 35 ; its membership now seems doubtful.

Tables VII and VIII are complete between the magnitude limits of Table VI, and inside the circles with a radius of 60′ around the centres of Table I.

9. *Luminosity Curves*

We have investigated the distribution of the Hyades stars according to absolute photographic magnitude and spectral class. All members of the cluster were used occurring on the field completely investigated in this paper, *i.e.* :

(1) The six circles with a radius of 60′ and centres as given in Table I. It appears from Table VI that the countings are complete between the photographic magnitudes 10·0 and 12·0. Some members of the cluster between the magnitude 12·0 and 14·0 may be missing, especially on the plates $\alpha = 4^h\ 24^m$, $\delta = +16°$ and $\alpha = 4^h\ 32^m$, $\delta = +16°$.

The number of members of the cluster between the photographic magnitudes 5 and 10 † on the area (1) cannot be found from the data of Table VII,

* Rasmuson, *Meddelanden Lund II*, **26**, 11, 1921.

† The members of the cluster brighter than the photographic magnitude 5 on the area (1) can of course be found from Boss's *Preliminary General Catalogue*.

which for the brighter stars is incomplete. It has been derived from countings of tables vi and viii of *Groningen Publications*, No. 35; some objects of the list of doubtful members of *Groningen Publications*, No. 35, which, according to the present paper, are members of the cluster, have been added to the countings.

We wish to find the numbers of Hyades between the photographic magnitudes 5 and 10 on the area (1). To this end we count the members of the cluster $m = 5$ to 10 on the overlapping area of the field (1) and the field completely observed in *Groningen Publications*, No. 35—*i.e.*:

(2) The circles with a radius of 55′ and the centres as given in table i of *Groningen Publications*, No. 35.

The overlapping area of (1) and (2) is smaller than the field (1), and the counted numbers magnitude 5 to 10 must therefore be multiplied by a factor in order to reduce them to the area (1). This factor has been found from the stars brighter than the visual magnitude 6, and from the objects photographic magnitudes 10 to 12. Both these classes of objects have been completely observed on the area (1), as well as on the overlapping field of (1) and (2), the stars brighter than the visual magnitude 6 being given in Boss's *Preliminary General Catalogue* and the stars photographic magnitude 10 to 12 in the present paper. It appears that the factor amounts to 1·1 for both classes of stars, and this factor has also been adopted for the stars with photographic magnitudes 5 to 10.

We thus find the following numbers of group-members on the area (1). The absolute photographic magnitudes M are $m + 5 + 5 \log 0''{\cdot}027$.*

TABLE IX

Members of the Cluster of the Hyades on the Area (1)

$m_{photogr.}$	$M_{photogr.}$	Spectral Class A	F	G	K	M	Sum	log Sum	*G.P.* 38, Table 71	Diff.
2·0 to 3·0	− 0·8 to + 0·2									
3·0 „ 4·0	+ 0·2 „ + 1·2	...	1	...	...	...	1	0·00	6·01	6·01
4·0 „ 5·0	+ 1·2 „ + 2·2	1	...	...	2	...	3	·48	6·55	6·07
5·0 „ 6·0	+ 2·2 „ + 3·2	2·2	3·3	...	...	...	5·5	·74	6·83	6·09
6·0 „ 7·0	+ 3·2 „ + 4·2	2·2	5·5	...	...	...	7·7	·89	7·06	6·17
7·0 „ 8·0	+ 4·2 „ + 5·2	...	3·3	3·3	...	...	6·6	·82	7·28	6·46
8·0 „ 9·0	+ 5·2 „ + 6·2	...	...	6·6	...	...	6·6	·82	7·53	6·71
9·0 „ 10·0	+ 6·2 „ + 7·2	...	...	2·2	3·3	...	5·5	·74	7·55	6·81
10·0 „ 11·0	+ 7·2 „ + 8·2	...	...	1	4	...	5	·70	7·44	6·74
11·0 „ 12·0	+ 8·2 „ + 9·2	...	...	1	6	...	7	·85	7·40	6·55
12·0 „ 13·0	+ 9·2 „ +10·2	...	...	1	2	...	3	·48	7·50	7·02
13·0 „ 14·0	+10·2 „ +11·2	...	...	1	3	...	4	·60	7·59	6·99
14·0 „ 15·0	+11·2 „ +12·2	...	1 †	1	1					

* Rasmuson's value of the parallax in *Meddelanden Lund II*, No. 26, 1921, has been adopted.

† This star is α 1900 $= 4^h\ 22^m\ 54^s$, δ 1900 $= +16°\ 44'{\cdot}8$. Professor Schwassmann is not sure about the spectral classification. If the spectral class is early F, the star is a white dwarf.

The spectral classes are from the Henry Draper Catalogue, or if the star did not occur there from an unpublished investigation by Professor Schwassmann. The photographic magnitudes are from Table VII of the present paper and the catalogue of *Groningen Publications*, No. 35. A correction of +0·2 has been applied to the magnitudes of *Groningen Publications*, No. 35, fainter than 9·5 in order to reduce them from the scale of *Harvard Annals*, **71**, No. 3, to the international photographic scale of *Harvard Bulletin* 781. The magnitudes of *Groningen Publications*, No 35, brighter than 9·5 are on the scale of the Göttingen Aktinometrie, which, according to an unpublished paper by Seares, does not differ more than $0^{m}.1$ from the international photographic scale. The correction has been neglected.

The groups between the apparent photographic magnitudes 12 and 14 are not complete, the plates 3, 5 and 6 of Table VI having a limiting magnitude of completeness brighter than 14. Probably only a small fraction of the stars between the magnitudes 12 and 14 is missing. This can be shown by forming the ratio :

$$\frac{\text{Number of group-members } m = 10 \text{ to } 12 \text{ on area } 60' \text{ from the centres of the plates 1 to 6 of Table VI}}{\text{Number of group-members } m = 10 \text{ to } 12 \text{ on area } 60' \text{ from the centres of plates 1, 2 and 4 of Table VI}}$$

This ratio amounts to 2. If this value also holds for the fainter stars the number of group-members $m = 12$ to 14 on all plates ought to be twice the numbers on the plates 1, 2 and 4—*i.e.* 6, whereas the actually counted number 7 is even larger. This shows that only few stars $m = 12$ to 14 are missing. The group $m = 14$ to 15 is incomplete.

The sum of the numbers for all spectral classes are in the column "Sum" of Table IX. The logarithms of these sums have been compared with the logarithms of the number of stars per cubic parsec near the Sun according to *Groningen Publications*, No. 38, table lxxi. It appears from the last column of the table that the frequency of the absolutely faint stars as compared with that of the bright ones is larger in the neighbourhood of the Sun than in the Hyades cluster. The same holds for other clusters.*

* See, for instance, *Groningen Publications*, No. 41, p. 34, 1927.

J. H. Reynolds, Photometric Measures of the Nebula N.G.C. 205.

PHOTOMETRIC MEASURES OF THE NEBULA N.G.C. 205.

J. H. Reynolds.

The photometry of extra-galactic nebulæ has received a good deal of attention in recent years in America, principally from the point of view of the integrated magnitudes, visual and stellar. The photometric curves of individual nebulæ have not received so much notice, but in *Mt. Wilson Cont.* 398 (1930) Hubble made a special investigation of the distribution of light intensity in the elliptical nebulæ and arrived at the formula $\log I = \log I_0 - 2 \log \left(\frac{r}{M} + 1 \right)$, which represented the distribution in average nebulæ of this class.

The distribution of intensity in the spiral class has been the subject of papers by the writer in *M.N.*, **74**, 132, 1913, and **80**, 746, 1920.

The elliptical nebulæ, besides being the most numerous, are now recognised to be of much smaller dimensions than the spirals, and resemble the amorphous nuclear regions of types of spirals where condensations near the nucleus are absent. Only in one instance have stars been photographed in elliptical nebulæ (N.G.C. 4866), and their distances are subject to considerable uncertainty compared with the spirals and the irregular nebulæ. The two to which the most reliable distances can be assigned are N.G.C. 205 and 221, both quite close to the Andromeda Nebula (N.G.C. 224). The former of these in general form and light distribution seems to be a good example of the class and, as undoubtedly the nearest, has been taken as the subject of the present paper.

The negatives were obtained at the Helwân Observatory with the 30-inch Reflector by Dr. Madwar in 1932 December, the exposures being 15 minutes and 30 minutes respectively. By the kindness of Professor Stratton and Mr. Stoy the negatives were put through the recording photometer of the Cambridge Solar Physics Observatory, and the resulting tracings are the basis of the diagrams given in figs. 1 and 2.

The calibration was made by means of a tube photometer. In the form adopted the ratios of densities to light intensities are found by a series of small holes in a brass plate, the diameters of which are graduated to give small illuminated areas ranging approximately in intensities from one to ten at the other end of the tubes. The plate to be exposed on the nebulæ is first exposed in the tube photometer, to an evenly illuminated surface, giving on development five small discs above and below the central part of the plate. In the telescope the calibration discs already exposed are screened off, so that on development the images of the nebulæ and the exposed field do not overlap.

The distribution of light intensity as shown by the curves is different from the impression got from a visual inspection of the negative under

magnification. The great concentration of density at the centre seems to the eye almost like a photographic star disc, but the curves prove that the intensity gradient is continued right up to a sharp peak. This is very similar in form to the curve found in the case of the nucleus of the Andromeda Nebulæ.*

Even with only 30 minutes' exposure the diameter of N.G.C. 205 is appreciably greater in the tracings than that given in L.O. XIII, being 12′. The same increase in diameter over visual inspection of the negative was given by the tracings of N.G.C. 3115 by Carroll in *M.N.*, **91**, 199, 1930.

The region of N.G.C. 205 was found by Hubble to contain eight of the indeterminate nebulous spots which he has provisionally identified with globular clusters in connection with M31. If this identification is a correct one, the clusters must be of considerably less absolute magnitude than the clusters connected with the Galaxy, and the distribution is very different as they extend in areas far beyond the photographic image of M31, whereas the galactic clusters are concentrated on each side of the central regions of the Galaxy.

The intense building up of light in the centre of N.G.C. 205 cannot satisfactorily be explained by a concentration of stars, although the spectrum is of the F type. Stars from the 17th to 20th magnitude are very numerous in M31 and M33, but there are no stars visible in N.G.C. 205, which is at approximately the same distance, although there are many field stars in this region of the sky, presumably galactic. It is, however, useful to compare the curve with the frequency curve of star distribution in the globular clusters.

In *Mt. Wilson Cont.* 129 (1917) Pease and Shapley deal with this subject for 12 clusters and give a diagram of the frequency curves of M12 and M13. For comparison with intensity distribution in N.G.C. 205 the curve of M13 is included in fig. 1. The general form is strikingly similar and that of the nebula is a near approach to the curve of inverse squares. The peak of the intensity curve of N.G.C. 205 terminates in a well-defined point, but in the case of the globular clusters the height of the centre is impossible to determine with accuracy owing to the "burning out" of the central regions in the photographs. Short exposures only bring out the brighter stars, while the fainter stars are so numerous that the light of the central area is massed together in longer exposures.

An interesting question arises as to the optical effect of a quasi-stellar central point such as is shown to exist in N.G.C. 205. If this central point were small enough in angular size to be regarded as a point source, its relative brightness would vary with distance in accordance with the inverse square law, while the surrounding nebulosity would remain of the same surface brightness with a diameter varying inversely with the distance. It seems possible that the effect of increasing distance would be to flatten out the central portion of the photometric curve. The point also arises whether the same photometric curve would be obtained with instruments varying in aperture and focal ratio.

* *M.N.*, 74, 132, 1913.

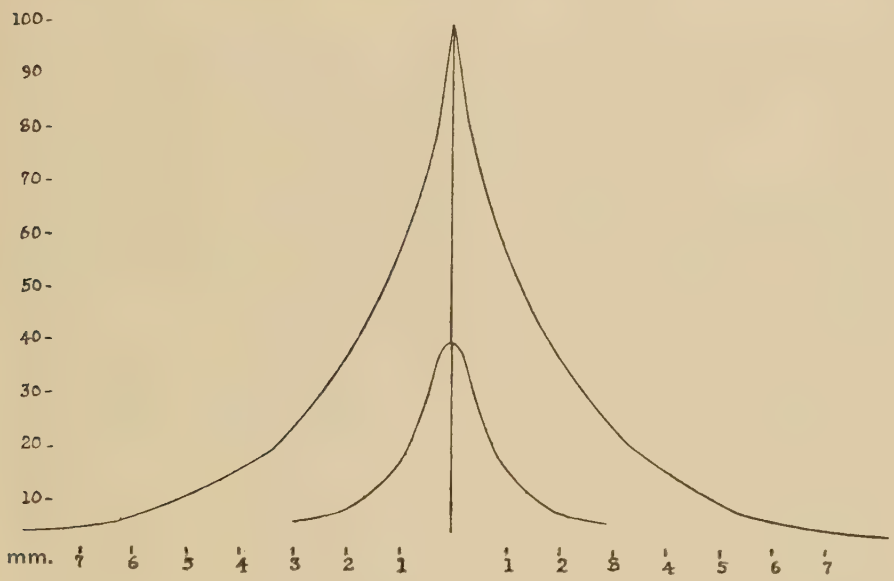

FIG. 1.—*N.G.C.* 205, *Plate* 2084, *No.* 10. 30 *min. exposure. Helwân Observatory*, 1932 *December.*

*Inner curve represents frequency counts of stars in globular cluster M*13 (*Shapley*).

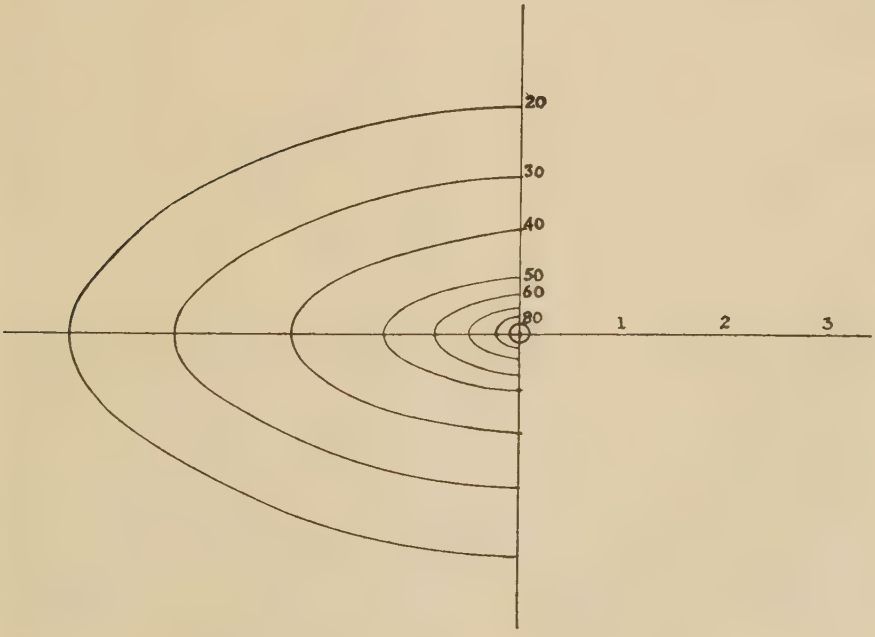

FIG. 2.—*Photometric Contours of the Nebula N.G.C.* 205.

NOTE CONCERNING MILBURN'S NEBULA.

B. Vorontsov-Velyaminov

Concerning the discussion published recently in *M.N.* on the planetary nebula observed by Mr. Milburn * the following information can be given.

The said planetary nebula is listed in my "General Catalogue of Planetary Nebulæ" † among other twenty-four objects not contained in N.G.C. The following data concerning this nebula are given there :—

R.A. $21^h\ 29^m{\cdot}1$, Dec. $+39°\ 11'$ (1900·0), l 54°, b $-9°{\cdot}8$; Class I (stellar); 5″ in diameter; integrated photographic magnitude, based on the international system of magnitudes, $12^m{\cdot}7$. The mean surface brightness is $7^m{\cdot}3$ per circle of diameter 1′. Observed radial velocity +9·8 km./sec.; peculiar radial velocity +35·8 km./sec.

This nebula was listed in the "Catalogue of Integrated Photographic Magnitudes of Planetary Nebulæ" ‡ compiled by the writer in collaboration with Dr. P. Parenago on the basis of our original measures, and it is listed in Dr. Moore's General Catalogue of Radial Velocities.§ The observed radial velocity quoted above is taken from Dr. Moore's measures.‖

The nebula was discovered on October 11 of 1920 by Humason ¶ at Mount Wilson, who estimated its magnitude to be 12·5 and its shape as nearly circular.

ON THE HYPOTHESIS OF THE RADIAL EJECTION OF HIGH-SPEED ATOMS FOR THE WOLF-RAYET STARS AND THE NOVÆ.

S. Chandrasekhar, Ph.D.

§ 1. *Introduction.*—In all recent discussions concerning the nature of the Wolf-Rayet emission a description of the observed phenomena has been attempted on the basis of a hypothesis which postulates a continual ejection of high-speed atoms by the parent star. These atoms, which are supposed to be ejected radially, are assumed to have maximum velocities ranging from 500–3000 km./sec. in the different stars. Further, it is assumed that these ejected atoms form an extensive envelope and that the broad emission bands which are characteristic of the Wolf-Rayet spectra (and also of the Novæ Spectra in their later stages of development) originate here. Though this hypothesis has been discussed in a general way by a number of investigators, and particularly Beals, yet so far no very serious attempt has been made to

* *M.N.*, **94**, 229–230, 1934.
† *Russ. A.J.*, **11**, No. 1, p. 40, 1934.
‡ *Ibid.*, **8**, Nos. 3–4, p. 207, 1931.
§ *Publ. Lick Obs.*, **18**, 1932.
‖ *Publ. A.S.P.*, **37**, 225, 1925.
¶ *Ibid.*, **33**, 175, 1921.

deduce all the consequences of the underlying hypothesis. But to find out whether this hypothesis is at all an appropriate one for the Wolf-Rayet stars we should really develop a dynamical theory of ejection and from the deduced velocity and density variations with the distance r derive the contours of the emission bands for comparison with observation. A dynamical theory of the ejection process itself is necessary only in so far as we require the emission per unit volume and the radial velocity as functions of r, and consequently even without any underlying dynamical theory we can formally examine the type of band contours that could be expected from assumed hypothetical laws of velocity variation, and from a comparison with the observed contours infer something about the actual conditions obtaining in the stellar atmospheres where such emission bands originate. Thus, as was first pointed out by Beals, an atmosphere consisting of atoms moving out radially with uniform velocities from a parent star of relatively small dimensions should produce a flat-topped contour with discontinuously dropping sides, and Beals argues from this that the existence even of a single flat-topped contour would support the hypothesis of the radial ejection of atoms. This question of the contours of emission bands has recently been discussed in some detail by Professor Gerasimovič * in a paper of great interest. Gerasimovič finds, for instance, that in Nova Aquilæ four days after the maximum the hydrogen shell should have been moving with a velocity varying as $r^{-1/4}$.† (We give a different interpretation of Gerasimovič's result in § 6.)

Now the hypothesis of the radial ejection of atoms is a very stringent one —very stringent in the sense that we cannot make this hypothesis and make others as well—and as this does not appear to be generally recognized, we shall attempt to develop some of the consequences of the underlying hypothesis, starting with a discussion of the dynamics of the ejection process itself.

§ 2. *The Possible Ways in which the Radial Ejection of Atoms could take Place.*—If one postulates that the parent star is continually ejecting atoms then from a dynamical point of view there are not many possibilities of the ways in which this could happen. The ejection process could, in fact, take place in one of two ways:—

(A) At the boundary of the star the atoms (presumably only those with a relatively small but finite outward velocities) are "repelled" by some kind of force which is, say, f times the gravitational attraction. Unless f is very nearly unity we could reasonably assume that f is a constant, *i.e.* the repulsive force—whatever its nature—falls off like gravity inversely as the square of the distance.

As we shall show in the sequel this hypothesis includes, as a special case, the emission of particles arising from unbalanced radiation pressure, which possibility was first pointed out by Milne ‡ in a well-known paper.

(B) The atom at the boundary of a star might receive a large initial

* *Zeits. für Astrophysik*, **7**, 335, 1933.

† Actually Gerasimovič gives $r^{-1/2}$, but this is due to a slight numerical error. His value of α is (1/3·83) and not (1/2·17) as he gives.

‡ *M.N.*, **86**, 459, 1926.

outward velocity (either in a single process or in stages), and in escaping from the star be continually de-accelerated in the gravitational field of the star, the atom either escaping from the star with a finite outward velocity, or after ascending a certain distance begin to fall back towards the parent star. We could have an atmosphere of high-speed particles set up in this way.

This underlying mechanism for the ejection process includes the "explosion hypothesis," which (even in its extreme form) appears to be favoured by some investigators.* It has a definite resemblance, for instance, with a point of view recently advocated by Zanstra † in a rather different connection. But a much more satisfactory explanation of an ejection process of this character is, as was kindly pointed out to the writer by Professor H. H. Plaskett, that as the Wolf-Rayet stars (and the Novæ stars after the initial outburst) are rich in ultra-violet light, the atoms near the boundary would receive large outward momenta in the process of getting ionized—the emission lines themselves originating from a recombination process, as in Zanstra's theory of nebular luminosity. Indeed, as Professor Plaskett points out, this kind of mechanism is the simplest one that can underlie a theory which postulates a radial ejection of atoms and also applies Zanstra's method to determine the temperature of the parent star. However, from a consideration of the high-lying metastable states, Plaskett concludes that both the mechanisms A and B might be of importance in discussing the nature of the Wolf-Rayet emission if the radial ejection hypothesis should finally prove satisfactory.

The main point is that both the mechanisms A and B for the ejection process lead to perfectly definite predictions for the types of emission band contours that should be obtained, and the comparison of these predicted contours with the observed ones should settle the tenability or otherwise of the radial ejection hypothesis.

Before proceeding to the calculations one point of general interest might be mentioned. In all the recent discussions (including Gerasimovič's) the occultation effect has been tacitly neglected, but we shall see that, as a consequence of this effect, very essential asymmetries in the band contours are produced. The reason is that any dynamical theory for the ejection of the atoms would not provide stellar atmospheres so extensive as to justify our regarding the parent star as of "negligible" dimensions.

I. *The Contours of Emission Bands on the Mechanism A for the Ejection Process*

§ 3. By hypothesis, an atom at a distance r from the centre experiences an outward acceleration specified by

$$\frac{d^2r}{dt^2} = (f-1)g\frac{a^2}{r^2}, \tag{1}$$

where a is the radius of the star and g the value of gravity at the boundary. From (1) it follows that

* *Cf.* J. Genard, *M.N.*, **92**, 400, 1932. † H. Zanstra, *M.N.*, **93**, 131, 1932.

$$\left(\frac{dr}{dt}\right)^2 = \text{constant} - 2(f-1)g\frac{a^2}{r}. \tag{2}$$

We now assume that the atom starts with a zero velocity at the boundary of the star. This is admittedly an approximation, but since the atom later acquires large macroscopic velocities of the order of 1000 km./sec. we can reasonably neglect the small initial velocities the atoms might possess. From (2) we then have

$$\frac{dr}{dt} = \sqrt{2(f-1)ag\left(1-\frac{a}{r}\right)}. \tag{3}$$

The limiting velocity with which the atom finally leaves the star is

$$v_\infty = \sqrt{2(f-1)ag}. \tag{3'}$$

We can therefore rewrite (3) in the form

$$v = \sqrt{1-r^{-1}}, \tag{4}$$

where we now measure the distances and velocities in scales where the radius of the star and the final limiting velocity v_∞ are respectively units. We shall adopt this convention consistently in Part I of this paper.

§ 4. Now, in Milne's original theory of the emission of high-speed particles the atom is at first supposed to be in equilibrium with the flux of the emergent radiation corresponding to the residual intensity in the absorption line, and an accidental outward velocity (large in this connection, but negligible in comparison with the velocity it subsequently acquires) will make it absorb in the wing of the line, where since it is now exposed to a greater flux of radiation it begins to be accelerated till it finally "climbs" out of the absorption line, being accelerated all the time and ending with a large limiting velocity. It is, however, clear that unless the width of the absorption line is unduly large the atom would have the same limiting velocity as specified by (3'), provided we substitute for f the value

$$f = I_1/I_0, \tag{5}$$

where I_1 is the intensity of the emergent radiation adjacent to the line and I_0 the residual intensity in the line. We verify that with this value of f in (3') we have recovered Milne's original result. But since Milne assumed that I_1 was constant outside the line it would appear that this restriction is necessary for our result to be valid. It can, however, be proved that for the expulsion of atoms by selective radiation pressure the result (4) is valid provided (i) f at (or near) the boundary of the star differs from unity, (ii) the maximum velocity acquired is such that $vf/(f-1)c$ (c = velocity of light) is small compared with unity, and (iii) the initial velocity is very small relative to the order of the velocity it subsequently acquires.

§ 5. We therefore proceed to calculate the emission band contours for the velocity law specified by (4). Write for the radial velocity u:

$$u = \sqrt{1-r^{-1}}\cos\theta = v\cos\theta. \tag{6}$$

We have to calculate then the intensity in the emission band $i(u)du$ for a frequency interval $d\nu$ corresponding to a velocity interval du where

$$d\nu = \frac{\nu_0 du}{c}. \tag{6'}$$

In (6') ν_0 is the frequency of the line emitted by an atom stationary with respect to the observer.

Let $i(r)$ be the emission per unit volume which clearly is a function only of r. Then

$$i(u)du = 2\pi \iint i(r) r^2 \sin\theta dr d\theta, \tag{7}$$

$$(u = \text{constant}),$$

the integration being carried out over such volume elements that u lies between the interval u, $u+du$ (*i.e.*) along the curves of constant u (see fig. 1).

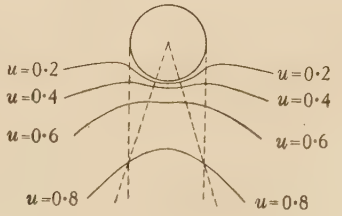

FIG. 1.—*Curves of Constant u.*

Then

$$i(u) = 2\pi \int_{\theta_1}^{\theta_2} \left[i(r) r^2 \frac{\partial r}{\partial u} \right] \sin\theta d\theta, \tag{8}$$

where the quantity in the brackets [ ] has to be expressed in terms of θ only by eliminating r by (6), and θ_1 and θ_2 are the appropriate limits. The question of the limits is a rather delicate matter, and we shall consider this in due course. By (6) we can rewrite (8) as

$$i(u) = \frac{4\pi}{u} \int_{\theta_1}^{\theta_2} \left[i(r) r^4 \left(1 - \frac{1}{r} \right) \right] \sin\theta d\theta. \tag{9}$$

To evaluate the integral we need $i(r)$ explicitly. Now, in a steady state the law (4) corresponds to a density law

$$\rho \propto \frac{1}{r^2 \sqrt{1 - r^{-1}}}. \tag{10}$$

The singularity at $r = 1$ arises on account of the approximation that the velocity is zero at $r = 1$. Actually, however, v, though small compared with unity, must be finite. We now assume that

$$i(r) \propto \rho^2 v^8, \tag{11}$$

v being specified by (4). Gerasimovič, in his paper already referred to, assumes the law $i(r) \propto \rho^2$, but this law does not appreciably differ from (11)

for large values of r. The law (11) is perhaps not so artificial as it looks,* but there can be no harm at any rate in formally investigating the consequences which happen to be of some interest. By (11) we then have (on a suitable scale)

$$i(r) = r^{-4} v^{\beta-2}. \tag{12}$$ †

Introducing (12) in (9) and eliminating r we have

$$i(u) = 4\pi u^{\beta-1} \int_{\theta_1}^{\theta_2} \sin\theta \sec^{\beta}\theta d\theta, \tag{13}$$

or

$$i(u) = \begin{cases} \dfrac{4\pi}{\beta-1} u^{\beta-1} \left[\sec^{\beta-1}\theta \right]_{\theta 1}^{\theta_2}, & \beta \neq 1, \\ 4\pi \left[\log \sec\theta \right]_{\theta_1}^{\theta_2}, & \beta = 1. \end{cases} \tag{14}$$

§ 6. *The Band Contour on the Violet Side of the Normal Frequency* ν_0.—We now need to consider only the curves of constant u in the hemisphere presented to the observer. Let $r = r_1 (\geqslant 1)$ be the inner boundary of the envelope responsible for the emission bands. At $r = r_1$,

$$v = \sqrt{1 - r_1^{-1}} = v_1 \text{ (say)}. \tag{15}$$

Now if $u \leqslant v_1$, obviously

$$\cos^{-1} u/v_1 \leqslant \theta \leqslant \cos^{-1} u, \tag{16}$$

which specifies the limits. By (14) then

$$i(u) = \begin{cases} \dfrac{4\pi}{\beta-1}(1 - v_1^{\beta-1}), & \beta \neq 1, \\ -4\pi \log v_1, & \beta = 1. \end{cases} \tag{17}$$

On the other hand, if $u > v_1$ then the limits are

$$\theta_2 = \cos^{-1} u, \qquad \theta_1 = 0. \tag{18}$$

By (14) now

$$i(u) = \begin{cases} \dfrac{4\pi}{\beta-1}(1 - u^{\beta-1}), & \beta \neq 1, \\ -4\pi \log u, & \beta = 1. \end{cases} \tag{19}$$

At $u = v_1$, (19) gives $i(u)$ identical with (17). Hence on the violet part of the band (by which we shall mean the part of the band to the violet of the

* Professor H. H. Plaskett has suggested to the writer that the law (11) could perhaps be justified physically by supposing that the mechanism of support was by resonance lines in the violet of the ionized atom, the visual luminosity arising from the recombination of the ionized atom and the free electrons giving neutral lines with an intensity distribution roughly as the density squared.

† If $\beta \geqslant 2$ there is no singularity for $i(r)$ at $r = 1$.

normal frequency ν_0) $i(u)$ is constant for $u \leqslant v_1$, and for $1 \geqslant u > v_1$ we have a sloping side. On a certain arbitrary scale of intensities we can write for the sloping sides

$$i(u) = \begin{cases} (1 - u^{\beta-1}), & \beta > 1, \\ -\log u, & \beta = 1, \\ (u^{\beta-1} - 1), & \beta < 1. \end{cases} \tag{20}$$

If $v_1 = 1$ then (20) defines the contour on the violet side for all values of u. We have then "peaked" or "rounded" types of contours.

It is remarkable that the families of contours predicted on this model are identical with the families obtained by Gerasimovič (*loc. cit.*) on the basis of quite different laws for velocity variation.

In particular, Gerasimovič found that for Nova Aquilæ four days after the maximum the contour could be approximately represented by

$$i(u) = 1 - u. \tag{21}*$$

By (20) this means on our model that $\beta = 2$. Thus to explain a contour of this character we have the possibilities :

	v	$i(r) \propto$
Gerasimovič .	$r^{-1/4}$	$\rho^2 \propto r^{-7/2}$
Mechanism (A)	$\sqrt{1 - r^{-1}}$	$\rho^2 v^2 \propto r^{-4}$

From a physical point of view there is clearly nothing to choose between the two laws for $i(r)$, but if the expulsion of atoms did take place by an unbalanced radiation pressure (as was first suggested by Milne) then the second possibility is to be preferred.

§ 7. *The Band Contour on the Red Side of the Normal Frequency ν_0. The Occultation Effect.*—Now, the emission in a region to the red of the undisplaced frequency ν_0 is contributed by the hemisphere on the antipodal side of the star. First we will consider, for the sake of simplicity, the case where the shell begins from $r = 1$. The problem is to find the appropriate limits of θ for a given value of u (*i.e.* at a frequency displaced by an amount $u\nu_0/c$ to the red of ν_0) for substitution in (14). Because of the occultation effect we are concerned only with those parts of the curves $u = \text{constant}$ which are to the right of the tangent at $\theta = \pi/2$ (see fig. 1). The upper limit of θ is clearly the same as before :

$$\theta_2 = \cos^{-1} u,$$

and the lower limit is determined by the intersection of the tangent at $\theta = \pi/2$ with the curve $u = \text{constant}$. At the point of intersection

* *Note added April* 29.—Professor Gerasimovič has kindly pointed out to the writer that the equation (21) for the contour should be regarded as only tentative, and that on the law $u = r^\alpha \cos\theta$ the observations can be taken as merely indicating a negative value for the exponent α.

$$\cos\theta = \frac{\sqrt{r^2-1}}{r} = \frac{u}{\sqrt{1-r^{-1}}}, \tag{22}$$

or

$$u = \left(1-\frac{1}{r}\right)\sqrt{1+\frac{1}{r}}. \tag{23}$$

For a given value of u we have to solve (23) for r. If we denote the solution by r_u then

$$\cos\theta_u = \sqrt{1-\frac{1}{r_u^2}}. \tag{24}$$

By (14) then

$$i(u) = \begin{cases} \dfrac{4\pi}{\beta-1}(1-u^{\beta-1}\sec^{\beta-1}\theta_u), & \beta \neq 1, \\ -4\pi \log u \sec\theta_u, & \beta = 1, \end{cases} \tag{25}$$

or by (22)

$$i(u) = \begin{cases} \dfrac{4\pi}{\beta-1}\left[1-(1-r_u^{-1})^{\frac{\beta-1}{2}}\right], & \beta \neq 1, \\ -2\pi \log(1-r_u^{-1}), & \beta = 1. \end{cases} \tag{25'}$$

A more convenient method of constructing the line contours is to calculate u from (23) for different values of r and tabulate $u \sec\theta_u (= \sqrt{1-r^{-1}})$ against u. Knowing the corresponding values of u and $u\sec\theta_u$ we can now calculate $i(u)$ for different values of u by (25).

In Table I some pairs of values of u, $u\sec\theta_u$ are given (the last column refers to the following section).

TABLE I

r	u, (v_2)	$u\sec\theta_u$, (v_1)	v_2/v_1
1·0	0·0	0·0	0·0
1·1	0·126	0·302	0·417
1·2	·226	·408	·553
1·25	·268	·447	·600
1·5	·430	·578	·745
2	·612	·707	·866
3	·770	·816	·942
4	·839	·866	·968
5	·876	·894	·977
6	·900	·913	·986
∞	1·	1·	1·

Using the results of Table I, the band contours for $\beta = 2$, 3, 4 were constructed and are illustrated graphically in fig. 2. There is a distinct asymmetry between the violet and the red parts of the contour. In fact,

if $\beta = 2$ the tangent to the line contour on the red side of the band is *vertical* at $u = 0$. The following analytical proof of this may be of interest:

If we write $r = 1 + \epsilon$ and treat ϵ as small then by (23)

$$u = \sqrt{2} \cdot \epsilon\,; \qquad u \sec \theta_u = \sqrt{\epsilon},$$

or

$$u \sec \theta_u = \sqrt{\frac{u}{\sqrt{2}}}, \tag{26}$$

so that while on the violet side of ν_0

$$i(u) \sim (1 - u^{\beta-1}), \qquad (\beta > 1), \tag{27}$$

on the red side we have

$$i(u) \sim \left[1 - (\sqrt{\tfrac{1}{2}} \cdot u)^{\frac{\beta-1}{2}}\right] \quad \text{as} \quad u \to 0. \tag{28}$$

From (28) we deduce that if $\beta = 2$, the tangent to the contour is vertical at $u = 0$. Also, if $\beta = 3$ the tangent to the contour on the red side makes an

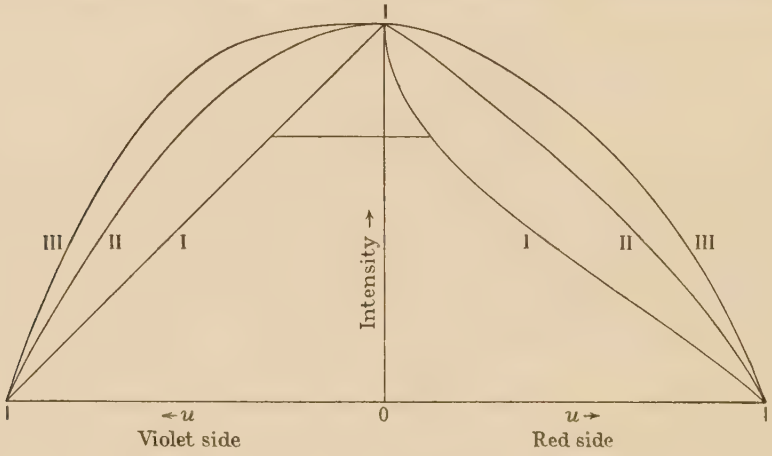

FIG. 2.—*I* $\to \beta = 2$; *II* $\to \beta = 3$; *III* $\to \beta = 4$.

angle $\theta = \tan^{-1}\sqrt{2}\,(= 54^\circ\,45')$ with the vertical. For $\beta > 3$ the tangents to the contour on both sides of ν_0 are horizontal.* In all cases, however, the asymmetry between the violet and the red parts of the contour consists mainly in the violet part being brighter than the corresponding red part. Gerasimovič mentions a case where the observations indicate just this kind of asymmetry, but it will be of interest to know if this asymmetry is of a general kind.

§ 8. *The Band Contour on the Red Side of* ν_0 (*continued*).—We will now consider the case where the shell begins at $r = r_1$. Then, as we have already shown, on the violet side of ν_0, $i(u)$ is constant for $u \leqslant v_1$ where v_1 is defined

* If $\beta > 2$, $i(r)$ defined by (12) takes the value of zero both when $r = 1$ and $r = \infty$. Hence in its *emission properties* the envelope is of the "*planetary-nebula*" type if the contour is of the "rounded type"—this, of course, on the hypothesis that ejection takes place according to mechanism A.

by (15). On the red part of the band there is also a flat part but *not* to an equal extent. For $u < v_1$ the lower limit θ_1 is defined by $\theta_1 = \cos^{-1}(u/v_1)$ or θ_u (as given by equations (22) and (23)), whichever is the *greater*. Clearly, then, if v_2 be such that

$$v_1 = v_2 \sec \theta_{v_2}, \tag{29}$$

then for $u \leqslant v_2$ the contour is flat and has the same intensity as on the violet part of the band. In the last column of Table I the ratio of the extents to which the contour is flat on the red side and on the violet side of ν_0 (when on the violet side it is flat to an extent $v_1/2$ of the *whole* width of the emission band) for different values of v_1 is tabulated. We see that this fraction is always less than unity. It should be finally mentioned that the ratios given in the last column of Table I are a direct consequence of the geometry and the dynamics of the problem, and is *independent* of our assumption regarding $i(r)$. Hence exact measures on line contours by determining this ratio should settle whether the radial ejection process takes place according to mechanism A or not.

II. *The Contours of Emission Bands on the Mechanism B for the Ejection Process*

§ 9. On this mechanism, according to H. H. Plaskett, the atom receives a large momentum mainly in the forward direction and is subsequently de-accelerated. Consistent with this hypothesis we should really allow some (perhaps considerable) spread in velocities, but to start with we shall suppose that all the atoms receive the same outward velocity v_0, at the boundary of the star. Let us now take as our unit of velocity the parabolic velocity of escape specified by

$$V_\infty = \sqrt{2ag}, \tag{30}$$

where, as before, a is the radius of the star and g the value of gravity at the boundary. Measuring, as before, distances in a scale where the radius of the star is unity we easily find that

$$v = \sqrt{v_0^2 + \left(\frac{1}{r} - 1\right)}. \tag{31}$$

From (31) it is clear that we should consider two distinct cases: $v_0 \leqslant 1$ and $v_0 > 1$. If $0 < v_0 < 1$ we can find $r = r_1$ (> 1) such that

$$v_0 = \sqrt{1 - \frac{1}{r_1}}. \tag{32}$$

Then by (31), at $r = r_1$, $v = 0$ and the envelope extends from $r = 1$ to $r = r_1$. On the other hand, if $v_0 \geqslant 1$ the atom goes off to infinity with a limiting velocity

$$v_\infty = \sqrt{v_0^2 - 1}, \tag{33}$$

and the atmosphere extends to infinity. The law (31) defines by the equation of continuity the density law

$$\rho \propto \frac{1}{r^2\sqrt{v_0^2+\left(\frac{1}{r}-1\right)}}. \tag{34}$$

When $v_0 < 1$, then at $r = r_1$ we have a singularity, and to get over this singularity we assume, as before, that (on a certain scale)

$$i(r) = \rho^2 v^\beta. \tag{35}$$

If $v_0 > 1$ the law (35) does not appreciably differ from $i(r) \propto \rho^2$, which law is what we should expect if the emission is due to a recombination process, as in Zanstra's theory. Further, if $v_0 < 1$, then the envelope extends to $r = r_1$ (defined in (32)), and hence $i(r)$ must tend to zero as $r \to r_1$ and a term of the form $v^\beta (\beta > 2)$ is necessary. Proceeding as in Part I we find that

$$i(u) = \begin{cases} \dfrac{4\pi}{\beta-1} u^{\beta-1}\left[\sec^{\beta-1}\theta\right]_{\theta_1}^{\theta_2}, & \beta \neq 1, \\ 4\pi\left[\log\sec\theta\right]_{\theta_1}^{\theta_2}, & \beta = 1. \end{cases} \tag{36}$$

Where θ_1 and θ_2 are the appropriate limits of θ on the curves $u =$ constant. (See fig. 3.)

§ 10. *The Band Contour on the Violet Side of* ν_0.—We have to consider two cases.

Case I ($v_0 \leqslant 1$).—Naturally we are only concerned with values of u less than v_0. The appropriate limits of θ are

$$\theta_2 = \cos^{-1}(u/v_0); \qquad \theta_1 = 0, \tag{37}$$

and by (36)

$$i(u) = \begin{cases} \dfrac{4\pi}{\beta-1}(v_0^{\beta-1} - u^{\beta-1}), & \beta \neq 1, \\ 4\pi \log(v_0/u), & \beta = 1. \end{cases} \tag{38}$$

We have then a peaked or rounded contour on the violet side with an intensity increasing from 0 at $u = v_0$ to a maximum at $u = 0$.

Case II ($v_0 > 1$).—If $u < v_\infty$ (*cf.* equation (33)) then

$$\theta_2 = \cos^{-1}(u/v_0); \qquad \theta_1 = \cos^{-1}(u/v_\infty), \tag{39}$$

and by (36)

$$i(u) = \begin{cases} \dfrac{4\pi}{\beta-1}(v_0^{\beta-1} - v_\infty^{\beta-1}), & \beta \neq 1, \\ 4\pi \log(v_0/v_\infty), & \beta = 1. \end{cases} \tag{40}$$

Hence this part of the contour is flat. On the other hand, if $v_\infty \leqslant u \leqslant v_0$ the limits are the same as (37) and the equation of the contour is specified by (38). Hence to the violet of the normal frequency ν_0 the contours have flat tops and sloping sides which are identical with those obtained on mechanism

A. Here the existence of a flat part means that the atoms receive initial velocities greater than the velocity of escape. If the initial velocity is less than v_0 then the contour is necessarily of a peaked or rounded character.

§ 11. *The Occultation Effect.*—As before, when we are considering the contour on the red side of ν_0 we must take into account the occultation effect, and we shall show presently that this effect produces an asymmetry in the line contour of an entirely different kind than is predicted on mechanism A. Now the main problem is, as before, to find the appropriate parts of the curves of constant u which contribute to the emission. From fig. 3 we see that only curves with u less than a certain critical value have intersections with the tangent at $\theta = \pi/2$, which means that to the red of ν_0 the intensity falls to zero at a frequency corresponding to a value of u less than v_0, at which place the intensity falls to zero on the violet side. This critical value of $u = u_{\text{red}}$ (say) at which the intensity is zero on the red side of ν_0 can be calculated quite easily as follows :—

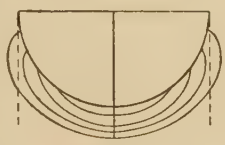

FIG. 3.—*Curves of Constant u* (=0·1, 0·2, 0·3, 0·4) $v_0 = 0{\cdot}5$.

Since at the point of intersection (assuming one exists)

$$\cos\theta = \sqrt{1 - \frac{1}{r^2}} = \frac{u}{\sqrt{(v_0^2 - 1) + \frac{1}{r}}}, \tag{41}$$

we have

$$u = \sqrt{\left(1 - \frac{1}{r^2}\right)\left(v_0^2 - 1 + \frac{1}{r}\right)}, \tag{42}$$

u defined by (42) has a maximum, and this maximum is clearly equal to u_{red}. Now (42) is found to have a maximum when

$$r = (v_0^2 - 1) + \sqrt{(v_0^2 - 1)^2 + 3}. \tag{43}$$

This value of r substituted in (42) gives us u_{red}. Having calculated u_{red} we can compute the ratio of the band widths to the red and to the violet of the normal frequency as a function of v_0. In Table II the results of such calculations are summarised.

Hence, if the ejection process in the Wolf-Rayet stars follows mechanism B then this asymmetry should exist, and we can from a measure of the band contour determine v_0 *in terms of the velocity of escape* (since the ratio of the band widths on the red and on the violet sides of the normal frequency ν_0 is by Table II a function of v_0 expressed in units of the velocity of escape), and knowing also its *absolute value* (determined from the band width on the violet side of ν_0) we can determine an observational value of $\sqrt{ag}$, and if, in addition, we know also the mass of the star, we can deduce the value of g. It has to be emphasised in this connection that the result of Table II is a consequence purely of the geometry and the dynamics of the problem, and is independent of our assumption regarding $i(r)$.

TABLE II

v_0	u_{red}	v_0/u_{red}
0·2	0·0281	0·141
0·4	0·1109	0·277
0·5	0·1712	0·343
0·6	0·2431	0·405
0·8	0·4166	0·521
1·0	0·6206	0·621
1·5	1·188	0·792
2·0	1·755	0·877
2·5	2·302	0·921
3·0	2·833	0·945
4·0	3·875	0·968
5·0	4·901	0·980
∞	∞	1·

Finally, the following approximate solution of (43) when $v_0 < 1$ may be noted. One finds that

$$u_{\text{red}} = \frac{1}{\sqrt{2}} v_0^2 (1 - \tfrac{1}{8} v_0^2) + O(v_0^6), \tag{44}$$

or, since on the violet side of ν_0 the width of the band is v_0, we have for our ratio tabulated in the last column of Table II approximately

$$\frac{u_{\text{red}}}{v_0} = \frac{1}{\sqrt{2}} v_0 (1 - \tfrac{1}{8} v_0^2). \tag{45}$$

This formula reproduces the results of exact calculation remarkably well when $v_0 \leqslant 1$. Thus, when $v_0 = 1$, while (45) gives a value 0·6197, the result of the exact calculation is 0·6206. Of course, when $v_0 > 1$, (45) should not be used.

§ 12. *The Band Contour on the Red Side of* ν_0.—We consider the two cases separately.

Case I ($v_0 \leqslant 1$).—Now, because of the occultation effect only when $u < u_{\text{red}}$ have we a non-zero intensity. It is clear from fig. 3 that the curves of constant $u(< u_{\text{red}})$ intersect the tangent at $\theta = \pi/2$ at two distinct points which correspond to the two roots of the equation (42) for a given value of $u < u_{\text{red}}$. If we denote the corresponding angles by θ_1 and θ_2 we have the required limits for use in (36).

A more convenient method to construct the line contour is to calculate u for different values of r (for a given v_0) and plot u against $u \sec \theta$. From this graph we can directly read off the values of $u \sec \theta_1$ and $u \sec \theta_2$ for any given value of $u(< u_{\text{red}})$. The contour can now be constructed according to (36). Fig. 4 illustrates the calculations for $v_0 = 0{\cdot}8$ and fig. 5 for the case $v_0 = 1{\cdot}0$.

Now observations seem to indicate that almost all the contours of emission bands in Wolf-Rayet stars are of the "peaked" or "rounded"

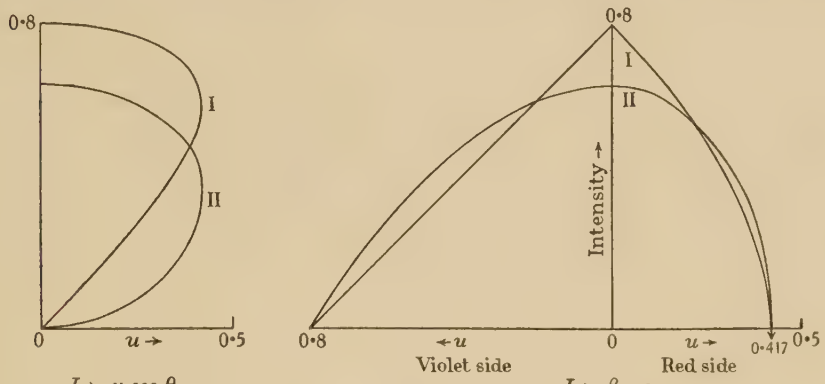

FIG. 4.

types,* and if the ejection process takes place according to mechanism B then careful measures on band contours must reveal asymmetries of the character illustrated in figs. 4 and 5.

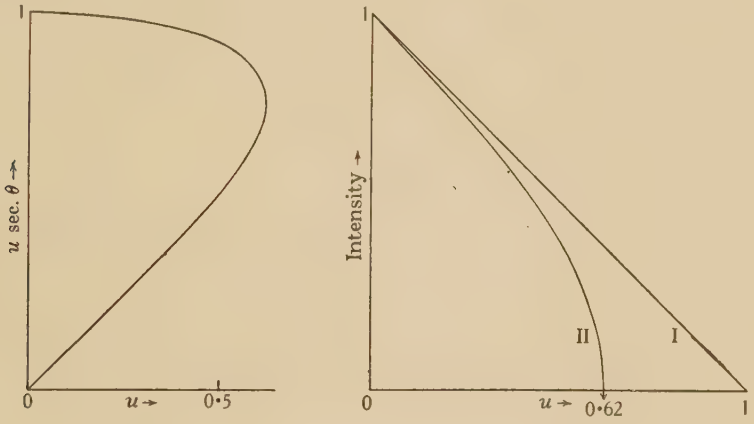

FIG. 5.

Case II ($v_0 > 1$).—On the violet side of ν_0 the contour is flat for $u < v_\infty (= \sqrt{v_0^2 - 1})$ and has a sloping side for $v_0 < u \leqslant v_\infty$. But on the red side the situation is quite different. If $u < v_\infty$ the curves of constant u have just *one* intersection with the tangent at $\theta = \pi/2$, and if we denote the solution by θ_u then the required limits are

$$\theta_2 = \theta_u\,; \qquad \theta_1 = \cos^{-1}(u/v_\infty). \tag{46}$$

* C. S. Beals, *Dominion Astro. Obs. Pub.*, **6**, No. 9 (in press). I am indebted to Professor H. H. Plaskett for the opportunity to see an advance manuscript copy of this paper.

Then

$$i(u)=\begin{cases}\dfrac{4\pi}{\beta-1}\{(u\sec\theta_u)^{\beta-1}-v_\infty{}^{\beta-1}\}, & \beta\neq 1,\\ 4\pi\log(u\sec\theta_u/v_\infty), & \beta=1.\end{cases}\qquad(47)$$

Thus the contour is not flat to the red of ν_0. When $v_\infty\leqslant u\leqslant u_{\text{red}}$ the curves of constant u have two intersections with the tangent at $\theta=\pi/2$, and these specify the limits θ_1 and θ_2 to be used in (36). In practice the contour can be constructed by the method sketched under Case I. In fig. 6 we illustrate the case where $v_0=1\cdot5$ and $\beta=2$. We notice that to the red of ν_0 the part corresponding to the "flat top" on the violet side is of a slightly

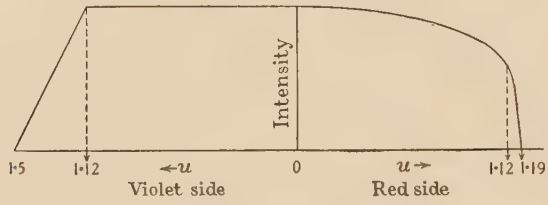

FIG. 6.—$v_0=1\cdot5$; $\beta=2$.

but definitely sloping nature. (When $v_0=1\cdot5$ this sloping is quite appreciable and should be capable of observational verification if the ejection takes place according to mechanism B.) The part corresponding to the sloping side to the violet of ν_0 is very much steeper on the red side. The band is, in fact, wholly unsymmetrical about ν_0.

Finally, the following geometrical properties of the curves (u, $u\sec\theta$) and their consequences might be noted :—

(i) If $v_0\leqslant 1$ the curve passes through the origin, making an angle $\tan^{-1}v_0\sqrt{2-v_0{}^2}$ with the $u\sec\theta$ – axis. Further, the curve also crosses the $u\sec\theta$ – axis at right angles on its "upper branch." Hence for $v_0<1$ the contour is unsymmetrical even about the immediate neighbourhood of $u=0$, and this in addition to the fact that the intensity on the red side falls to zero for a value of $u=u_{\text{red}}$, less that at which it tends to zero on the violet side. If $v_0=1$ the curve passes through the origin, making an angle of 45° with both the axes. Hence in this case the contour is symmetrical about the neighbourhood of $u=0$.

(ii) If $v_0>1$ the curve crosses the u – axis at $u=v_\infty$, making an angle of 45° with it. Also the curve crosses the $u\sec\theta$ – axis at right angles when $u=0$. Hence when $v_0\geqslant 1$ the band contours are symmetrical about the *immediate* neighbourhood of $u=0$.

§ 13. There is one point of importance which has to be mentioned here. In calculating the line contours we have assumed that when $v_0<1$ only those atoms which have an outward radial velocity contribute to the emission. But when $v_0<1$, the atoms after "ascending" to a distance r_1 (see equation (32)) begin to fall back towards the parent star. If these "descending" atoms are equally efficient in contributing to the emission then it is clear that the asymmetry between the red and the violet parts of the band is

removed and that the contour on both sides of v_0 will be represented by summing up the intensities calculated in §§ 10, 12 for the "violet" and the "red" parts of the band separately. But if we assume that the descending atoms are equally efficient in the emission process then it is clear that we no longer have a strict radial ejection hypothesis ; in particular the explanation generally given for the "violet absorption" will not be valid. This, however, is not so important as the fact that when $v_0 < 1$ the density will rise rather steeply near the boundary $r = r_1$, and if the emission arises by some kind of recombination process then the probability is that an atom which has been ejected from the boundary in an ionized state will have recaptured an electron before it begins to fall back towards the parent star. Of course, we must now consider the possibility of an atom getting ionized once again when it would receive an additional outward momentum. This introduces further complications, and it is best to avoid these, in the first instance, by neglecting the emission by the "descending" atoms. It is, however, important to bear these reservations in mind in accepting the conclusions stated in the following section.

§ 14. *Concluding Remarks.*—The observational material is not extensive, but they appear to indicate, firstly, that "the centres of the Wolf-Rayet bands are approximately in their normal positions," * and secondly, that "flat-topped contours are exceptions rather than the rule." †

Now, on the basis of mechanism A, though the maximum intensity occurs at the centre of the band, the band contours are not symmetrical, the asymmetry consisting essentially in the violet part being brighter than the corresponding red part. Further, the contours are of the "peaked" type if $\beta \leqslant 3$, but develop "rounded" tops for $\beta > 3$. Even for $\beta = 4$ (see curve III, fig. 2) the contour has a more or less flat top. It is worthy of note here that if $\beta > 2$ the envelope of the high-speed particles in its emission properties is of the "planetary nebula" type.‡

On the other hand, on the basis of mechanism B a "peaked" or "rounded" contour means that the atoms are ejected with velocities less than or equal to the velocity of escape. Even when $v_0 = 1{\cdot}5$ (*cf.* fig. 6) the contour has a pronounced flat top on the violet side. But when $v_0 \leqslant 1$ the contours are very unsymmetrical. Thus for $v_0 = 1$ the band width on the red side is only 0·6 of the band width on the violet side, and one would expect that observations could easily detect a difference of 40 per cent.

Broadly speaking, then, the band contours on mechanism A show much less asymmetry than the band contours on mechanism B. One could conclude then that the existing observational material is formally more consistent with the ejection process taking place according to mechanism A

* C. S. Beals, *Pub. Dom. Astro. Ob.*, 4, No. 17.

† *Ibid.*, 6, No. 9 (in press).

‡ If we write $\beta = n + 2$ then on a certain scale

$$i(r) = \frac{1}{r^4}\left(1 - \frac{1}{r}\right)^{n/2},$$

from which we deduce that $i(r)$ attains its maximum when $r = (n+8)/8$.

than according to mechanism B. But if the ejection process takes place according to mechanism A then one meets with a number of difficulties. For instance, the limiting velocity must depend on the atom. Actually, however, it appears that there is not much difference between the band widths of the different atoms. There are, in fact, a number of other difficulties, but this is not the place to go into such matters. The purpose of this paper was merely to work out the formal consequences of the radial ejection hypothesis.

I have great pleasure in expressing my thanks to Professor H. H. Plaskett and Dr. Redman for much valuable advice and stimulating discussions.

Trinity College, Cambridge:
1934 *April* 6.

SODIUM AND MAGNESIUM IN STELLAR SPECTRA.

A. D. Thackeray, B.A.

In a previous paper * the results of a spectrophotometric study of some late-type stars photographed with the Huggins 15-inch refractor at Cambridge were discussed. Attention was then confined to the comparison of intensities of lines in an iron multiplet. The present paper deals with the measures of the *D* lines of sodium and the *Mg* "*b*" lines 5183, 5172 from the

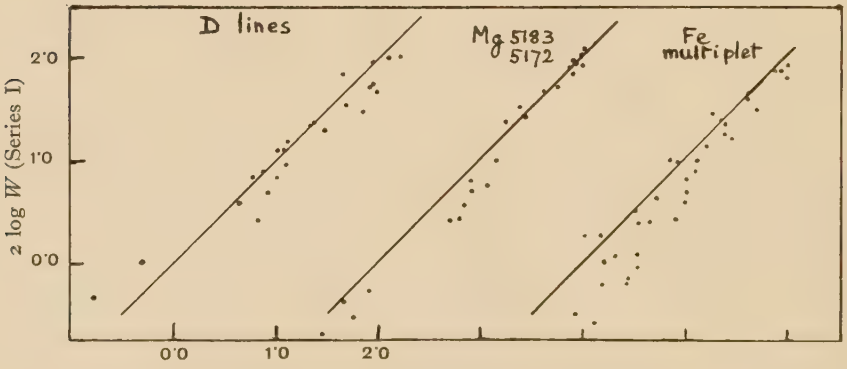

FIG. 1.—*Comparison of Series I and II.*

same series of plates (referred to in future as "Series I"). Meanwhile a valuable second series ("Series II") has been obtained with the Newall 25-inch refractor; these measures lay claim to a higher order of accuracy, since the spectrograph employs four prisms (recently refigured by Hilger to a $\frac{1}{4}$ wave-length), gives higher dispersion (32 A./mm. at 5183), and further has the great advantage of thermostatic control. It was therefore possible to obtain tolerable measures of the lines near their marginal appearance in Ao and B8 stars which had not been practicable in Series I. The

* *M.N.*, 94, 99, 1933.

photometric procedure was the same as before ; Series II, however, was taken almost without exception on Ilford Rapid Process Panchromatic plates, thus greatly reducing the errors due to grain effects.

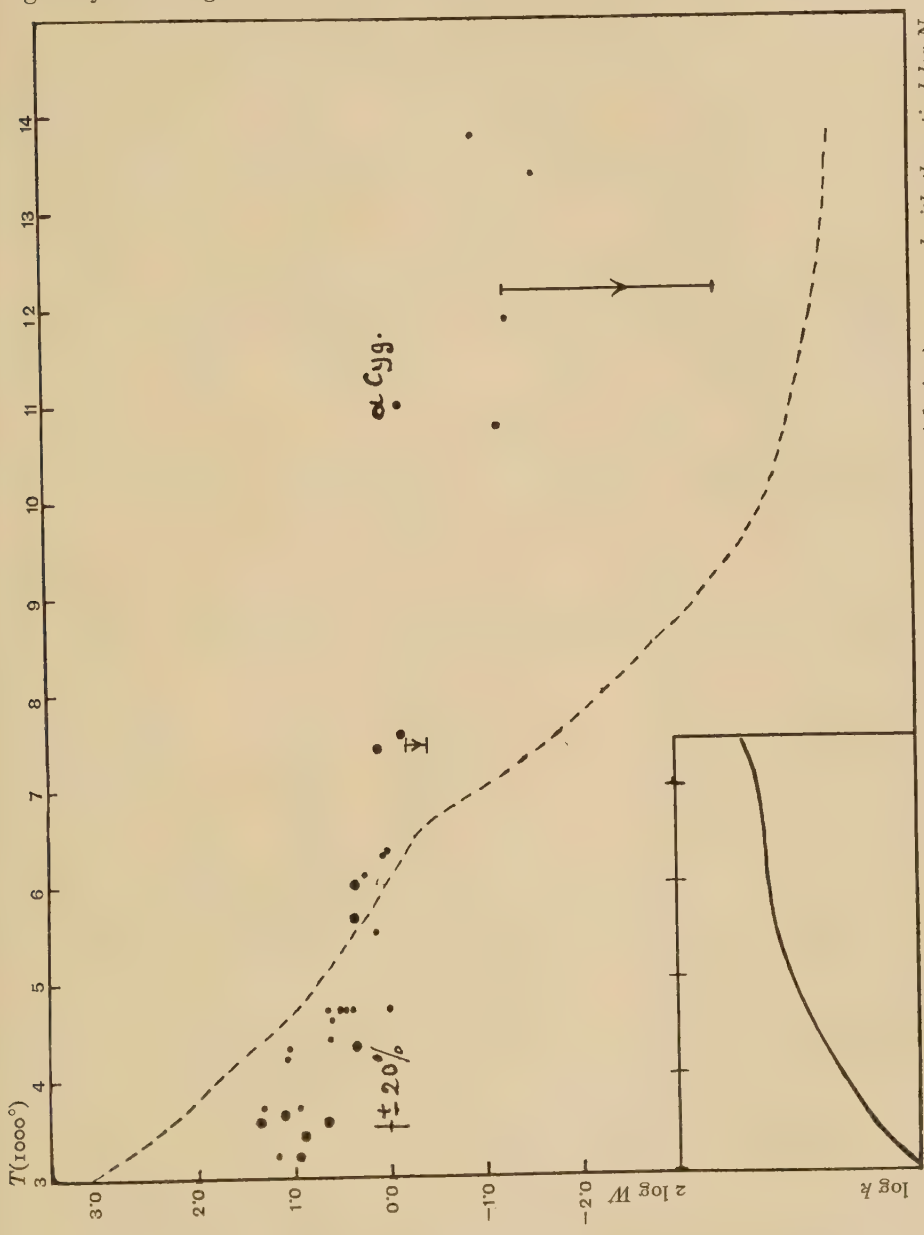

FIG. 2.—*Na* 5890, 5896. 2 log $(D_1 + D_2)$ (*ordinates*) *against temperature* (*abscissæ*), *compared with theoretical log N* (*shown by dotted line*). *Extent of Doppler correction shown thus* ⊦. *Inset—computed log k on same scale.*

Comparison of Series I and II is shown in fig. 1. The scatter is consistent with a probable error of 20 per cent. estimated for Series I. There appear to be systematic errors depending on line-intensity which differ*

* Probably due to an effect of density. In both series the *D* lines were more densely exposed than the 5000 region.

TABLE I

Equivalent Widths (in Angstroms)

(1) Star	(2) T_e	(3) *Na* 5890		(4) *Na* 5896		(5) *Na* 5682	(6) *Na* 5688	(7) *Mg* 5183		(8) *Mg* 5172		(9) *Mg* 5528	(10) 2 log *W* *Na* 5890	(11) 2 log *W'* *Mg* 5183	(12 2 log *W''*
α CMa	13,800	*0·12* :	0·25	*0·05* :	0·19	..	..	*0·13* :	0·16	*0·09* :	0·135	..	$\bar{2}$·63	$\bar{2}$·36	
β Ori	13,400		0·105		·06 :	..	..	..		..		..	$\bar{3}$·97		
α Lyr	11,900	*·18* :	·125	*·12* :	·074	..	..	*·12*	·115	*·08* :	·095	..	$\bar{2}$·27	$\bar{2}$·13	
α Cyg	11,000	*·45*	·50	*·29*	·39	..	..		·08 :		·055 :	..	$\bar{1}$·39	$\bar{3}$·78 :	
α^1 Gem *	10,600		·16		·095	..	..		·075 :		·06 :	..	$\bar{2}$·35	$\bar{3}$·76 :	
ε UMa *	10,200	..		..		..	..		·08 :		·07 :	..	..	$\bar{3}$·84 :	
γ Boo	9,400	*·33* :		*·13* :		..	..	..		..		..	$\bar{2}$·87		
β Cas	8,000		·37		·39	..	..	*·34* :	·47	*·29* :	·40	..	$\bar{1}$·31	$\bar{1}$·29	
α CMi	7,550	*·47*	·43	*·35*	·37	..	..	*·56*	·67	*·45*	·50	0·195	$\bar{1}$·36	$\bar{1}$·60	$\bar{2}$·53
α Per	7,400	*·63*	·61	*·48*	·48	0·10 :	..	*·38*	·49	*·29*	·45	·21	$\bar{1}$·62	$\bar{1}$·34	$\bar{1}$·00
η Boo *	6,380	*·60*		*·45*		..	..	*·90* :		*·59* :		..	$\bar{1}$·58	$\bar{1}$·87	$\bar{1}$·23
α UMi	6,350	*·47*	·57	*·39*	·52	..	..	*·43*	0·61	*·38*	·51	·18	$\bar{1}$·53	$\bar{1}$·54	$\bar{2}$·89
γ Cyg	6,100	*·79*		*·54*		..	..	*0·68*		*0·63*		..	$\bar{1}$·79	$\bar{1}$·72	$\bar{1}$·40
Sky	(6,000)	*·87*	·86	*·63*	·58	·12 :	0·11 :	*1·23*	1·13	*1·04*	·87	..	$\bar{1}$·86	0·17	$\bar{2}$·95
α Aur *	5,630	*·86*	·88	*·69*	·61	·19 :	·12 :	*0·93*	·93	0·86	0·74	·195	$\bar{1}$·88	$\bar{1}$·96	$\bar{1}$·27
ε Leo	(5,200)	*0·64*		*0·51*		..	..	*0·83*		*·66*		..	$\bar{1}$·66	$\bar{1}$·84	
η Dra	5,200	*1·02* :		*0·55* :		..	..	*1·09* :		*0·88* :		..	0·93 :	0·09 :	
μ Her	(5,200)	*1·30* :		*1·00* :		..	..	*1·28*		*1·02*		..	0·26 :	0·22	$\bar{2}$·81
β Dra	4,900	*0·59* :		*0·41* :		..	..	*0·86* :		*0·72* :		..	$\bar{1}$·54 :	0·89 :	
ε Gem	(4,700)	*1·18*		*·93*		..	..	*1·12* :		*1·23* :		..	0·19	0·19	$\bar{1}$·54
α UMa *	4,700	*1·05*		*·65*		..	..	*1·44*		*1·39*		..	0·00	0·38	$\bar{1}$·43
γ^1 Leo	4,700	*1·03*		*·70*		..	..	*1·36*		*1·12*		..	0·02	0·29	$\bar{1}$·37
β Gem	4,610	*1·04*	1·25	*·66*	·84	·21	·18	*1·49*	1·59	*1·30*	1·34	·30	0·12	0·41	$\bar{1}$·50
α Ari	(4,400)	*1·28*		*·82*		..	..	*1·92*		*1·63*		..	0·18	0·59	$\bar{1}$·52
α Boo	4,340	*0·79*	0·98	*0·53*	0·63	·15	·15	*1·86*	1·78	*1·77*	1·59	·35	$\bar{1}$·89	0·56	$\bar{1}$·43
γ^1 And	4,300	*2·03*		*1·29*		..	..	*1·29* :		*0·88* :		..	0·58	0·19 :	$\bar{1}$·81
α Hya	(4,200)	*1·97*		*1·47*		..	..	..		..		..	0·61	..	$\bar{1}$·34
β UMi	3,700	*1·72*	1·70	*1·51*	1·19	·22	·18	*1·73*	1·65	*1·62*	1·52	·36	0·49	0·50	$\bar{1}$·84
γ Dra	3,700	*2·59*		*2·01*		..	..	*0·90*		*0·73* :		..	0·87	$\bar{1}$·96	$\bar{1}$·72
β And	3,630	*1·80*	2·06	*1·30*	1·64	·18	·20	*1·55* :		*1·36* :		·335	0·63	0·41 :	$\bar{1}$·89
α Tau	3,560	*1·84*	2·34	*1·30*	1·68	·22	·24	*1·99*	1·81	*1·66*	1·79	·45	0·88	0·59	$\bar{1}$·90
μ Gem	3,560	*0·87* :	1·11	*0·75*	0·85	·075	·12	..		..		·28	0·17	..	$\bar{1}$·86
α Cet	3,500	*1·45*	1·76 :	*1·41*	1·19	·165	..	*1·26* :		*1·11* :		·255	0·47	0·24 :	$\bar{1}$·48
α Ori	3,400	*1·12*	1·76	*0·97*	1·49	0·25 :	0·29 :	..		..		0·37	0·45	..	2·07
α Sco	(3,400)	*2·04*		*1·74*		..	..	..		..		..	0·70		

* Spectroscopic binaries. Series I (Huggins) in italics.

curiously for the *Na*, *Mg* lines and the iron multiplet which was remeasured in most of the late-type stars in Series II. In the latter case this error is

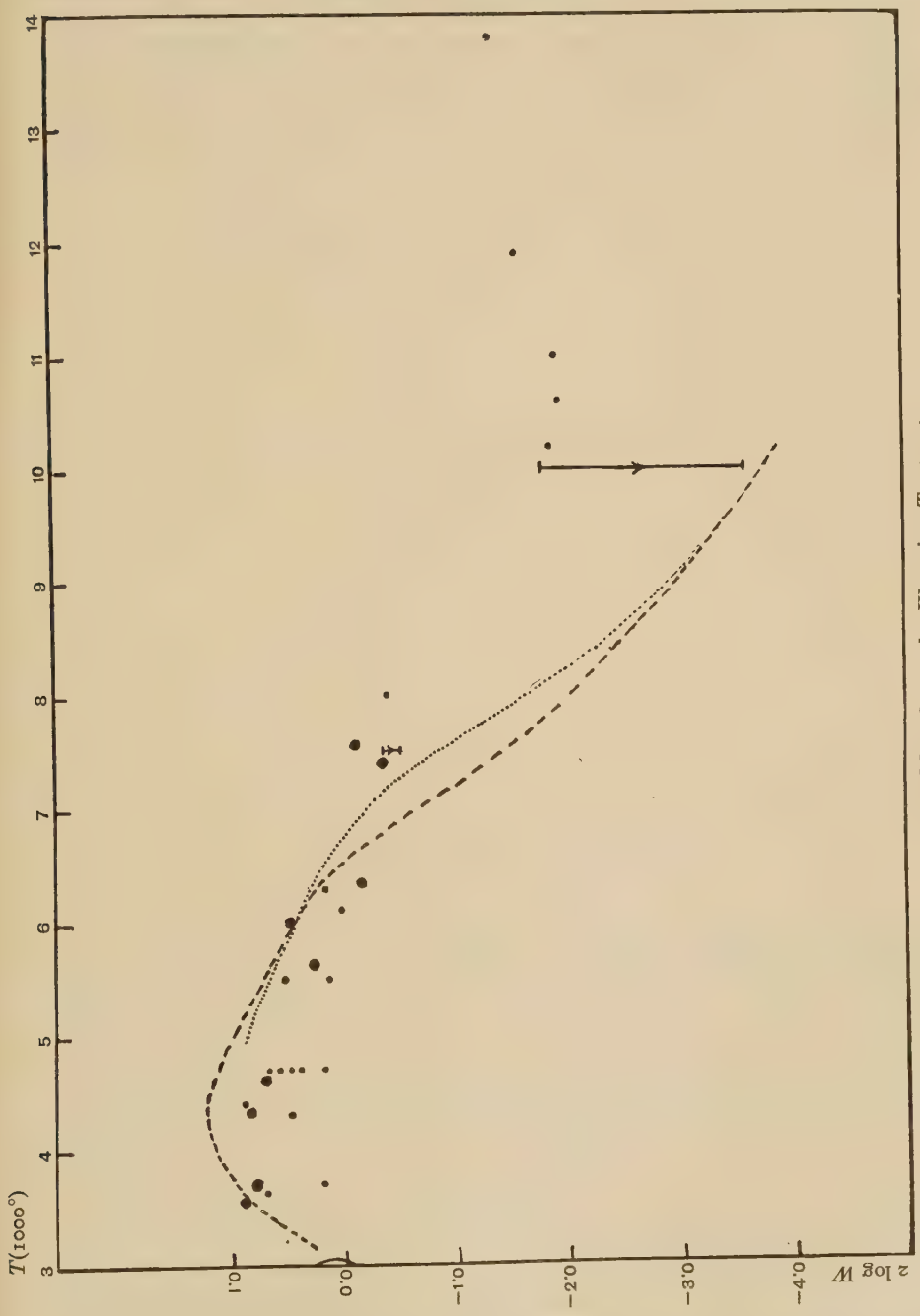

FIG. 3.—*Mg* 5183. 2 *log W against Temperature.*
– – – – *giants* } *computed log N (Russell).*
. . . . . *dwarfs* }
Extent of Doppler correction shown thus ⊥.

(as we should expect) largest for the weakest lines, which appear too weak in Series I, and therefore has the effect of generally *increasing* the multiplet anomalies. The conclusion of the previous paper that the anomalous

behaviour increases in the latest types is unaffected by a systematic error which, as here, increases linearly with line-intensity.

Table I gives measures of equivalent widths W (*i.e.* the breadth in angstroms of a line with rectangular contour and zero central intensity which absorbs the same total amount of light as the observed line). Series I and II are given separately, the first in italics. In Columns (10) and (11) values of 2 log W are given for *Na* 5890 and *Mg* 5183 ; in order to reduce accidental

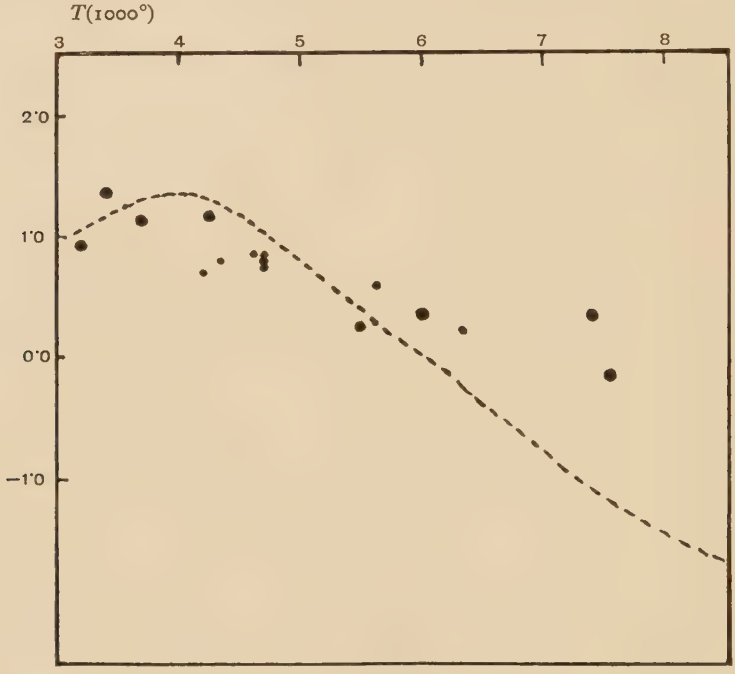

FIG. 4.—*Fe* 5371. 2 *log W against T.*
– – – – *computed log N.*

errors, Columns (3), (4) and (7), (8) were combined to derive these values, assuming the multiplet intensities to be obeyed (2 : 1 for *Na*, 5 : 3 for *Mg*). The two series have been combined where possible, double weight being given to Series II. Subordinate lines of *Na* and *Mg* are also given in Columns (5), (6) and (9). Effective temperatures given in Column (2) are taken from Brill * and Sampson.† Column (12) gives values of 2 log W for *Fe* 5371 derived in a similar way (*i.e.* using theoretical ratios) from the four best lines in the iron multiplet.

In figs. 2, 3 and 4 the values of 2 log W in the last three columns of Table I are plotted against T and compared with the theoretical values of log N, N being the number of atoms in the ground state associated with the line above a given optical depth. The ordinate-zero has been chosen in each case to give agreement for the Sun. The curve for *Mg* 5183 is given by Russell;‡ the other two have been computed by the writer from Russell's

* *Handbuch der Astrophysik*, V/1, p. 151. † *M.N.*, **90**, 636, 1930.
‡ *Ap. J.*, **78**, 290, 1933.

equations, using his computed values of the electron pressure P. Milne's formula * for Problem I gives essentially the same curves for temperatures less than 6000°, above which the ionisation of hydrogen rapidly reduces the extent of the atmosphere.

These figures all agree in indicating that the change of equivalent width with temperature is not so rapid as the change in the number of atoms producing a line predicted by theory. For *Na* the observed width is too small by a factor of ten at 3000° and too large by a factor of fifty at 10,000°. It looks as if there must be some process at work causing a given number of atoms above constant optical depth to be less effective in producing absorption lines at low than at high temperatures.

(a) *Doppler Broadening.*—One such process is the broadening due to thermal agitation of the atoms, which of course increases with the temperature. This probably explains why the *Na* and *Mg* lines are visible at all in the Ao stars, for it appears that 90 per cent. of the observed width of such weak lines at temperatures of 10,000° are due to Doppler broadening. For estimating the correction, the approximate formula for the modified line-absorption coefficient κ' given by Minnaert † was used :

$$\kappa' = \frac{2\sqrt{\pi}e^2Nf}{\omega bm}\left\{\frac{\sqrt{\pi}}{4}\frac{b\omega'}{\mu^2} + \frac{\pi}{2}e^{-\mu^2/b^2}\right\}, \qquad (1)$$

where

$$b = \frac{2\pi\nu_0}{c}\sqrt{\frac{2RT}{M}}, \quad \mu = 2\pi\Delta\nu, \quad \omega = 2\pi\nu, \quad \omega' = \text{damping constant},$$

$$N = \text{number of atoms per c.c.}, \qquad f = \text{oscillation factor.}$$

In this approximation the first term is that part due to radiation damping and falls off as the inverse square of the distance μ from the line-centre ; the second term due to thermal agitation is of exponential form and is negligible compared with the first term for large and small μ. But intermediately this term becomes predominant and may increase the total absorption considerably. The modified coefficient κ' is always greater than the unmodified coefficient, κ, for thermal motion of the atoms always increases the chance of absorption off the line-centre without decreasing absorption at the line-centre.

Calculations of κ' and κ were made for various $\Delta\nu$ (having chosen the appropriate T, ν_0 and atomic mass M) ; the ratio η of line to continuous absorption is proportional to κ, whence using Eddington's ‡ approximate formula

$$r = \frac{1 + \frac{2}{3}q}{1 + \eta + \frac{2}{3}q}, \qquad (2)$$

the broadened and unmodified contours could be calculated and the corresponding widths W', W derived.

* *M.N.*, **92**, 156, 1931, equation (23).

† *Zeit. f. Ast.*, **2**, 168, 1931.

‡ *M.N.*, **89**, 620, 1929.

Fig. 5 shows the results diagrammatically, the broadened width W' being plotted against $2\Delta \log W$, the correction to be applied to the observed width to derive the number of atoms that would be producing the line if there were no Doppler broadening.

The correction depends on four factors—line-strength, atomic weight, temperature and wave-length ; it is largest for weak lines due to light atoms

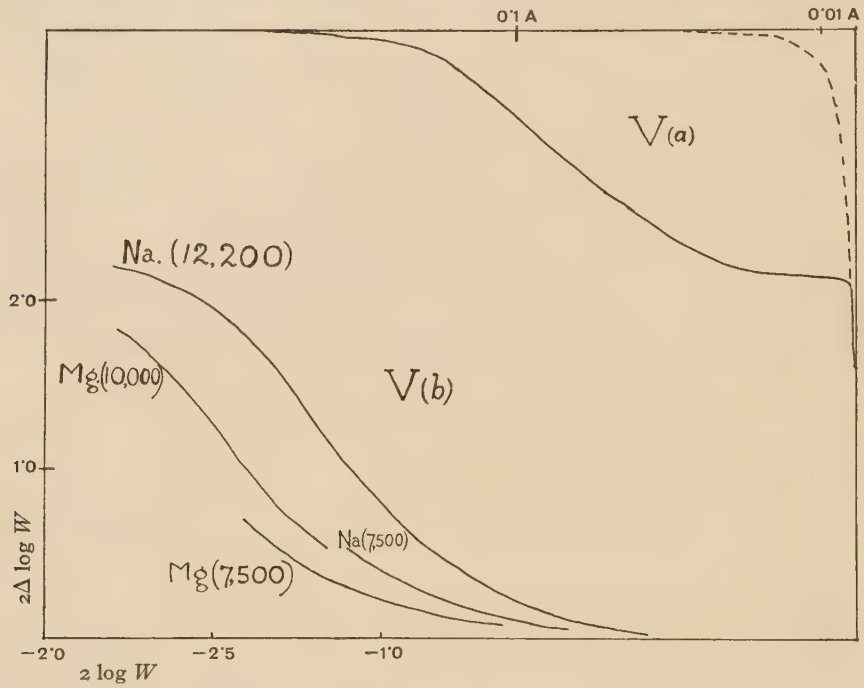

Fig. 5.—(a) *Contour of* 5890 (*Na*) *at* $T = 12{,}200$ *modified by Doppler broadening.*
(b) *Variation of correction for Doppler broadening* (*ordinates*) *with strength* (*abscissæ*), *for Na* 5890, *Mg* 5183 *at different temperatures.*

at high temperature. When a line is weakening with increasing T, the correction increases rapidly with T and causes the observed width to be much less sensitive to T. Thus the change in observed width with temperature will be more rapid for a heavy atom like *Fe* than for light elements like *H* and *He*.

The variation of the correction with temperature will shift observed maxima to earlier types, and this may be appreciable in types B and A.

The computed corrections are indicated by the lengths of the downward arrows in figs. 2 and 3 ; it will be seen that Doppler broadening is almost large enough to account for the whole discrepancy between theory and observation at 10,000°. In the computations we have used the classical value of ω' ; in a recent paper Struve and Elvey * derive from stellar contours in A stars a value of ω' ten times as great. This would make the corrections smaller and increase the discrepancy. The excess width might be attributed to turbulence after Struve and Elvey, but they have not found

* "The Intensities of Stellar Absorption Lines." I have been privileged to see this unpublished paper in manuscript.

this present in either α Lyr or α CMa, both of which show a large discrepancy in the present observations.

Owing to the large corrections due to Doppler effect and the great uncertainty of the measures in the A stars, the observations can hardly be used to test Russell's interesting prediction of the rapid drop in number of atoms above the photosphere due to the ionisation of *H*, but they suggest that it cannot begin till after spectral type F5, for two well-observed stars (α Per and α CMi) lie well above the theoretical curve for both *Na* and *Mg*, and the lines are too strong for Doppler broadening to be the cause.

In the later types Doppler broadening is negligible owing to the strength of the lines and the low temperatures.

(b) *Temperature Scale.*—Woolley * has found calcium ionisation temperatures for K and M stars somewhat higher than the usually adopted temperature scale; this would help to fit the present observations with theory, but the whole of the discrepancy can hardly be attributed to temperature, since M stars would then have to be about 4800° to 5000°. The maximum of the *Mg* lines, although ill-defined owing to the difficulty of measurement in M stars where they are badly blended with a *TiO* band, seems to come certainly later than Ko and perhaps as late as K5. The predicted maximum is at 4300°. With Russell's computed pressures this suggests a high temperature scale like Woolley's, or with the normally adopted temperatures a pressure of 10^{-8} atm.

(c) *The Square-root Law.*—We should expect the relation

$$N \propto W^r \qquad (3)$$

connecting equivalent width *W* with the number *N* of atoms producing a line to hold with $r = 2$ for such simple multiplets as the *Na* doublet and *Mg* triplet under discussion, which should not suffer from interlocking effects. Fig. 6 shows the ratios of the line-pairs 5890 : 5896, 5183 : 5172, plotted against spectral type. Both ratios decrease in the latest types in a manner recalling the behaviour of the *Fe* multiplet; we should expect another decrease from type G to A owing to Doppler broadening. This appears to begin in type F5, but the ratio is again normal in Ao stars (where, however, the measurements do not carry much weight). The mean ratios are 1·31 and 1·18 as compared with the theoretical ratios 1·41 and 1·29 for *Na* and *Mg* respectively. The best agreement with the theoretical ratio would be obtained by taking as mean values of *r* in (3) 3·3 for *Mg* and 2·6 for *Na*. Such values would be sufficient to make the values of *N* for *Mg* derived from the observations follow the theoretical curve, but the mean value of *r* would have to be 5 to give agreement for *Na*. It would be more satisfactory to find some common physical cause giving simultaneous agreement in both cases.

It should be remembered that the square-root law as given by Woolley † is

$$W^2 \propto Nf/k \qquad (4)$$

for a given distribution of η with τ.

* *M.N.*, **93**, 709, 1933.

† *Ibid.*, **93**, 694, 1933.

The general absorption coefficient k does not enter when we compare lines of a multiplet in the same star, but it should be taken account of when comparing the same line produced in different stars under very different physical conditions. Chandrasekhar gives *

$$k \propto \frac{\alpha P \bar{x}}{T^{11/2}}, \tag{5}$$

where α increases slowly with T and with decreasing P, and consequently remains approximately constant with spectral type. Using Russell's values of P and $\bar{x}$, and $\alpha = 10^{21}$, we find the following values of log k:—

$z' = \frac{5040}{T}$	1·6	1·4	1·2	1·0	0·9	0·8	0·7
log k	2·22	2·56	2·94	1·34	1·51	1·55	1·70

These values are shown in the inset to fig. 2 on the same scale.

Following (4) these values should be added to the observed 2 log W to give log (Nf). The increase of k with T is just sufficient to make Nf practically constant from $T = 3000°$ to 7000°, thus greatly increasing the difficulty of fitting theory with observation. Perhaps the most reasonable explanation is that for temperatures less than 7000° molecular dissociation plays so important a part in the general opacity that k actually decreases with increasing T instead of increasing as it does in the above table. The fact that molecular lines are visible in the Sun's spectrum shows that this form of opacity is present, and it must increase rapidly in the later types. It is noteworthy that Shane † has found the D lines in N stars (which probably differ from M stars only in composition) to be very broad—up to 100 A.—and this is sufficiently strong to lie on the theoretical curve at 3000°. It may be that oxygen compounds have a higher coefficient of opacity than compounds of carbon, and if so this would support this explanation of the behaviour of lines at low temperature.

The distribution of η with τ is another point needing investigation with respect to the square-root law. This can be calculated by Woolley's ‡ method using the ordinary ionisation formula, Pannekoek's correction for departure from thermodynamical equilibrium, and Chandrasekhar's absorption coefficient. The results of the calculation are shown in Table II, α, β being the parameters in the relation

$$\frac{1}{1+\eta} = \alpha + \beta\tau, \tag{6}$$

describing the variation of η with τ. In some cases the linear approximation fails and a second pair of parameters α', β' is needed above an optical depth τ_1. The ratio r of line- to continuous-intensity is given by Eddington's §

* *M.N.*, **92**, 152, 1932, neglecting 1 with respect to $\frac{2{\cdot}4\chi}{kT}$.

† *L.O.B.*, **329**, 89, 1920. ‡ *M.N.*, **93**, 697, 1933. § *Op. cit.*, 633.

equation in terms of α, β. Woolley * has given the solution for the case where two pairs of parameters are needed.

TABLE II

T / g ($\odot$ =1)	3000 0·001						5000 0·1						10,000 1·0		
Value of η at τ =·3	α	β	α'	β'	τ_1	r	α	β	α'	β'	τ_1	r	α	β	r
10	0·33	·192	...	...	...	0·24	0·043	·188	...	...	...	0·30	0·070	·080	0·30
3	·130	·394	...	...	...	·46	·133	·388	...	...	...	·47	·200	·162	·51
1	·343	·496	·253	1·11	·14	·69	·363	·400	·320	·600	·3	·72	·429	·220	·735
0·3	·667	·326	·537	1·28	·13	·90	·688	·280	·618	·500	·3	·90	·710	·176	·86
0·1	·864	·144	·780	·77	·13	$\cdot 95_6$	·875	·116	·832	·259	·3	$\cdot 96_6$	·884	·078	·96

It will be seen that although the distribution of η with τ depends on the physical conditions to a certain extent, the resulting values of r are almost identical and the consequent effect on the equivalent width is negligible.

Absolute Magnitude Effects.—Only a few dwarfs were available for observation, none of spectral type later than Go. In Table III line-intensities of stars with different surface gravities (computed from absolute magnitude, temperature and the mass-luminosity relation) are compared.

TABLE III

Star / Type	α CMi dF5	α Per gF5	η Boo dGo	γ Cyg gGo	$\odot$ dGo	α Aur gGo	β Gem Ko	α Boo* Ko	α Hya* K2	γ Dra K5	UMi K5
log g	4·3	2·8	3·7	2·2	4·4	2·8	2·8	2·2	1·3	2·5	1·3
Na 5890		+		+		o		−	+ +		−
Mg 5183		−		−		−		+	...		+ +
Fe 5371		+ +		+		+		o	−		+

* Both stars compared with β Gem.

\+ indicates line strengthened in giant.
− ,, ,, weakened ,, ,,
+ + ,, 2 Δ log $W > 0.4$.†
o ,, 2 Δ log $W < 0.1$.

The numerous factors contributing to the observed line-width renders it dangerous to compare this table with the effects predicted by theory for the number of atoms above a given optical depth in giants and dwarfs; *e.g.* the general absorption is greater in dwarfs owing to the higher pressures, so that if we use (4) this will give a $+ve$ absolute magnitude effect for 2 log W

* *M.N.*, **92**, 495, 1932.
† Δ log W represents change in log W from giant to dwarf.

where theory predicts a null effect for *N*. This may possibly explain the *+ve* effect observed for *Na* in some of the pairs (theory predicts a *−ve* effect for a heavily ionised element in the presence of an excess of atoms slightly ionised). It is noteworthy that the effects for *Na* and *Mg* are in no case of the same sign.

Russell's curves for *Mg* 5183 predicts a *+ve* effect for $T < 6000°$, *−ve* for $T > 6000°$. This agrees with Table III, except that the critical temperature seems to lie between spectral types Go and Ko (*i.e.* about 5000°).

α Boo (Ko) is interesting. The *D* lines are about as strong as in the Sun—*i.e.* much weaker than in other stars of the same type, and a similar weakness is also shown by the subordinate lines 5682, 5688. Since *Na* provides most of the electrons in this type any unusual lack of abundance might have a pronounced effect on the general spectrum; such an explanation might lie behind the discrepancy between the spectroscopic (0·16) and trigonometric (0·08) parallaxes of this star.

α Cyg (A2p) shows the *D* lines abnormally strong—as strong as in type F5. This is probably due to interstellar sodium, as the star is a very distant super-giant. Merrill * has found some sixth and fifth magnitude stars showing a spectrum similar to α Cyg with the *D* lines stronger than in the Sun. It is unlikely that interstellar sodium causes any appreciable strengthening in any other stars in the present list; three distant stars—γ And, α Hya and γ Dra—show the lines rather strong, but other stars equally distant appear normal.

Subordinate Lines.—These are too weak to place much weight on the measures, but they suffice to bring out the phenomenon noted by Adams and Russell † (and attributed by them to lack of thermodynamical equilibrium) that they are much stronger relative to the principal lines than we should expect with a Boltzmann distribution of the atoms. The "contrast factor," describing the agreement between theoretical and observed relative intensities, remains consistently less than unity and shows no systematic variation with temperature. A systematic increase with temperature of turbulence, as discussed by Struve and Elvey in the paper referred to above, would be a very satisfactory explanation of the slow change of line-width with temperature. But this would involve a systematic decrease in the contrast factor from type M to A, and this is not shown by what evidence there is available from the subordinate lines or by the relative intensities of the *D* lines and *Mg* 5183, 5172 as shown in fig. 6.

Summary.—Measures of total intensities of the *D* lines (*Na*) and *Mg* 5183, 5172, and some subordinate lines are given from two separate series of plates taken with different instruments, for a number of stars of spectral type M to A.

If these measures are interpreted by means of the square-root law it is found that in all cases the change with temperature is not nearly so rapid as that given by theory for the number of atoms above a given optical depth. If a modification of the square-root law, involving the opacity coefficient, is used the discrepancy is increased.

* *P.A.S.P.*, 45, 305, 1933. † *Ap. J.*, 68, 20, 1928.

Doppler broadening is found to account for most of the excess strength in the Ao stars ; it appears to be difficult to account for the weakness in the latest types without postulating a greatly increased opacity coefficient,

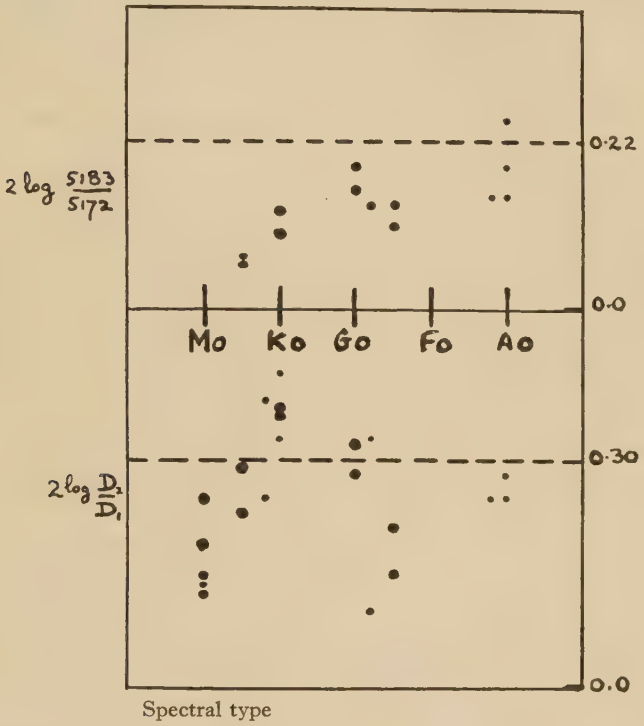

FIG. 6.—*Change of line-ratio with spectral type for Mg* 5183 : 5172 (*above*), *and Na* 5890 : 5896 (*below*). *Dotted lines indicate theoretical ratios.*

perhaps due to molecular dissociation. A somewhat higher temperature scale is another possibility.

Another possible explanation is turbulence found by Struve and Elvey in some early-type stars. No systematic decrease in the contrast factor, however, is observed with increasing temperature.

Absolute magnitude effects and certain peculiarities of individual stars are discussed.

I again wish to express my heartiest thanks to Professor Stratton, in particular for a much-valued opportunity of taking a series of plates with the Newall telescope which has added great weight to the observations. I am further indebted to all those of the observatory staff who assisted in obtaining this series of plates.

Solar Physics Observatory,
Cambridge :
1934 *March* 27.

ON THE EQUILIBRIUM OF AN INCOMPRESSIBLE SPHERE.

N. R. Sen.

(Communicated by Sir Arthur Eddington)

1. *Introduction*

Since Schwarzschild gave a solution of Einstein's equations with material tensor representing the equilibrium of an incompressible fluid sphere (of constant energy density), it has been pointed out that, strictly speaking, the condition for incompressibility is the constancy of proper density, the scalar formed by the diagonal sum of T_k^i, rather than the constancy of T_4^4, as taken by Schwarzschild.* This suggestion has not as yet been worked out. The equations in this case are complicated and do not lend themselves to integration in closed forms. Nevertheless, there are certain interesting points, such as the existence of a possible limit to the size and mass of such an incompressible sphere, which require to be cleared up. Besides, the problem of equilibrium of an incompressible spherical mass has assumed interest from another quarter. Milne, in his new theory of stellar structure considers it probable that the core of a star may be so compressed as to possess a density equal to the maximum density of matter possible, in the neighbourhood of 10^{12}, or possibly higher. Firstly, such high density is sure to produce some curvature of space making a relativity calculation of equilibrium necessary.† Secondly, in such a case it is the invariant density that should be considered. Though we have not succeeded in integrating the equations in finite forms, the interest of the problem, we consider, justifies the decision of the above points by numerical integration which has been adopted here. The results obtained are somewhat unexpected. There exists really for a given density a sphere of maximum radius as well as a sphere of maximum gravitational mass, these two spheres not being identical. Conversely, for a given radius and density there are two spheres of different masses and central pressures, of which one has a central pressure smaller than that of the one with maximum radius and the other greater.

The numerical calculations we have made show that the incompressible sphere of water of maximum size will have a radius of 230 million kilometres, whereas if the material has the maximum density of matter, say $3 \cdot 10^{12}$, the largest sphere will have a radius of only 133 kilometres. The most massive sphere of this density will have a mass nearly 24 times that

* Eddington, *The Mathematical Theory of Relativity*, p. 168.

† *Zeitschrift f. Astrophysik*, **7**, 188, 1933. It has been shown in this paper that if the central (energy) density of a polytrope is of the order 10^{12}, the curvature of space produced by this mass concentration has considerable effect on the equilibrium, though for central density of the order 10^6, the effect is inappreciable and Emden's tables remain practically unmodified.

of the Sun. In all the calculations we have assumed the surface to be free (pressure vanishing). For given pressure on a surface, as in Milne's problem of an incompressible core with the maximum density of matter, the solution can be obtained from the system of curves shown in fig. 1, or an analogous one.

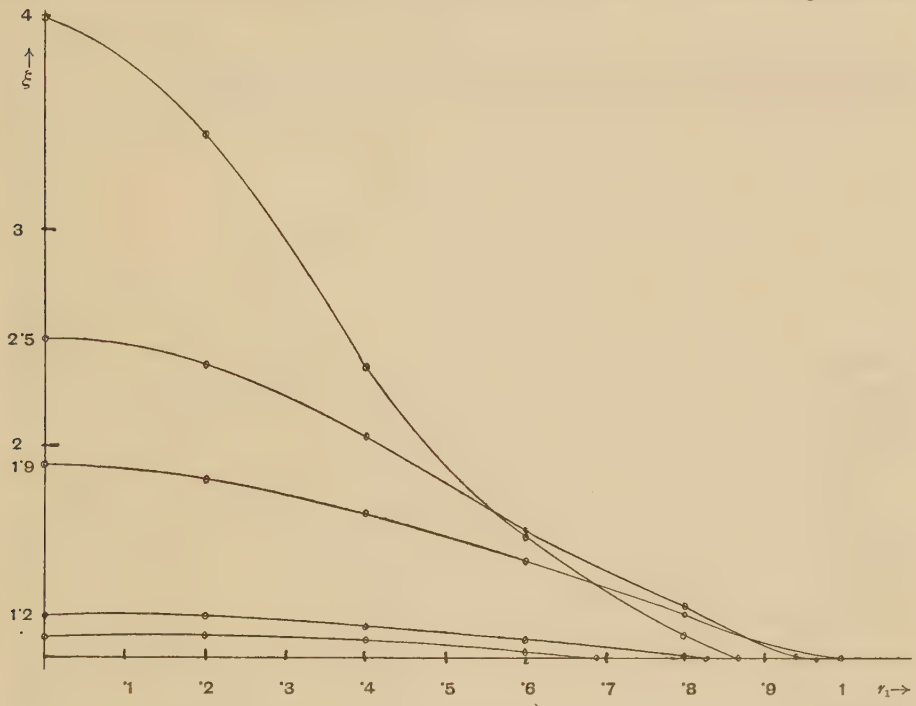

FIG. 1.—*This fig. shows the* (ξ, r_1) *curves for different spheres. The sphere of maximum radius corresponds to* $\xi = 1{\cdot}90$ *at the centre.*

2. *The Equations of Equilibrium*

For numerical integration we have to choose some suitable form for our equations. It is found that the equations derived from the variation principle are of the first order and very convenient for our numerical computation. Besides, the variables can be easily connected with physical quantities.

We take the line element in the form

$$ds^2 = \frac{dr^2}{1 - \frac{w}{r}} + r^2(d\theta^2 + \sin^2\theta d\phi^2) - V^2 dt^2, \tag{1}$$

$$V^2 = v^2\left(1 - \frac{w}{r}\right), \tag{2}$$

and the material tensor as

$$T_i^{\,i} = p(i = 1, 2, 3), \qquad T_k^{\,i} = 0(i \neq k), \qquad T_4^{\,4} = -\mu c^2, \tag{3}$$

where p is the pressure and μ the density in grammes/(cm.)^3. The variation principle gives the two following equations * for w and v :—

* M. v. Laue, *Die Relativitatstheorie*, ii, p. 228.

$$\frac{dw}{dr} - \kappa c^2 \mu r^2 = 0, \tag{4}$$

$$\frac{dv}{dr} - \tfrac{1}{2}\kappa \frac{p + c^2\mu}{r - w} r^2 v = 0. \tag{5}$$

$\kappa = 8\pi G/c^4 = 2{\cdot}07 \,.\, 10^{-48}$ is Einstein's gravitational constant. The energy-momentum principle gives an additional independent equation,

$$\frac{dp}{dr} + \frac{p + c^2\mu}{V} \cdot \frac{dV}{dr} = 0. \tag{6}$$

For an incompressible sphere we introduce the condition

$$c^2\mu - 3p = c^2\delta, \tag{7}$$

where the constant δ is the invariable density in grammes/(cm.)^3. Equations (4), (5), (6), (7) and (2) are sufficient for the determination of the sphere. Only those integrals are of interest to us for which p is positive, whereas zero value of p will indicate the free surface of the sphere.

Since μ is positive, equation (4) shows that w is a monotone increasing function of r. Further, from (2) $w < r$; the extreme value $w = r$ will give a singularity and is to be interpreted as indicating a natural boundary. From (6) dp/dr and $d(\log V)/dr$ are of opposite signs. Hence if we take the pressure to decrease continuously from the centre towards the surface, V must be increasing continuously in the same direction. Equation (5) now shows that v also increases continuously from its minimum value at the centre towards the constant value c on the surface. Just on the surface Schwarzschild's outer solution will apply, and by comparison we have

$$v_s = c, \qquad w_s = \frac{2G}{c^2} M,$$

where M is the gravitational mass of the sphere. Writing equation (4) as

$$w(r) = \kappa c^2 \int_0^r \mu r^2 dr = \frac{2G}{c^2} M(r) \tag{8}$$

and noting its resemblance with the corresponding non-relativity equation, we can call $M(r)$ the "gravitational mass" within the sphere r. In the present case two other masses can be defined by the integrals

$$4\pi \int_0^r \frac{\mu r^2 dr}{\sqrt{1 - \frac{w}{r}}} \quad \text{and} \quad 4\pi \int_0^r \frac{\delta r^2 dr}{\sqrt{1 - \frac{w}{r}}}.$$

The former gives the total relative mass of the sphere, and the latter its proper mass, where each mass element is referred to a local system in which it is at rest.

3. *Transformation of the Equations.*

The equation (6) can immediately be integrated by taking (7) into consideration. This gives

$$4p + c^2\delta = \left(\frac{A}{V}\right)^4,$$

where A is an integration constant. We put $V = V_s$ on the surface, where $p = 0$, evaluate A, and have thus

$$p = \tfrac{1}{4}c^2\delta(\xi^2 - 1), \tag{9}$$

where

$$\xi = \left(\frac{V_s}{V}\right)^2. \tag{10}$$

This gives further

$$\mu = \tfrac{1}{4}\delta(3\xi^2 + 1), \qquad p + c^2\mu = c^2\delta\xi^2. \tag{11}$$

Equations (4), (5), and (2) then assume the forms

$$\frac{1}{r_1^2}\frac{dw_1}{dr_1} = \tfrac{1}{4}(3\xi^2 + 1), \tag{12}$$

$$\frac{1}{r_1}\frac{dz}{dr_1} = -\xi^3, \tag{13}$$

$$\frac{w_1}{r_1} + \frac{z}{\xi} = 1; \tag{14}$$

for the substitutions

$$\left(\frac{V_s}{v}\right)^2 = z, \qquad r_1 = \kappa^{\frac{1}{2}}\delta^{\frac{1}{2}}cr, \qquad w_1 = \kappa^{\frac{1}{2}}\delta^{\frac{1}{2}}cw. \tag{15}$$

(12), (13) and (14) are equations in dimensionless quantities. The differential equations are of the first order and in their normal form. For a given set of initial values for w, z and ξ for a definite value of r_1 (agreeing with equation (14)), which is an ordinary point, there is a single set of solutions giving w, z and ξ as functions of r_1. We shall start integration at $r_1 = 0$, where $w_1 = 0$ for a definite value of $\xi(> 1)$, and continue the integration till $p = 0$; that is, $\xi = 1$.

We note, as in the last paragraph, that w_1 starts with the value zero at the centre and increases continuously with r_1. $\xi = \xi_0$ at the centre is greater than 1, and decreases monotonously to the value 1 on the free surface. In the same manner z decreases monotonously from the centre to the surface. Since we are interested in those solutions for which w_1 vanishes at the centre $r_1 = 0$, it is evident from (12) that $\frac{dw_1}{dr_1}$, $\frac{w_1}{r_1}$, $\frac{w_1}{r_1^2}$ all vanish at the centre. Hence, initially at the centre $z = \xi = \xi_0$. Thus at $r_1 = 0$ all the three variables are known when $\xi = \xi_0$ is given, so that a complete integral curve can be obtained corresponding to that value of ξ_0. This only means that for a given density the central pressure determines the sphere completely.

When the integration is completed, $(w_1)_s$, the value of w_1 on the surface, is obtained. Then, remembering Schwarzschild's outward solution, we have from continuity

$$V_s = \left[1 - \left(\frac{w_1}{r_1}\right)_{\text{surface}}\right]^{\frac{1}{2}}. \tag{16}$$

V_s being thus known, equations (10) and (15) give V and v, and so the gravitational field is completely determined.

The above considerations immediately suggest the following functional forms:—

$$p = \delta F_1(p_0/\delta,\ \sqrt{\delta}\ .\ r), \qquad M(r) = \frac{1}{\sqrt{\delta}} F_2(p_0/\delta,\ \sqrt{\delta}\ .\ r).$$

If the sphere closes for $r_1 = R_1$, then R_1 is a function of ξ_0 only. If $r = R$ when $r_1 = R_1$, then from (9) and (15) we have

$$R\ .\ \sqrt{\delta} = f(p_0/\delta). \tag{17}$$

Hence if there are two spheres, one of density δ and central pressure p_0, and in the second these values are $n^2\delta$ and $n^2 p_0$ respectively, then the radius of the first sphere is n times that of the second. Their masses are also in the same ratio.

We can construct Taylor's series for the functions w_1, z and ξ in the neighbourhood of the origin. In equations (12), (13) and (14), if the signs of both w_1 and r_1 are changed, while the signs of z and ξ are both changed or both unchanged, the equations are unaltered. Hence w_1 is an odd function of r_1, and as regards z and ξ there are two types of solutions : for one both are odd functions, and for the other both are even functions of r_1. In the case in which we are now interested z and ξ are both even functions of r_1. Constructing the solutions as Taylor series in the usual manner we have

$$\left.\begin{aligned} w_1 &= \tfrac{1}{12}(3\xi_0^2 + 1) r_1^3 + \ \ldots \\ \xi &= \xi_0[1 - \tfrac{1}{12}(3\xi_0^2 - 1) r_1^2 + \ \ldots]. \end{aligned}\right\} \tag{18}$$

If $\xi_0 - 1$ is small we have from (9) and (15)

$$p_0 - p = \tfrac{1}{4} c^2 \delta(\xi_0^2 - \xi^2) \sim \frac{2\pi}{3} G\delta^2 r^2 (r_1 << 1),$$

which is really the classical pressure equation. Here r_1, being small, we have stopped at the first term of the series. If then the sphere closes for

$$r_1 = R_1, \qquad R^2_1 = 12\left(1 - \frac{1}{\xi_0}\right)\Big/(3\xi_0^2 - 1),$$

so that comparatively larger values of ξ_0 give larger spheres.

4. *On some Approximations.*

That r_1 will have a maximum under the conditions laid down can be easily seen. The minimum value of the right-hand side of (12) is unity (on the surface). Hence

$$\frac{1}{r_1^2}\frac{dw_1}{dr_1} \geqslant 1,$$

giving

$$w_1 > \tfrac{1}{3}r_1^3$$

when we consider those solutions for which w_1 and r_1 vanish together.

But since $w_1/r_1 < 1$ we must have

$$r_1 < \sqrt{3}. \tag{19}$$

Equation (15) now gives an upper limit to the "radius"

$$R_{\max} < \frac{\sqrt{3}}{c\sqrt{\kappa\delta}}. \tag{19'}$$

This is only a rough upper limit. We shall find the exact upper limit by actual integration. It can be shown that the above upper limit is obtained also in Schwarzschild's solution. For Schwarzschild's sphere (μ = constant) equation (12) is replaced by

$$\frac{1}{r_1^2}\frac{dw_1}{dr_1} = 1.$$

From this immediately follows the existence of the limit (19'). The attainment of this limit really means the breakdown of the metric ($w_1 = r_1$). But Schwarzschild's sphere of maximum size is really conditioned by other circumstances.

Though complete integration of the equations is not possible, we can get much useful information in the form of inequalities, which often serve as good checks in course of numerical calculations. For instance, when ξ_0 is not very far removed from the value giving the maximum radius we can use the following approximation. w_1/r_1 being less than $\frac{1}{3}r_1^2$, $z/\xi = 1 - w_1/r_1 < 1 - \frac{1}{3}r_1^2$. Again from (13)

$$\left(-\frac{dz}{dr_1}\right) \leqslant \xi_0{}^3 r_1,$$

so that on integration

$$z_0 < z + \tfrac{1}{2}\xi_0{}^3 r_1{}^2 < \xi(1 - \tfrac{1}{3}r_1{}^2) + \tfrac{1}{2}\xi_0{}^3 r_1{}^2.$$

Taking the case $\xi \to 1$, $r_1 \to R_1$ we have

$$R_1 > \sqrt{\frac{\xi_0 - 1}{\frac{1}{2}\xi_0{}^3 - \frac{1}{3}}}. \tag{a}$$

The maximum value of the right-hand side, namely 0·62, is evidently a lower limit to $R_{1\,\max}$. The following table shows the usefulness of (a) :—

ξ_0	$R_1 >$ (Calculated by 2)	Correct Value of R_1
1·10	0·54	0·69
1·20	0·61	0·83
1·30	0·62	0·90 *
2·00	0·52	0·99

* This value is obtained from the curve in fig. 2.

For the type of solutions we are seeking now ($\xi_0 \to$ definite finite number > 1, as $r_1 \to 0$), w_1/r_1 increases in the neighbourhood of the origin, and in fact w_1/r_1 is a monotone increasing function throughout.* We can obtain many good approximations (giving rough limits) in the form of inequalities. We do not give the proofs here, but simply mention them. They are all subject to the condition that w_1/r is monotone increasing.

Firstly,

$$R_1 < \sqrt{\frac{2(\xi_0 - 1)}{1 - \frac{2}{3}\eta_0}}, \qquad \eta_0 = \tfrac{1}{4}(3\xi_0^2 + 1), \tag{b}$$

but it is useful so long as $\xi_0 < \sqrt{\frac{5}{3}} = 1{\cdot}29$. For small values of $\xi_0 - 1$ (a) and (b) give two suitable limits.

Another approximation for (w_1/r_1 monotone increasing) R_1 is

$$R_1^2 > A\left(1 - \frac{1}{\xi_0^2}\right),$$

where A is a constant not greater than the minimum value of z/ξ, for which we can evidently substitute z_s, the value on the surface. As z_s changes regularly from one sphere to another we can guess a lower limit for R_1 by substituting the value of z_s for that contiguous sphere which has a lower value of this function.

5. *Numerical Integration*

Equations (12), (13) and (14) have been integrated numerically, starting from $\xi_0 = 1{\cdot}01$, and for about 12 values of ξ_0 up to $\xi_0 = 10$. Fortunately, each integration does not require large number of steps. Table I shows the radii of the spheres whose central pressures can easily be calculated from ξ_0 by (9), as well as their gravitational masses, etc.

TABLE I

ξ_0	R_1	$\frac{(w_1)_s}{R_1}$	$(w_1)_s$	z_s
1·01	0·240	0·019	0·0046	0·981
1·10	·695	·182	·1266	·818
1·20	·831	·258	·2141	·742
1·40	·955	·375	·3587	·625
1·80	·990	·485	·4800	·515
1·90	·996	·496	·4940	·504
2·00	·990	·514	·5093	·486
2·40	·967	·536	·5188	·464
2·50	·965	·545	·5260	·455
2·60	·948	·548	·5199	·452
3·00	·924	·554	·5127	·445
4·00	·867	·553	·4795	·447
10·00	·736	·492	·3623	·508

* For the shell type of solutions discussed in § 6, maximum and minimum are present in every solution.

Fig. 1 gives (ξ, r_1) curves for different values of ξ_0 (central pressures). As the spheres close for $\xi = 1$ the portions $0 < \xi < 1$ have been omitted. The points where the curves end on $\xi = 1$ (r_1 axis in the figure) give the radii of the corresponding spheres. Fig. 1 shows that as ξ_0 (central pressure) increases, at first, the "radius" which is proportional to R_1 also increases, till $R_{1\,\max} = 0{\cdot}996$ is reached for $\xi_0 = 1{\cdot}90$. As ξ_0, or the central pressure, increases further the spheres shrink in size. For a given "radius" corresponding to given R_1, there are two spheres possible, one of which has a central pressure less than that of the sphere of maximum "radius," and the other greater. The spheres thus fall into two classes, which we shall call A class and B class (ξ_0 larger) respectively. In this respect the relativity sphere differs from the classical sphere, where for a given radius and density only one sphere is possible. The classical sphere belongs to A class as $\xi_0 - 1$ for the classical sphere is small, as is evident from equation (11). Differentiating (14) and using equations (12) and (13), we have on the surface of the sphere, *i.e.* $\xi = 1$,

$$\left(-\frac{d\xi}{dr}\right)_{R_1} = \frac{1}{R_1}\left(\frac{1}{z_s} - 1\right) = \frac{1}{R_1^2}\frac{w_s}{z_s}.$$

Hence of the two curves that end at the same point on the r_1 axis the steeper one (with greater central pressure) belonging to B class has the greater value of w_s (smaller value of z_s) than the other one. The complete value of $\left(-\frac{d\xi}{dr}\right)$ when calculated shows that $\left(-\frac{d\xi}{dr}\right)$ is always positive ($\xi \geqslant 1$), except at $r_1 = 0$, where it vanishes. Fig. 2 (p. 558) shows the radii of the spheres against ξ_0 (connected with square root of central pressure). For small values of $\xi_0 - 1$ the curve is steep and nearly straight, representing the conditions in a classical sphere. Table I further shows that the sphere of maximum radius is not the sphere of maximum mass. The maximum value of w_s is 0·526, corresponding to $R_1 = 0{\cdot}948$, and $\xi_0 = 2{\cdot}50$. Substituting from (15) we have

$$\sqrt{\delta}\,.\,R_{\max} = 0{\cdot}996\,.\,\frac{1}{c\kappa^{\frac{1}{2}}} = 0{\cdot}23\,.\,10^{14}.$$

The largest sphere of water will have a "radius" of 230 million kilometres. The radius of the Schwarzschild sphere of water of maximum size is about 370 million kilometres.* If the material has density 10^6, $R_{\max}$ (for an incompressible sphere) is 230,000 kilometres, whilst for density of the order of the maximum density of matter, say $\delta = 3{\cdot}10^{12}$, the largest sphere has a radius of only 133 kilometres.†

The central pressure of the incompressible sphere of maximum radius is given by $p_0 = \delta\,.\,5{\cdot}8\,.\,10^{13}$ atmospheres.

* Eddington, *The Mathematical Theory of Relativity*, p. 170.

† When converted into real length by the integral $\int dr_1 \Big/ \left(1 - \frac{w_1}{r_1}\right)^{\frac{1}{2}}$, this value is somewhat raised.

Again from equations (8) and (15) we have

$$M_{\max} \cdot \delta = 0{\cdot}526 \frac{4\pi}{c^3 \kappa^{\frac{3}{2}}} = 8{\cdot}2 \cdot 10^{40}.$$

For $\delta = 3 \cdot 10^{12}$, $M_{\max} = 4{\cdot}7 \cdot 10^{34}$ grm. $= 24 \times$ (mass of the Sun).

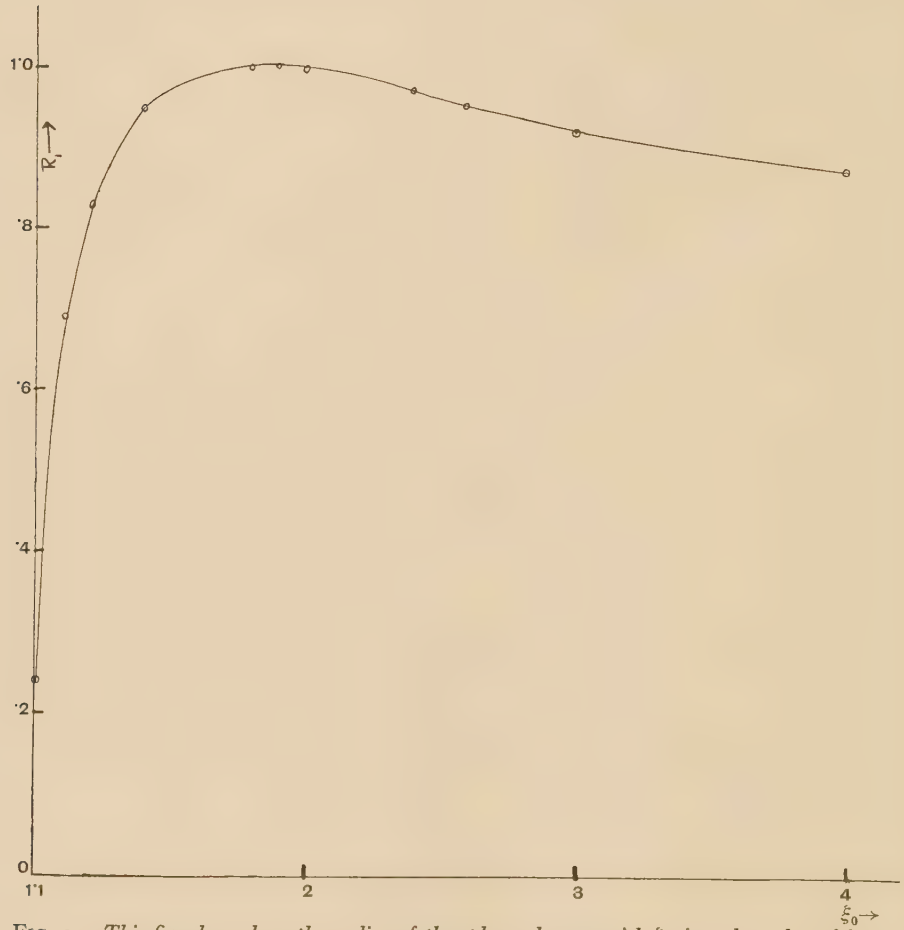

FIG. 2.—*This fig. shows how the radius of the sphere changes with* ξ_0, i.e. *the value of* ξ *at the centre. The central pressure is proportional to* $(\xi_0^2 - 1)$.

In fig. 3 the masses of the spheres are plotted against their radii.

6. *Discussion of the Solutions.*

With regard to the maximum values for radius and mass, it should be noted that the circumstances under which these values arise in the present case are different from those in the case of the Schwarzschild sphere. For this latter, $R_{1\,\max} = \sqrt{\frac{8}{5}} = 1{\cdot}63$, and at this extreme value the line element becomes singular on account of the vanishing of V (velocity of light) just at the centre of the sphere. Since V is monotone increasing from the

centre, this is the first point where V can be expected to vanish. In this case $V=0$ arises through $v=0$. Another way in which a natural boundary can arise is by w_1/r_1 attaining the value 1, which evidently can be expected to happen for the first time on the surface of a sphere. But this contingency does not as a matter of fact arise. For the incompressible sphere neither of these cases happens, since for the sphere of maximum size V is positive

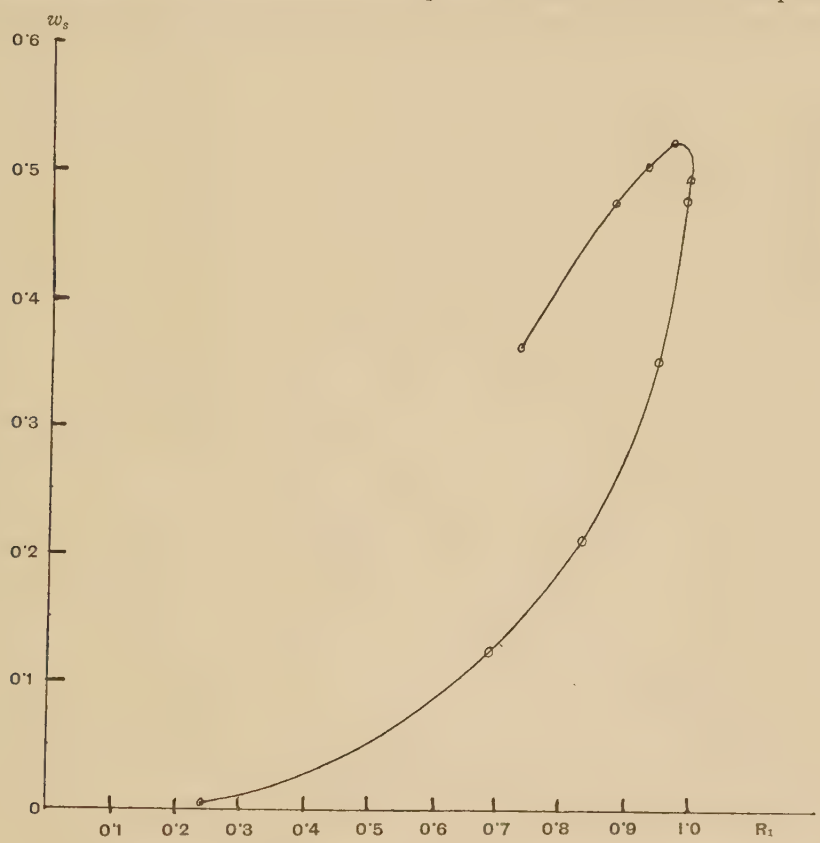

FIG. 3.—*This fig. shows the masses of the spheres against their radii in proper units. There is a maximum for "radius" (R_1) as well as for "mass" (w_s).*

and $w_1 < r_1$ everywhere. The passage from A to B class of spheres arises in a different way. In the classical sphere of constant density the pressure gradient at a point is proportional to the distance of the point from the centre. The greater the central pressure the greater is the distance required for this initial central pressure to sink to the value zero at the free surface, and the greater is the size of the sphere. In the present case

$$\left(-\xi\frac{d\xi}{dr_1}\right)=\frac{r_1}{4z}\xi^3(\xi^2-1)+\frac{\xi^2}{r_1}\left(\frac{\xi}{z}-1\right).$$

The left-hand side measures the pressure gradient by (9), and on the right both terms are positive. For large values of ξ_0 these terms are evidently large near the centre, and the fall of pressure there is far quicker than in

the classical case. For very small values of $\xi_0 - 1$ we have the classical sphere, which is a sphere of A class. As ξ_0 increases, the radius of the corresponding sphere also increases, but the fall of pressure also becomes very rapid from one sphere to the next one. A higher central pressure will have a tendency to give a bigger sphere on the one hand and produce very rapid fall of pressure on the other. In all the spheres of A class the first tendency is predominant, and after the value $\xi_0 = 1{\cdot}9$ the second tendency predominates and the spheres

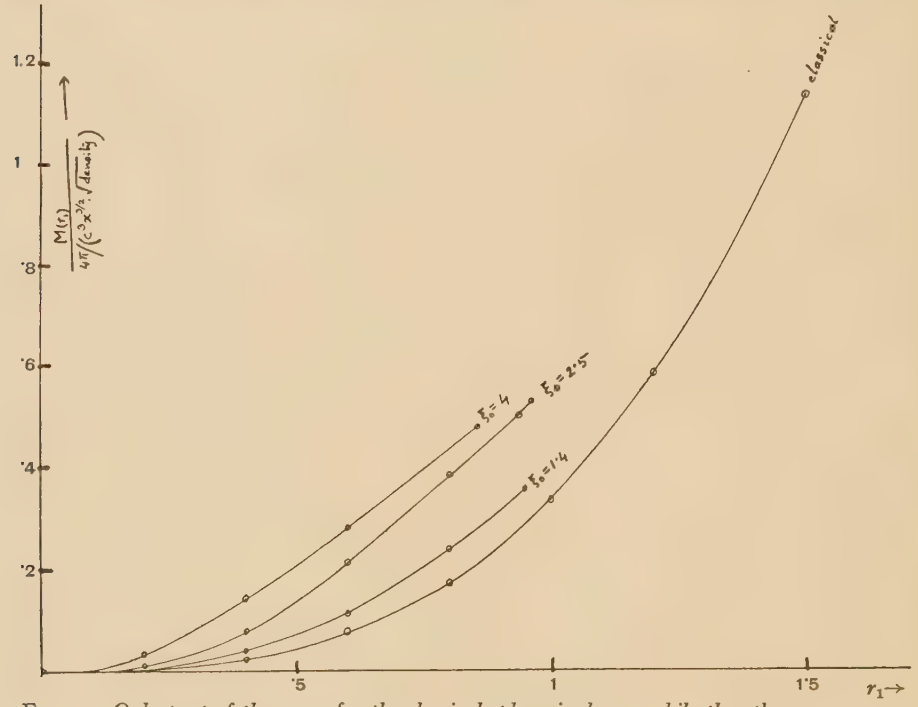

FIG. 4.—*Only part of the curve for the classical sphere is shown, while the other curves are for complete spheres.*

Note that distance for distance the sphere with higher central pressure contains greater mass.

begin to shrink in size and fall under B class. Curiously, for spheres after $\xi_0 = 2{\cdot}5$ as the central pressure increases the spheres not only shrink in size but have less and less mass. This is rather puzzling, since the warping of space near the centre which ultimately produces B class of spheres is to be expected in spheres with greater accumulation of mass. But the factor which plays the decisive part here is rather the concentration of mass or the packing of matter than the total mass. From fig. 4 it will be apparent that higher central pressure means closer packing. Moreover, the relative mass, given by μ, is very high near the centre in these spheres of high central pressures. It may be mentioned in this connection that this complication is peculiar to the present problem, since for a given radius there is only one Schwarzschild sphere ($\mu = \text{constant}$) with a definite central pressure.

An attempt has been made to study another type of solutions of equations (12), (13) and (14), which throw some light on the problem we are studying.

It has been noticed that for a given radius there are two spheres, one of A class and the other of B class. Let (w_1, r_1) curves for the spheres be drawn. The lower curve OA is for a sphere belonging to A class with mass W_1, while the upper curve OB is for a sphere of B class with mass W_2, both having the same radius R_1. We next investigate what would be the nature of the solution if for radius R_1 the mass be arbitrarily given, say W'. We have only to continue the solution backwards, starting from the surface towards the origin. There exist three types of solutions, S_1 for $W' < W_1$, S_2 for $W_1 < W' < W_2$, and S_3 for $W' > W_2$. All these give shell solutions for which w_1 vanishes before $r_1 = 0$ is attained. For S_1 class the inner radius of the shell (the outer radius for all shells is R_1) starts from R_1 with $W' = 0$, and decreases continuously to the value zero as W' tends to the value W_1 *from below*. The pressure (value of ξ) on the inner surface also increases continuously to the value of the central pressure of the complete sphere for which $W' = W_1$. The solutions of S_3 class have also similar property, only the shells with W' just greater than W_2 have inner surfaces with small radii, which, however, increase continuously as W' increases, whilst the pressures on the inner surfaces also increase continuously. Thus for a given inner radius (the outer radius is R_1 and fixed) there is one shell of S_1 class and another of S_3 class, the inner pressure for S_3 shell being greater than that for S_1 shell. For S_2 class there is a value W_{12} between W_1 and W_2, for which the inner surface of the shell has the maximum radius (the maximum value is quite small). The inner pressure is large compared to the inner pressures on the shells of S_1 and S_3 classes. As W' increases from W_{12} to W_2, the radius of the inner surface decreases continuously from the maximum value to the value zero for $W' = W_2$, but the inner pressure increases rapidly, and in fact appears to increase indefinitely as W_2 is approached. Thus there is a discontinuity in pressure as W' attains the value W_2 from above or below. If W' attains the value W_2 through decreasing values the inner pressure decreases continuously to the value of the central pressure of the complete sphere for $W' = W_2$, but if W' approaches W_2 from below the inner pressure appears to increase indefinitely. There is a similar discontinuity in pressure as W' attains the value W_1 from below or above. Here as W' approaches W_1 from above the inner pressure increases indefinitely. Thus the two different spheres of A and B class for a given value of R_1 correspond to two points of discontinuity in the solutions of the equations. Corresponding to a given inner radius, provided it lies within a definite limit, there are two shells of S_2 class which are characterised by large inner pressures (in addition to two shells of S_1 and S_3 classes mentioned above). These shell solutions help us to understand properly the behaviour of those integral curves in which we are interested.

7. *Comparison of the Classical, Schwarzschild and Incompressible Sphere*

A classical sphere of uniform density ρ obeys the following law of pressure :—

$$P_0 - P = \frac{2\pi}{3} G\rho^2 r^2,$$

which by putting $r = r_1/(c\sqrt{\kappa\rho})$ we rewrite as

$$\frac{P_0 - P}{\frac{1}{4}c^2\rho} = \tfrac{1}{3}r_1^2. \tag{A}$$

The pressure equation for the incompressible sphere of proper density δ is, by (9),

$$\frac{p_0 - p}{\frac{1}{4}c^2\delta} = \xi_0^2 - \xi^2. \tag{B}$$

Similarly, if we calculate the masses we have for the classical sphere

$$\frac{M_{\text{cl}}(r_1)}{(4\pi/c^3\kappa^{3/2}\rho^{1/2})} = \tfrac{1}{3}r_1^3, \tag{C}$$

whereas for the incompressible sphere we have by (8) and (15)

$$\frac{M(r_1)}{(4\pi/c^3\kappa^{3/2}\delta^{1/2})} = w_1(r_1). \tag{D}$$

The basis of our comparison we take to be the equality of densities and central pressures. We have then from (A) and (B)

$$\xi_0^2 - 1 = \tfrac{1}{3}(R_1^2)_{\text{cl}}. \tag{E}$$

This equation enables us to compare the sizes of the two spheres. Consider, for instance, the incompressible sphere of maximum radius. $\xi_0 = 1{\cdot}90$, $R_1 = 0{\cdot}996$. By (E) the corresponding classical sphere has $(R_1)_{\text{cl}} = 2{\cdot}8$; that is to say, a radius almost three times as large. The fall of pressure in these two spheres can be compared by (A) and (B), as ξ is known as function of r_1 and is shown in fig. 5. We can also compare the gravitational masses of these two spheres thus :

$$\frac{\text{Mass of incompressible sphere of maximum radius}}{\text{Mass of corresponding classical sphere}} = \frac{0{\cdot}494}{\frac{1}{3}(2{\cdot}8)^3} = {\cdot}06.$$

Similarly comparing the incompressible sphere of maximum mass with that of the classical sphere of same density and central pressure (which by (E) has $R_1 = 3{\cdot}7$), the ratio comes out to be only 0·03.

Fig. 4 compares the distribution of mass in the incompressible sphere and the classical sphere of same density and central pressure. The lowest curve shows the classical distribution, and the three upper curves the distributions for $\xi_0 = 1{\cdot}4$, $2{\cdot}5$, 4. For the same distance (r) the relativity sphere contains more mass than the classical sphere, and for the former the higher the central pressure, the greater is the mass, distance for distance from the centre. The diminution of masses for higher central pressures is due to the earlier closing of the spheres and not to looseness of packing of matter.

Fig. 5 compares the fall of pressure in the incompressible sphere and the classical sphere of the same density and central pressure. The steeper gradient of the relativity spheres is to be noticed.

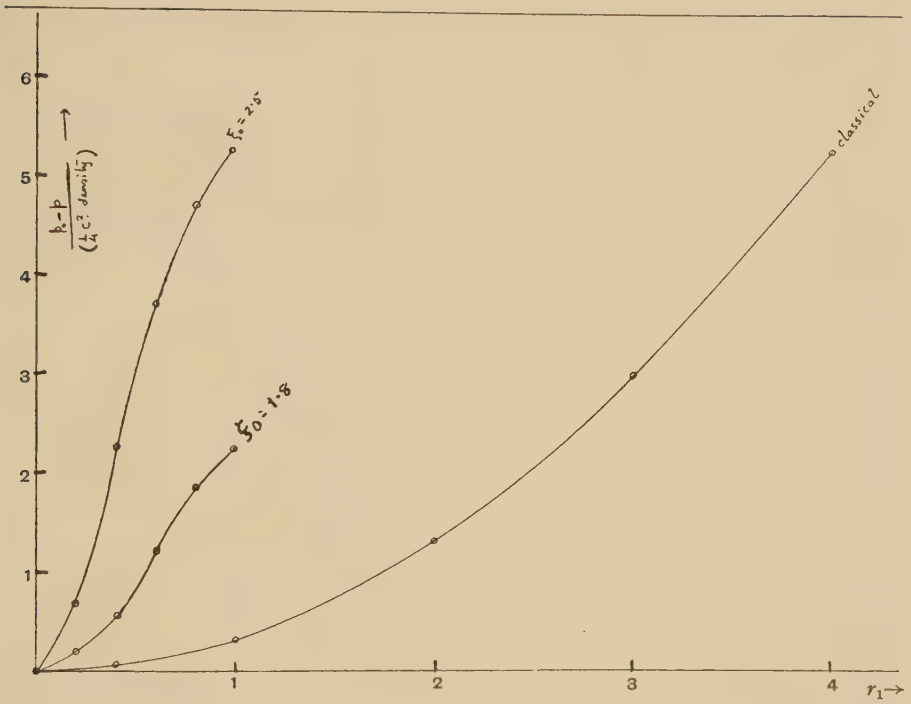

FIG. 5.—*This fig. shows the drop of pressure in the classical and in two relativity spheres.*

For the Schwarzschild sphere of central density μ we have

$$\frac{M_s(r)}{(4\pi/c^3\kappa^{3/2}\mu^{1/2})} = \tfrac{1}{3}r_1{}^3 \qquad \text{(F)}$$

and

$$\frac{p_0{}^s - p^s}{\frac{1}{4}c^2\mu} = \frac{8\cos\theta_m(1-\cos\theta)}{(3\cos\theta_m - 1)(3\cos\theta_m - \cos\theta)}, \qquad \text{(G)}$$

where $\sin\theta = \frac{1}{\sqrt{3}}r_1$ and θ_m = value of θ on the surface.

If, as before, we put $p_0{}^s = P_0$, $\mu = \rho$ we have

$$\cos\theta_m = \frac{1 + \frac{1}{12}(R_1)^2_{\text{cl}}}{1 + \frac{1}{4}(R_1)^2_{\text{cl}}}.$$

Taking $(R_1)_{\text{cl}} = 2{\cdot}8$ as calculated above, we have

$$\cos\theta_m = 0{\cdot}55, \quad \text{and} \quad \sin\theta_m = 0{\cdot}83 = \frac{(R_1)_s}{\sqrt{3}},$$

giving $(R_1)_s = 1{\cdot}42$. Hence, for the sphere of that particular type

$$\frac{\text{Mass of classical sphere}}{\text{Mass of corresponding Schwarzschild sphere}} = \frac{(2{\cdot}8)^3}{(1{\cdot}42)^3} = 7{\cdot}7.$$

Taking $(R_1)_{\text{cl}} = 3{\cdot}7$ this ratio is nearly 16.

It may be noted that the mass distributions in the classical and Schwarzschild sphere as given by (C) and (F) are identical.

I desire to thank Mr. Samarendra Ray, Research Student, for kindly undertaking the work of numerical solution of the equations in this paper, which he accomplished with great energy and extraordinary patience, and also Prof. P. C. Mahalanobis of the Presidency College, for kindly placing at our disposal the calculating machines, tables, etc. of his Statistical Laboratory.

ON THE DISTRIBUTION OF STELLAR LUMINOSITIES DERIVED FROM TRIGONOMETRIC PARALLAXES.

J. J. Nassau and S. W. McCuskey.

1. *Introduction.*—A method of correcting statistical distributions for the effect of a known probable error has been given by Eddington,* and applied by Dyson,† Nassau ‡ and others, for the purpose of eliminating the negative values which enter into parallax determinations. One of the ultimate goals, of course, has been to improve and increase the absolute magnitude data for studies of luminosity distribution.

The present discussion follows the method given in *M.N.*, **88**, 441, with the trigonometric parallax material available at the end of May 1933, some 4000 determinations in all. Only those lists of parallaxes have been used which were large enough for statistical discussion.

For each observatory a number of frequency distributions were plotted as follows :—

(A) A distribution of all the parallaxes in intervals of 0″·005.

(B) Distributions of two or three sub-groups chosen according to the magnitude of the probable error.

(C) A distribution of all the probable errors.

As may be seen from the reference (‡) given above, the corrections used in this method must be applied to uniform data. To test for uniformity we applied the following criteria :—

(*a*) The sub-group distributions of parallaxes should be approximately of the same form.

(*b*) The distribution of probable errors should follow the Gaussian error law.

The Mt. Wilson and Allegheny data presented the only discordance from these criteria.

2. *Mt. Wilson Parallaxes.*—In the case of the Mt. Wilson observations the magnitude of the probable error was apparently a function of the

* *M.N.*, **73**, 359, 1913. † *Ibid.*, **86**, 686, 1926.

‡ *Ibid.*, **88**, 441 and 583, 1928.

parallax and no single distribution was valid for the whole. Corrections applied to the three sub-groups (B) yielded new distributions which were practically the same, indicating that the applied corrections were rational.

Similar trial distributions were made by dividing the parallaxes into groups according to the telescope used in their determination. This, however, failed to fulfil criteria (*a*) and (*b*) above.

3. *Allegheny Parallaxes.*—When plotted in the usual way the Allegheny frequency curves were very discordant among the sub-groups (B), and a decidedly skew curve (fig. 1, *b*) for the probable error distribution (C) resulted. It was then noted that the observational methods of the observatory had been changed somewhat during the course of years so as to include more plates for each parallax determination. A scrutiny of the catalogue revealed two rather abrupt changes in the number of plates per star. Three divisions of the parallaxes were then made as follows :—

Group I.—The early lists of parallaxes comprising 549 stars with an average number of plates per determination equal to 15.

Group II.—An intermediate group with average number of plates 21. 191 stars were present in this list.

Group III.—A total of 317 stars with average number of plates 29.

Each group was treated as if it were from an independent source. The sub-group plots of parallax frequencies and probable errors indicated definitely a conformity with criteria (*a*) and (*b*) of § 1, and the corrections were accordingly applied. Hence in Table I the parallax correction is divided according to the average number of plates used in each determination.

4. *The Form of the Correction.*—Using the formula

$$\epsilon = \frac{1}{2h^2} \cdot \frac{\Delta y}{\Delta x} \cdot \frac{1}{y},$$

where ϵ is the error in π, y the ordinate of the smooth curve of parallax frequencies, Δy the average increment on either side of π,

$$h = \frac{0{\cdot}477}{\text{average p.e. of the group}}.$$

With intervals of parallax $\Delta x = 0''{\cdot}005$, the corrections of Table I were applied to the parallax in the sense $\pi_{\text{corr}} = \pi + \epsilon$.

5. *Probable Errors and the Number of Plates.*—The precision of the mean probable error can be found in three ways :

(*a*) From the residuals in probable error about the arithmetic mean.

(*b*) From the constants of the Gaussian curve best fitting the observed frequency distribution of probable errors.

(*c*) From the average number of plates used per parallax determination by the formula *

$$\frac{\text{p.e. of p.e.}}{\text{p.e.}} = \frac{0{\cdot}477}{\sqrt{n-1}},$$

where n = average number of plates − 3.

* Brunt, *Combination of Observations*, p. 57 (Second Edition).

TABLE I

Relative Parallax	McC.	Allegheny I 15 pl.	Allegheny II 21 pl.	Allegheny III 29 pl.	Gr.	Yerk.	Yale	Spr.	Mt. Wilson P.E. 0″·001 to 0″·004	Mt. Wilson P.E. 0″·005 to 0″·006	Mt. Wilson P.E. 0″·007 to 0″·016	Cape
″												
−0·020	+24	+23	+22	+15	+21	+25	+23	+21	+10	+12	+14	+17
−0·015	+20	+18	+18	+11	+17	+23	+18	+17	+ 7	+ 9	+11	+14
−0·010	+16	+14	+14	+ 8	+13	+18	+14	+13	+ 5	+ 7	+ 9	+11
−0·005	+11	+10	+ 9	+ 5	+10	+13	+10	+11	+ 5	+ 7	+ 9	+ 9
0·000	+ 7	+ 7	+ 6	+ 4	+ 8	+ 9	+ 7	+ 8	+ 3	+ 6	+ 8	+ 7
+0·005	+ 4	+ 5	+ 3	+ 1	+ 5	+ 5	+ 6	+ 8	+ 1	+ 3	+ 4	+ 6
+0·010	+ 1	+ 4	0	0	+ 3	+ 1	+ 4	+ 6	− 1	0	+ 1	+ 5
+0·015	− 1	+ 2	− 2	− 1	0	− 1	+ 3	+ 3	− 2	− 3	− 3	+ 4
+0·020	− 2	+ 1	− 4	− 2	− 2	− 2	+ 1	− 1	− 2	− 4	− 5	+ 3
+0·025	− 3	+ 1	− 5	− 3	− 4	− 4	− 1	− 5	− 1	− 4	− 4	+ 1
+0·030	− 4	− 3	− 5	− 4	− 6	− 5	− 4	− 5	− 1	− 3	− 4	0
+0·035	− 5	− 6	− 5	− 5	− 8	− 5	− 5	− 6	− 1	− 3	− 4	− 2
+0·040	− 6	− 8	− 5	− 5	− 9	− 5	− 4	− 5	− 1	− 3	− 4	− 3
+0·045	− 7	− 8	− 6	− 5	− 9	− 5	− 4	− 5	− 1	− 4	− 4	− 4
+0·050	− 7	− 6	− 6	− 5	− 8	− 5	− 5	− 5	− 1	− 3	− 5	− 5
+0·055	− 8	− 6	− 7	− 6	− 7	− 5	− 6	− 6	− 1	− 2	− 6	− 5
+0·060	− 8	− 5	− 8	− 5	− 7	− 5	− 6	− 5	− 1	− 2	− 6	− 6
+0·065	− 7	− 5	− 7	− 3	− 8	− 6	− 7	− 6	− 1	− 1	− 8	− 6
+0·070	− 8	− 6	− 6	− 4	− 9	− 6	− 8	− 6	− 1	− 1	− 9	− 5
+0·075	− 7	− 4	− 3	− 6	−10	− 6	− 9	− 6	− 1	0	−10	− 5
+0·080	− 7	− 5	0	− 2	− 7	− 7	− 9	− 8	0	0	−11	− 5
+0·085	− 6	− 6	0	0	− 4	− 8	− 5	− 7	0	0	−13	− 6
+0·090	− 5	− 4	0	0	0	− 9	− 3	− 8	0	0	−11	− 5
+0·095	− 3	− 5	0	0	0	− 9	0	− 5	0	0	− 9	− 4
+0·100	0	0	0	0	0	− 8	0	0	0	0	− 5	− 4
+0·105	0	0	0	0	0	− 5	0	0	0	0	− 2	− 4
+0·110	0	0	0	0	0	− 2	0	0	0	0	0	0

Table II presents a summary of the probable errors together with their precision computed by the foregoing methods for each observatory under discussion. Column (1) gives the probable error and its precision using residuals from the mean; (2) the probable error and precision from the frequency curve; (3) the precision obtained from the average number of plates per determination, utilizing the probable error of column (1). Column (4) gives the average number of plates per determination.

In order to show more clearly the effect of the number of plates per determination on the size and precision of the probable error, the frequency curves for the three Allegheny groups are exhibited in fig. 1A. A curve showing the distribution of all the probable errors is given in fig. 1B, to bring out the asymmetry due to the change in observational methods.

From the above considerations it is clear that the individual probable error given for each parallax determination does not measure its precision, and that the magnitudes of probable error in each series are distributed according to the Gaussian law irrespective of the magnitude of the parallaxes.

TABLE II

Observatory	(1)	(2)	(3)	(4)
McC.	96 ± 16	96 ± 15	± 11	20
Ally. I	80 13	80 13	12	15
,, II	64 09	63 10	07	21
,, III	53 07	53 08	05	29
Gr.	77 13	76 12	09	22
Yerk.	95 22	91 19	14	14
Yale	74 11	74 11	09	19
Spr.	94 20	92 21	14	15
Mt. W.*	...	...	...	16
Cape	79 10	79 11	09	22

The unit in this table is 0″·0001.

* Non-Gaussian distribution of p.e.

6. *Absolute Parallaxes.*—The corrected relative parallaxes were reduced to absolute by using the *Publications of the Leander McCormick Observatory*,*

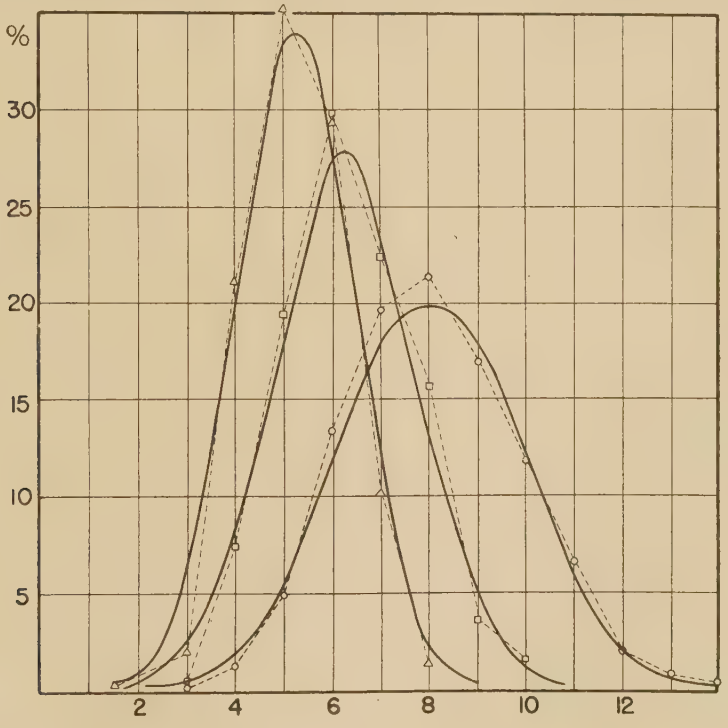

FIG. 1A.—*The Distribution of probable Errors for the Three Allegheny Groups. Abscissæ are given in units of* 0″·001.

when the mean magnitude of the comparison stars was about 10; *i.e.* for the McCormick and Yerkes data, and for all other cases Table I of

* *Publications of the Leander McCormick Observatory*, 4, 280, 1927.

Groningen Publications.* The two sources agree well except for stars near the galactic poles, where the McCormick values are somewhat higher.

7. *Absolute Magnitudes*.—The parallaxes corrected statistically for their probable errors and reduced to absolute by the methods stated in the foregoing section were used to obtain absolute magnitudes, and a numerical distribution diagram was constructed as indicated in Table III.† The number of stars in each interval of 0·3 absolute magnitude is given for the several spectral sub-classes. All stars with insufficient spectral classification

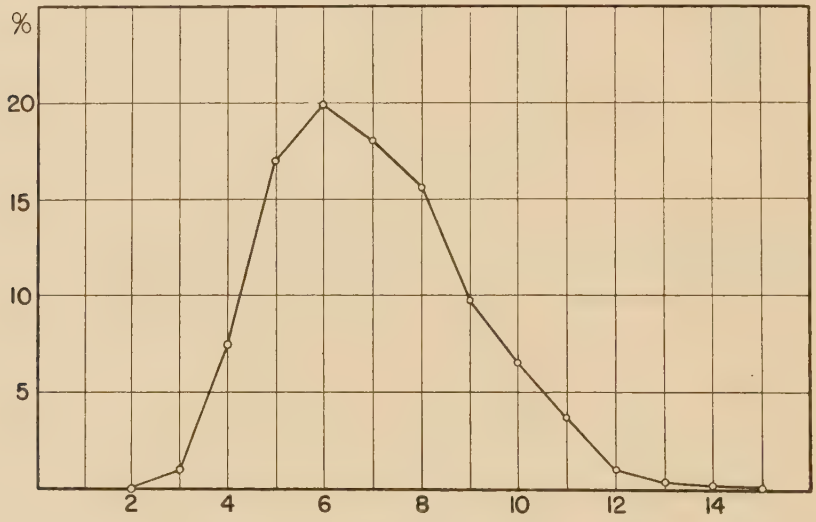

FIG. 1B.—*The Distribution of probable Errors for all the Allegheny Parallaxes. Abscissæ are in units of* 0″·001.

were placed in the zero of the group, *e.g.* K stars in the Ko division. In the horizontal direction the stars given under absolute magnitude 3·0, for example, include those with $M = 2{\cdot}9, 3{\cdot}0, 3{\cdot}1$.

Inasmuch as numerous data with regard to spectral type and apparent magnitude were missing or uncertain in some of the earlier parallax lists, the Henry Draper Catalogue was used to fill in the gaps. If the spectrum given was composite, the first value stated in the Catalogue was used. Although the Mt. Wilson spectral classification used with some of their stars differs from the Henry Draper Catalogue, it was not thought necessary to convert the Mt. Wilson values into the others. Since in the final analysis several sub-classes were in most cases used as one group, the discrepancies were absorbed.

Variable stars were given a mean magnitude based on the limits of their variation.

* P. J. van Rhijn, *Groningen Publications*, **37**, 3, 1925.

† In addition to the entries in Table III there are the following:—

1 star, $M = 14{\cdot}1$, Fo ; 1 star, $M = 14{\cdot}4$, Fo ; 1 star, $M = 16{\cdot}5$, Mo.

Binary stars were treated in the following manner :—

(*a*) When the magnitude, spectral class and π of each component was stated, the stars were used individually.

(*b*) When only one value of π was given, it was combined with the magnitude of the brighter component and the spectrum of the latter (or the combined spectrum).

(*c*) When individual parallaxes were available but a combined magnitude and spectral class was given, the average value of the parallax was used.

8. *Mean Values of Absolute Magnitude.*—With the extensive parallax material at hand it seemed advisable to compute the mean absolute magnitudes for giant and dwarf series according to the method of *M.N.*, **88**, 583. In the case of spectral sub-classes with too few values of M to treat separately they were joined with an adjacent large sub-class.

From the Russell diagram of each observatory the separation point between giants and dwarfs was assumed, beginning at spectral class Fo. The stars were examined for one magnitude on either side of this assumed value by means of the absolute magnitude yielded by the spectroscopic parallax or by the value given in Cecchini's catalogue,* when more than one determination was listed. The stars so examined were classified as giants and dwarfs, very few remaining in the intermediate zone.

A computed parallax π_c for each star was obtained from an assumed value of M near the centre of the group, and the equation $M = m + 5 + 5 \log \pi_c$. Residuals π (corrected absolute) $- \pi_c$ were formed, and by trial that value was chosen for M, which made, as far as possible :

(*a*) The sum of the positive residuals equal to the sum of the negative residuals.

(*b*) The number of positive residuals equal to the number of negative residuals.

(*c*) The arithmetic sum of the residuals a minimum.

The criteria proved to be quite sensitive. Many times a change of 0·1 magnitude in the assumed value of M caused a reversal in the sums.

The mean of these central values for each spectral class is shown in fig. 2 (p. 572). The means were obtained by using the number of determinations entering into each central value as weights (Tables V and VII).

9. *Dispersion of Absolute Magnitudes.*—For each observatory the measure of the spread of absolute magnitude about the mean values of the individual spectral groups is expressed in terms of probable error.

Let M_c represent the mean value of absolute magnitude as it has been determined in § 8. Then we have for each star in the same group

$$\log \pi_c = \tfrac{1}{5}(M_c - m - 5),$$

and hence the residual

$$M - M_c = 5 \log_{10} \frac{\pi}{\pi_c}.$$

* *Catalogo Generali Parallassi Stellari*, 1931.

TABLE III *

Sp. / M	Oe5	Bo	B1	B2	B3	B5	B8	B9	Ao	A2	A3	A5	Fo	F2	F3	F5	F8	F9	Go	G2	G5	G8	Ko	K2	K3	K4	K5	K6	K7	K8	Mo	M3	M8	Md
−6·3									1																									
−6·0																							1											
−5·7		1						1	1																									
−5·4										1																								
−5·1													1																					
−4·8									1																						1			
−4·5								1	2														1								1			
−4·2							1																	1										
−3·9							1					1					1																	
−3·6		1							1	1			1				1						2									1		
−3·3						1			1				1			1	1	1			1		1	1										
−3·0																1	2						3				2				1			
−2·7		1		1	2		1					1							1				3	1							2	2		
−2·4			2		1					1									1		2	1	3	1								1	1	
−2·1		1	2		1		1		1	1	1		1			1	3		3		2	1	4	2			2				3			
−1·8		2		1	1	3	1		5	1		1							7		2		10				1				4	1		
−1·5		1	2	2	3	2			3	2			1			1	3		2		3		16	3			2			1				
−1·2	1		1	1	6	3	2		6	3	1		1	2		2			5		2		18				3			1	5	1		
−0·9	1				6	1	1	1	10	4	2	1	3			3	2		10		6		23	1			8				1			
−0·6	3	1	2		2	3	6		14	3		5	5	1		2			6		5	2	20	1			10				7	1		
−0·3	1	3	2	1	1		1	1	12	6		1	2	2		3	2		4		7		39	4			7				8	1		
−0·0	2	1	2		3	2	5	2	16	5	3	5	5			3	6		7		4		31	9			11				10	3		
0·3	2	1	2	1	2	2	2	2	16	3	4	2	6	2		4	1		12		11	1	36	5			9				7			
0·6	1	1	2	1	2		1	2	24	10	4	4	4	4		4			3	1	13		45	8			4				13	6		
0·9		2		2	2	4	2		15	12	1	8	7	2		9	3		4		11		47	2			8				9	4	1	
1·2	1		2			2	1	3	20	17	9	14	9	6	2	9	5		9		11	2	52	5			4				7	1	2	1
1·5	3	1			2		3	3	20	12	4	10	10	3		9	7	2	3		15		51	4			6				3			
1·8				2	2	1	1	3	14	14	6	7	6	2		11	2	1	6	2	14	1	36	5			7				2	2		
2·1	1								16	8	6	8	21	2		22	7		9		19	1	40	4			4				4	6		1
2·4						1	2	1	7	4	8	6	19	7	1	21	12		14		20		35	4			2				4		1	
2·7	2								7	5	4	11	10	5	1	20	11		15		11	1	18	2			5				3	2	1	

| | | |

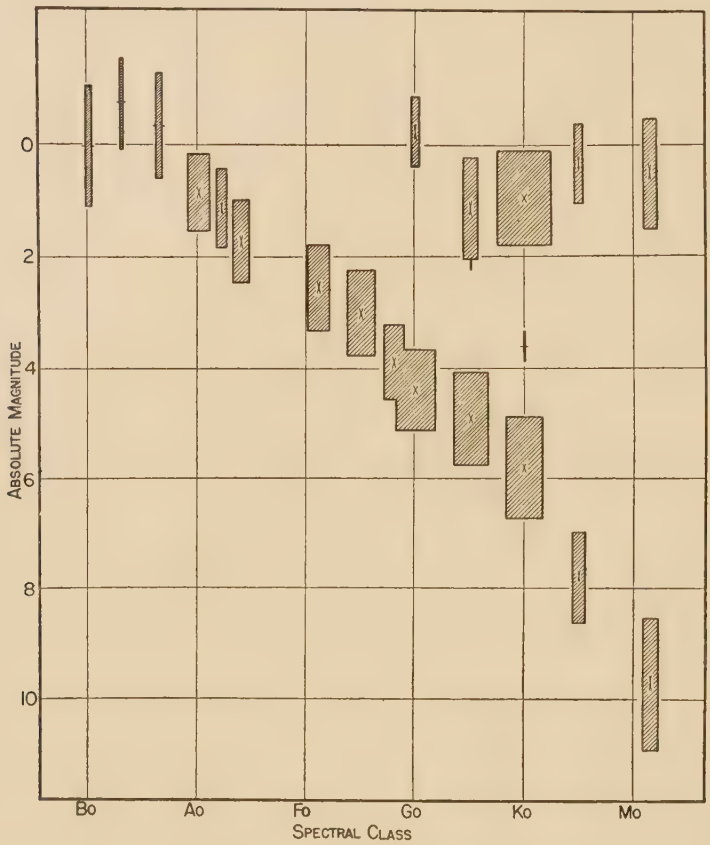

Fig. 2.—*Results obtained from all Trigonometric Parallaxes. The dispersion in magnitude is represented by the height of the rectangle whose width gives the relative number of determinations in the group.*

The probable error, r, based on these residuals is

$$r = 5\left[0{\cdot}845\frac{\sum\left|\log\frac{\pi}{\pi_c}\right|}{n}\right]. \qquad (1)$$

It is of course evident that when the parallax is small the ratio $\frac{\pi}{\pi_c}$ becomes uncertain, and therefore better results are obtained from

$$r' = 0{\cdot}845\frac{\Sigma|v|}{n} \qquad (2)$$

and

$$r = 5\frac{\text{I}}{\bar{\pi}}r'\log_{10}e, \qquad (3)$$

where $v = \pi - \pi_c$ and $\bar{\pi}$ is the average parallax of the group under consideration.

These values of r are termed the spread or dispersion in absolute magnitude.

When sufficient stars were available in each division, two or three sub-groups were formed according to the magnitude of π_c or its equivalent, the apparent magnitude, with the idea that each sub-group must contain as far as possible the same number of positive and negative residuals. The weighted mean value of r from the sub-groups yielded invariably the r obtained from the entire group.

Table IV gives 205 Ko–K2 Stars of the Allegheny Observatory, divided as follows :—

Sub-group	Apparent Magnitude
A	< 4.0
B	$4.0 - 5.0$
C	> 5.0

TABLE IV

Giants Ko–K2 of the Allegheny Observatory

Group	No. Stars	$\bar{\pi}$	r (Eq. 1)	r (Eq. 3)
A	53	22·6	1·01	1·07
B	73	17·9	0·81	0·80
C	79	13·0	0·95	0·87
Mean of r	...	...	0·92	0·91
From all stars	205	17·25	0·92	0·91

The above method was used for a detailed treatment, by observatories, for all the Ko–K2 stars, since they contributed one-fourth of the total number of trigonometric determinations. Two or three sub-groups were formed as far as the numbers permitted.

Table V presents a summary of spectral class Ko–K2 for all observatories. Column (2) gives the number of parallaxes. Columns (3) and (4) present the values of r as obtained from equations (1) and (3). The mean of these values is given in column (5), and shows good agreement between the values of the individual observatories. Column (6) gives the value of M obtained according to the method explained in § 8 ; and column (7), a similar value obtained from the uncorrected absolute parallaxes. The mean values of corrected and uncorrected parallaxes are given in the last two columns.

The values of dispersion given in column (5) exhibit no marked variation between observatories, and hence, assuming that each determination tends to express the actual spread in absolute magnitude for the type of stars under consideration, we obtain the mean ($\bar{r}$) from the equation

$$\bar{r} = \frac{\Sigma nr}{N},$$

where n stands for the number of stars per observatory, and N the total number of determinations in the spectral class.

TABLE V

Giant Ko–K2

	No.	$r\left(\log \frac{\pi}{\pi_e}\right)$	$r(v)$	$\bar{r}$	M_{corr}	M_{unc}	$\bar{\pi}_{corr}$	$\bar{\pi}_{unc}$
McC.	136	± 0·89	± 0·89	± 0·89	+0·4	+0·6	20·9	24·5
Ally.	205	0·92	0·91	0·91	+0·7	+0·8	17·3	19·1
Gr.	48	0·98	0·92	0·95	+1·0	+1·2	11·5	15·7
Yerk.	17	0·77	0·67	0·72	−0·3	0·0	19·0	22·5
Yale	154	0·82	0·74	0·78	+1·3	+1·4	24·3	25·7
Spr.	16	0·80	0·98	0·89	+1·7	+1·4	23·1	25·3
Mt. W.	31	1·00	0·98	0·99	+1·6	+1·8	17·4	18·6
Cape	...	...	...	...	...	...	...	...
Mean	607	...	...	0·88	+0·9	+1·0	...	...
			Dwarf Ko–K2					
McC.	122	± 0·99	± 0·89	± 0·94	+6·0	+6·2	61·5	68·4
Ally.	46	0·78	0·73	0·76	+5·7	+6·0	64·6	68·3
Gr.	76	0·82	0·82	0·82	+5·1	+5·3	28·1	30·1
Yerk.	37	1·30	1·41	1·35	+5·9	+6·1	59·1	66·8
Yale	19	0·85	0·69	0·76	+6·3	+6·3	135·0	143·2
Spr.	25	1·23	1·12	1·17	+6·0	+6·2	77·4	79·9
Mt. W.	11	...	0·62	0·62	+6·0	+6·1	60·8	62·1
Cape	64	0·99	0·87	0·93	+5·8	+5·9	44·7	48·8
Mean	400	...	...	0·92	+5·8	+6·0	...	...

Further reflection on this point might be of interest. Since the mean value of M was obtained from $\bar{M} = \frac{\Sigma nM}{N}$, the dispersion about this mean may be obtained from the fact that $\bar{M}$ is a linear function of the M's. Let $\bar{r}_1$ represent this spread. Then we have

$$\frac{\bar{r}_1^2}{N} = \sum \left(\frac{n_i}{N}\right)^2 \left(\frac{r_i}{\sqrt{n_i}}\right)^2$$

or

$$\bar{r}_1^2 = \frac{1}{N} \Sigma n_i r_i^2.$$

The numerical result for the Ko–K2 stars is :

$\bar{r} = 0{\cdot}88$ $\qquad$ $\bar{r}_1 = 0{\cdot}88$ (for giants)
$\bar{r} = 0{\cdot}92$ $\qquad$ $\bar{r}_1 = 0{\cdot}94$ (for dwarfs)

which indicates that $\bar{r}$ approaches $\bar{r}_1$. This is possible when the standard deviation (σ) about the mean of the r's expressed by

$$\sigma^2 = \frac{\Sigma n_i (r_i - \bar{r})^2}{N}$$

approaches zero, as may be easily shown. Therefore, in each division (giant or dwarf) all the observatories yield sensibly the same spread.

10. To gain greater confidence in the corrections applied to the observed parallaxes, and at the same time to show that the spread (r) obtained above is more or less free from spread due to the probable errors of the parallaxes of the different observatories, we will give a method of obtaining r directly from the uncorrected parallaxes.

Taking, for example, the Allegheny Ao stars, where the number is sufficient to illustrate the method, we have in Table VI, column (1), the catalogue star number; (2), the apparent magnitude; and (3), the uncorrected absolute parallax. Column (4) gives a parallax, π_c', computed from $M = m + 5 + 5 \log \pi_c'$, by assuming such a value of M that the residuals ($v = \pi' - \pi_c'$) of column (5) satisfy as far as possible the following: (*a*) the sum of positive residuals equal to the sum of the negatives, (*b*) the same number of positive and negative v's, and (*c*) the total absolute sum as small as possible.

Equations (2) and (3) yield a spread (r'') in absolute magnitude from the uncorrected parallaxes. If the mean probable error in the parallaxes of the observatory is expressed in magnitude by means of equation (3) and denoted by r_1'', then the probable error of the spread, free of r_1'', will be given by

$$r^2 = r''^2 - r_1''^2.$$

In the case under consideration we have

$$M = +0.4 \qquad r'' = 1.42$$
$$\bar{\pi}' = 12.2 \qquad r_1'' = 1.22 \qquad \text{and} \qquad r = \pm 0.73$$

This agrees well with the value, $\pm$ 0·74, given in Table VIIa. A number of such comparisons were made, all with satisfactory agreement.

11. In § 9 and Table V we have shown the data and treatment for the Ko–K2 stars. Table VII presents the results obtained in a similar manner for all spectral groups.

Spreads of the Main Sequence.—It is evident from Table VII and the latter part of § 9 that, with perhaps the exception of the Yale and McCormick values, no systematic deviations are present. In the case of the McCormick Observatory, particularly in the earlier lists of parallaxes, many stars with incomplete spectral classification were placed in the zero of the group. This, in addition to the selection of parallax stars, may have a tendency to increase the spread. The dispersion for Yale appears to be consistently low, due probably to selection of material and highly homogeneous spectral data.

Absolute Magnitudes of the Main Sequence.—The deviation of the mean absolute magnitudes of the different observatories from the weighted mean of each spectral group is usually less than a half magnitude. The Allegheny determinations are systematically smaller than the mean. A similar effect

TABLE VI

Allegheny Ao Stars

No.	m	π'	π'_e	v	No.	m	π'	π'_e	v
16	3·9	− 7	16	−23	677	4·7	9	11	− 2
31	3·0	39	24	15	690	4·8	1	10	− 9
44	3·9	42	16	26	702	3·8	− 8	17	−25
50	5·5	15	8	7	707	3·3	12	21	− 9
51	6·7	3	4	− 1	712	4·5	3	12	− 9
65	4·7	9	11	− 2	716	3·8	5	17	−12
67	3·8	15	17	− 2	736	5·1	1	9	− 8
76	5·6	16	7	9	751	5·5	− 2	8	−10
81	4·3	21	13	8	769	3·6	− 6	18	−24
82	3·6	18	18	0	800	6·3	− 8	5	−13
99	3·9	28	16	12	802	5·5	11	8	3
105	3·2	32	22	10	804	6·6	7	5	2
110	5·2	− 9	9	−18	817	2·4	47	32	15
119	4·0	− 2	15	−17	818	2·5	27	30	− 3
144	5·7	3	7	− 4	820	2·9	26	25	1
167	3·8	30	17	13	823	3·8	34	17	17
191	4·3	40	13	27	827	4·5	33	12	21
202	5·1	9	9	0	830	5·3	14	8	6
212	5·5	3	8	− 5	833	3·6	24	18	6
239	5·0	15	9	6	836	5·5	11	8	3
241	3·9	12	16	− 4	843	5·1	13	9	4
248	2·8	57	27	30	845	5·5	− 6	8	−14
262	3·8	34	17	17	847	4·9	10	10	0
321	6·5	− 1	5	− 6	851	5·5	0	8	− 8
323	4·4	11	13	− 2	867	4·6	12	11	1
371	4·5	− 2	12	−14	873	5·4	14	8	6
420	6·9	− 5	4	− 9	874	5·2	11	9	2
421	3·9	16	16	0	883	5·3	22	8	14
437	6·0	13	6	7	897	5·4	19	8	11
453	5·9	6	6	0	903	5·4	− 8	8	−16
477	5·9	− 2	6	− 8	912	5·1	− 2	9	−11
481	9·6	− 2	2	− 4	921	2·0	88	38	50
517	4·3	12	13	− 1	932	5·7	3	7	− 4
541	7·5	28	3	25	946	6·8	4	4	0
566	6·2	3	5	− 2	950	6·0	− 1	6	− 7
583	4·8	− 4	10	−14	954	5·4	17	8	9
589	5·0	1	9	− 8	961	2·2	29	35	− 6
595	5·0	0	9	− 9	965	5·4	11	8	3
600	2·7	17	28	−11	967	5·2	19	9	10
621	4·3	8	13	− 5	968	5·2	− 4	9	−13
628	4·5	19	12	7	971	4·1	14	14	0
640	5·4	21	8	13	990	5·4	6	8	− 2
653	5·5	19	8	11	997	5·5	5	8	− 3
654	5·2	−11	9	−20	1045	5·5	5	8	− 3
665	5·4	13	8	5	1049	5·4	− 6	8	−14

is more or less present in the McCormick group. Our weighted means differ but little from the results obtained by other investigators who have used different data and different methods of treatment.

The systematic variations in M might be due largely to the systematic differences in the parallax determinations or to the non-uniformity of parallax programmes.

Spreads of the Giant Sequence.—There is again no evidence of systematic change in the value of the spread between observatories.

Absolute Magnitudes of the Giants.—It is difficult to point out any striking variation among the values for the different observatories. The Allegheny and McCormick results are inclined to be somewhat lower and the Mt. Wilson and Yale somewhat higher than the mean values for the various spectral classes.

12. *Comparing Results.*—Many investigators have considered the determination of mean values in absolute magnitude together with the actual dispersion in their distributions. A summary table of mean values is given in *Handbuch der Astrophysik* * by Lundmark, and more recent work has been carried out by Stromberg, Wilson and many others. Inasmuch as our data deal strictly with trigonometric determinations of parallax, and the method of treatment is in many respects different from previous investigators, it is felt that a comparison of results will prove interesting. R. E. Wilson, in his paper "On the Distribution of Stellar Luminosities," † gives the mean absolute magnitudes derived from the weighted mean parallaxes of 5651 stars, together with the results obtained from stars brighter than 6·0 visual magnitude by Stromberg. Their results, with ours, are given in Table VIII. When the stars are numerous the agreement is good. The discrepancies in some of the luminous groups is of course due to the uncertainties in the trigonometric determinations of small parallaxes, and to the fact that the number of determinations is insufficient for statistical treatment.

The column headed "From Uncorrected Parallaxes" gives the mean absolute magnitudes obtained from the absolute parallaxes by omitting the corrections of Table I, and of course disregarding all negative parallaxes. The treatment of the data is otherwise the same.

A comparison of these results shows that in the long run the corrections applied to the parallaxes yield mean magnitudes in better agreement with the results given by Wilson and Stromberg.

13. The method of separating giants and dwarfs for each spectral group and each observatory has been fully explained in § 8. A more or less clear-cut division was apparent in all but the G5–G8 and K0–K2 stars. For these groups a further consideration was deemed advisable.

The absolute magnitudes derived from corrected parallaxes are shown as frequency distributions in figs. 3 and 4. Counts in absolute magnitude were made between limits of 0·3 magnitude and the data smoothed by taking the running means of three points.

Each distribution suggests a combination of two probability functions

* *Handbuch der Astrophysik*, Band V/1, first half.

† *Astronomical Journal*, p. 968, 1932 February.

TABLE VIIa

Main Sequence

	Mo–M3					K5				
	No.	r	M_{corr}	M_{unc}	$\bar{\pi}_{corr}$	No.	r	M_{corr}	M_{unc}	$\bar{\pi}_{corr}$
McC.	25	± 1·08	+ 9·4	+ 9·8	110·8	30	± 0·88	+8·5	+8·7	119·5
Ally.	...	...	...	...	...	12	1·05	7·7	7·7	118·1
Gr.	...	...	...	...	...	5	...	7·1	7·3	58·0
Yerk.	17	0·85	9·5	9·6	133·4	18	0·77	8·0	8·2	91·2
Yale	10	0·80	9·4	9·4	155·2	14	0·86	7·8	7·8	132·6
Spr.	7	...	10·4	10·6	236·7	6	...	7·2	7·4	131·9
Mt. W.	22	1·80	10·4	10·4	142·9	8	...	7·8	7·8	144·6
Cape	6	...	8·7	8·7	152·3	28	0·66	7·4	7·5	85·5
Mean	87	± 1·20	+ 9·7	+ 9·9	...	121	± 0·82	+7·8	+8·0	...
	G5					G0				
McC.	75	± 0·89	+5·0	+5·2	44·8	77	± 0·81	+4·2	+4·4	40·9
Ally.	68	0·85	4·8	5·0	44·1	89	0·70	3·9	4·1	35·1
Gr.	68	0·69	4·6	4·9	22·6	40	0·70	4·3	4·4	21·9
Yerk.	27	1·02	4·6	4·8	36·0	24	0·86	4·7	5·0	46·1
Yale	24	0·73	5·3	5·4	83·6	34	0·48	4·4	4·5	48·4
Spr.	27	0·91	4·7	5·0	37·0	30	0·65	4·7	4·9	51·7
Mt. W.	4	...	5·9	6·0	34·5	9	...	4·6	5·0	35·3
Cape	81	0·85	5·1	5·2	36·7	122	0·67	4·8	4·8	35·0
Mean	374	± 0·84	+4·9	+5·1	...	425	± 0·70	+4·4	+4·6	...
	F8					F5				
McC.	51	± 0·72	+3·9	+4·1	49·5	63	± 0·95	+2·8	+3·0	35·4
Ally.	61	0·66	3·7	3·9	37·5	94	0·68	2·9	3·0	28·5
Gr.	23	0·58	4·2	4·4	24·3	19	0·93	3·2	3·6	25·2
Yerk.	12	0·71	3·6	3·8	37·2	21	0·89	3·2	3·5	30·0
Yale	24	0·67	3·5	3·6	50·1	24	0·43	3·3	3·5	43·8
Spr.	20	0·80	4·3	4·4	40·5	41	0·92	3·5	3·5	31·0
Mt. W.	7	...	4·0	4·2	36·9	20	0·86	3·0	3·3	23·0
Cape	39	0·65	4·4	4·5	34·3	18	0·66	4·7	4·8	36·0
Mean	237	± 0·68	+3·9	+4·1	...	300	± 0·79	+3·1	+3·3	...

	F0–F2					A3–A5				
	No.	r	M_{corr}	M_{unc}	$\bar{\pi}_{corr}$	No.	r	M_{corr}	M_{unc}	$\bar{\pi}_{corr}$
McC.	38	± 0·82	+2·3	+2·5	32·0	36	± 0·83	+1·8	+2·1	38·8
Ally.	83	0·85	2·4	2·7	29·7	55	0·74	1·4	1·6	22·4
Gr.	18	0·50	3·1	3·3	22·5	7	...	2·4	2·6	33·9
Yerk.	13	1·03	2·8	3·1	31·3	11	0·35	0·5	0·4	20·7
Yale	36	0·67	2·4	2·4	35·3	30	0·52	1·9	1·9	33·9
Spr.	33	0·82	3·0	3·1	29·1	17	1·29	2·9	3·3	26·9
Mt. W.	15	0·79	2·4	2·7	18·5	5	...	2·0	...	19·2
Cape	(3)	...	(6·7)	(6·5)	...	...	...	...	...	...
Mean	236	± 0·79	+2·5	+2·7	...	161	± 0·75	+1·7	+1·9	...
	A2					A0				
McC.	25	± 0·88	+1·0	+1·0	22·2	63	± 0·80	+0·5	+0·5	29·3
Ally.	45	0·72	0·7	0·9	17·4	90	0·74	0·4	0·5	15·3
Gr.	7	...	0·7	0·3	16·7	8	...	1·0	1·0	15·2
Yerk.	7	...	1·5	1·5	29·4	20	0·68	1·0	1·2	55·9
Yale	25	0·58	1·5	1·5	24·2	44	0·47	1·6	1·5	30·4
Spr.	8	...	1·9	1·9	27·5	18	0·74	2·0	1·6	20·7
Mt. W.	...	...	...	...	...	3	...	0·9	...	10·3
Cape	(4)	...	(4·2)	(4·2)	...	(4)	...	(5·8)	(4·5)	...
Mean	117	± 0·72	+1·1	+1·1	...	246	± 0·70	+0·8	+0·9	...
	B5–B8					B3				
McC.	25	± 0·96	−0·7	−0·5	16·7	26	± 0·91	−0·8	−0·7	13·1
Ally.	9	...	−0·8	0·0	9·0	5	...	−1·2	−1·2	8·0
Gr.	4	...	+0·7	+1·0	17·5	3	...	+0·1	−2·0	11·0
Yerk.	7	...	−0·6	−1·2	15·1	8	0·48	−0·5	−0·5	12·8
Yale										
Spr.	7	...	+0·7	+0·2	17·7	4	...	−0·9	...	9·2
Mt. W.	3	...	+1·0	...	8·3					
Cape										
Mean	55	± 0·96	−0·3	−0·3	...	46	± 0·81	−0·7	−0·8	...
	B0–B1									
McC.	24	± 0·97	−0·6	−0·5	14·7					
Ally.	4	...	−1·2	...	7·9					
Gr.	3	...	+0·5	−0·2	14·7					
Yerk.	17	1·26	−0·1	−0·7	10·6					
Yale										
Spr.	7	...	+1·1	+0·8	20·1					
Mt. W.	9	...	+1·5	+1·5	6·7					
Cape										
Mean	64	± 1·09	0·0	−0·1	...					

TABLE VIIB

Giant Sequence

	Mo–M3					K5				
	No.	r	M_{corr}	M_{unc}	$\bar{\pi}_{corr}$	No.	r	M_{corr}	M_{unc}	$\bar{\pi}_{corr}$
McC.	26	± 0·99	−0·2	−0·3	17·0	27	± 0·82	−0·1	+0·2	16·0
Ally.	39	0·85	+0·1	+0·2	14·9	37	0·73	+0·1	−0·2	12·5
Gr.	5	...	0·0	−1·0	12·8					
Yerk.	4	...	+1·3	+1·3	23·8	2	...	−0·2	−0·4	28·5
Yale	29	0·99	+0·7	+0·4	20·2	24	0·68	+0·7	+0·4	19·8
Spr.										
Mt. W.	38	1·13	+1·0	+1·0	11·6	7	...	+1·0	+1·3	26·0
Cape										
Mean	141	± 1·00	+0·4	+0·4	...	97	± 0·74	+0·3	+0·2	...
	G5					G0				
McC.	31	± 1·04	+0·8	+0·8	20·8	26	± 0·65	−0·5	−1·0	15·0
Ally.	53	0·72	0·9	1·0	16·2	19	0·60	−0·8	−1·2	10·1
Cr.	4	...	1·4	1·2	11·3	2	...	+0·5	−0·1	14·5
Yerk.	4	...	0·9	0·7	13·5	4	...	−0·3	−0·6	28·2
Yale	33	0·79	1·3	1·2	21·4	12	0·74	0·0	−0·5	14·3
Spr.	4	...	0·7	0·7	15·5	4	...	+0·5	+1·1	19·2
Mt. W.	24	1·40	1·5	1·6	16·5	6	...	+1·0	+1·5	10·5
Cape										
Mean	153	± 0·92	+1·1	+1·1	...	73	± 0·65	−0·3	−0·6	...

fitted about the known mean values. Although we are fully aware of the objections to this procedure, the application of the normal error law to such frequencies has been found satisfactory by Wilson * and others, so we thought best to try it in these two cases.

For the G5–G8 dwarfs Table VIIA gives $M = 4{\cdot}9$, $r = 0{\cdot}84$ and $n = 374$; hence the probability curve for this group takes the form

$$y = C_1 e^{-{\cdot}322(M-4{\cdot}9)^2}.$$

In the case of the giants, from Table VIIB, $M = 1{\cdot}07$, $r = 0{\cdot}92$, $n = 153$, and for the probability curve we have

$$y = C_2 e^{-{\cdot}269(M-1{\cdot}1)^2}.$$

These curves, when plotted to suitable scale on the observed frequency curve of magnitudes, show definitely the presence of a third theoretical

* *Astronomical Journal*, p. 968, 1932 February.

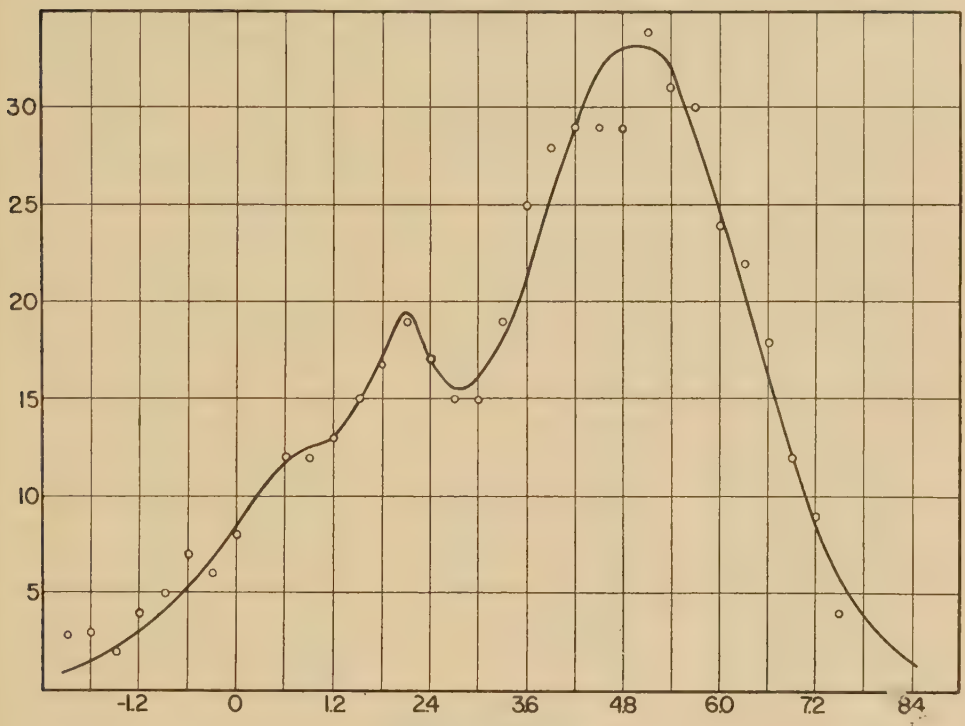

FIG. 3.—*G5–G8 Absolute Magnitude Distribution. The smooth curve represents the theoretical distribution.*

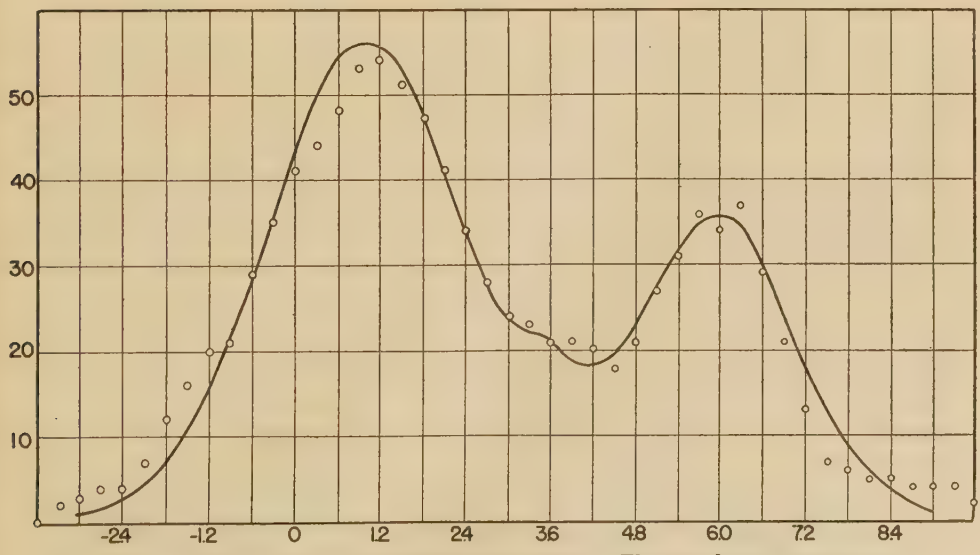

FIG. 4.—*K0–K2 Absolute Magnitude Distribution. The smooth curve represents theoretical distribution.*

TABLE VIII

Spectra	From π_{corr}	From π_{unc}	Wilson	Stromberg
Main Sequence				
Bo–B1	0·0	−0·1	−2·2	−2·1
B3	−0·7	−0·8	−1·1	−1·2
B5	−0·3	−0·3	−0·6	−0·5
B8			−1·0	−1·0
A0	0·8	0·9	0·7	0·6
A2	1·1	1·1	1·1	1·0
A3	1·7	1·9	1·6	1·4
A5			1·8	1·9
F0–F2	2·5	2·7	2·2	2·3
F5	3·1	3·3	3·5	3·0
F8	3·9	4·1	3·8	3·8
G0	4·4	4·6	4·5	4·3
G5	4·9	5·1	5·5	5·2
K0	5·8	6·0	5·9	5·9
K5	7·8	8·0	7·5	8·0
M0	9·7	9·9	8·3	9·2
M3			10·9	
Giant Sequence				
G0	−0·3	−0·6	0·5	0·1
G5	1·1	1·1	0·8	0·7
K0	0·9	1·0	0·7	0·7
K5	0·3	0·2	0·2	0·3
M0–M3	0·4	0·4	−0·2	−0·2

distribution. This may be obtained roughly from the observed distribution and the sum of the two distributions already given. After some slight readjustment of the three frequency functions, a satisfactory agreement between the observed and the computed distribution is easily obtained. The form of the theoretical function is :

$$Y = N_1\Phi_1(M - 1{\cdot}1) + N_2\Phi_2(M - 2{\cdot}1) + N_3\Phi_3(M - 5{\cdot}0),$$

where the number of absolute magnitude determinations between M_1 and M_2 is

$$N\frac{h}{\sqrt{\pi}}\int_{M_1}^{M_2} e^{-h^2(M-M_0)^2}dM = N\Phi(M - M_0).$$

The number of determinations in each of the three groups (giants, faint giants and dwarfs) is denoted by N, and it is of course evident that no particular meaning is attached to it. The values of N are relative, and change with a change in the selection of data.

The treatment of the K0–K2 group is the same. A summary of results

is given in Table IX. The smooth curves in figs. 3 and 4 represent the distributions computed from the theoretical functions described above.

TABLE IX

Type	N	M_0	r
G5–G8 :			
Giants	141	1·1	0·93
Faint giants	18	2·1	0·25
Dwarfs	368	5·0	0·90
K0–K2 :			
Giants	640	1·0	0·92
Faint giants	27	3·6	0·28
Dwarfs	340	5·9	0·77

We are indebted to Mr. E. J. Cerny and to Mr. W. A. Rense for many of the tabulations and much of the numerical work.

Warner and Swasey Observatory,
Case School of Applied Science :
1934 *February.*

EPHEMERIS OF THE RADIANT-POINT OF THE DELTA AQUARID METEOR STREAM.

R. A. McIntosh.

The prominent southern meteor shower emanating from the constellation of Aquarius at the end of July and early in August has been well observed in New Zealand in recent years by members of the Meteor Section of the New Zealand Astronomical Society. A total of 44 radiants, comprising 515 meteors, has been secured in the years 1926–33.

There is continuous activity of this shower from July 22, when the radiant is situated near R.A. 335°, Dec. −19°, until August 9, when it is at R.A. 352½°, Dec. −12°. The maximum activity of the shower occurs on July 28 (Greenwich date), when the radiant-point lies close to the star Delta Aquarii, from which the shower derives its name. The observed duration of the shower is nineteen days.

The observed rate of activity of the shower is shown in fig. 1. The number of Aquarid meteors visible per hour during the period July 20 to August 10 is shown by the continuous line in the figure, while the broken line represents the rate of all meteors seen, irrespective of radiant. Hindrances to observing have been taken into account, but not the time spent

in recording—generally about 40 seconds per meteor. It will be seen that the rate for the Aquarids shows a sharp maximum on July 28.

Some time ago it occurred to the writer that a much better method existed for forming the ephemeris of the motion of a radiant-point than the usual one of averaging the various radiants observed on the one date. The only co-ordinates of a group of radiants which do not vary during the whole

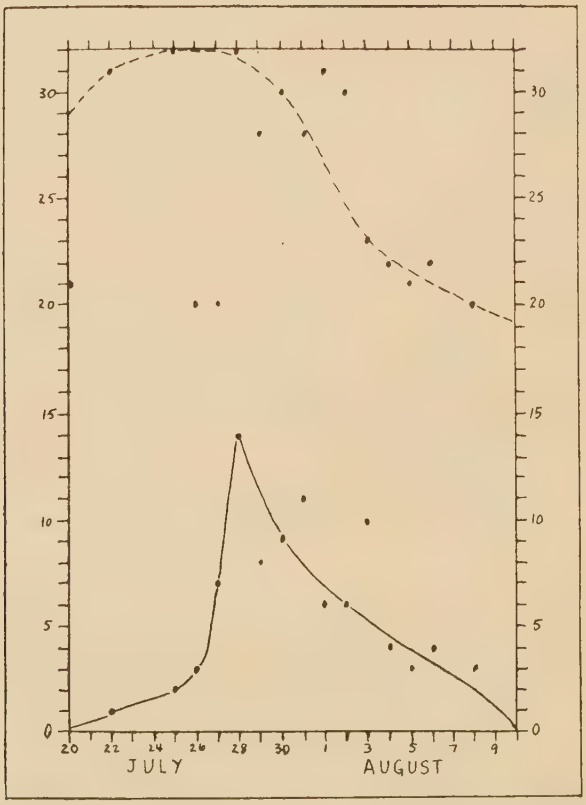

Fig. 1.—*Number of Meteors visible per hour.*

period of activity of the shower are the celestial latitude of the radiants and the difference in longitude between the radiants and the apex of the Earth's motion, termed the meteoric apex. Consequently, if a group of related radiants is reduced to these co-ordinates the whole should closely agree. Taking the mean position of the whole and translating it again into right ascension and declination an ephemeris is easily formed.

The principal advantage of this method is that the whole of the available data is used to determine the mean radiant, whereas under the earlier method the radiants observed on each day were treated separately, the mean daily positions being used to show the motion of the radiant-point.

Only those radiants observed by members of the Meteor Section of the New Zealand Astronomical Society have been used in this paper. Several reasons exist for this procedure. The use of the many Delta Aquarid

radiants observed in the northern hemisphere would have involved the selection of some which were determined according to the modern definition of radiation—each night's work being treated separately—and the rejection of many that were not. The necessity of correcting northern hemisphere work for zenith attraction, when in many cases the data necessary for the computations were not published, ruled out a further number of radiants. Again, a certain amount of material published on the Continent was not available. Rather than include only a portion of the observations, the discussion has been confined to the work performed south of the equator.

The New Zealand observers find the Delta Aquarid radiant lying close to the zenith. The meteoric display it provides therefore consists mainly of swift, short-pathed objects, generally rather faint. Very similar meteors were witnessed in Europe from the Draconid shower on 1933 October 9. The absence of bright, long-pathed meteors with a high proportion of trains makes the accurate plotting of radiants rather difficult, a point which is demonstrated by the published radiants of the Draconids. In 15 radiants deduced on the Continent, the positions vary between 19° of right ascension and 10° of declination.

In the radiants under discussion the divergence is fortunately not so great, probably owing to the observations being performed by persons experienced in the work. The poorest radiant is only 3°·6 from the mean position, while if 14 of the poorly determined radiants (those weighted as 1) are omitted only three radiants are more than a degree in either co-ordinate from the adopted centre.

The following Delta Aquarid radiants have been determined by the writer from the observations of the following members of the Meteor Section of the New Zealand Astronomical Society: F. M. Bateson, Wellington (Ba); A. Bryce, Hamilton (By); M. Geddes, Otekura (G); and R. A. M'Intosh, Auckland (M). The radiants have not been corrected for zenith attraction, as in all cases the amount of the correction is considerably less than the errors of observation. The columns are self-explanatory. The equatorial co-ordinates of the radiants (R.A. and Dec.) have been transferred to ecliptic co-ordinates (l and b) and finally referred to the meteoric apex (L). The weights allotted to the various radiants and the residuals from the mean are shown.

The mean position of the Aquarid radiant-point has been determined by weighting the individual radiants according to the square of the number of meteors composing them. The mean position derived was:

Longitude of radiants minus longitude of meteoric apex, 301°·0.
Latitude, −8°·1.

The fact that for a period of nineteen days the radiants observed are clustered about a fixed point in space, while in the time that point moved through an arc of 17° in the sky, clearly establishes that the radiant-point of the Delta Aquarid stream moves in the manner required by theory. This has already been established in the case of other prominent meteor showers, notably the Perseids, Eta Aquarids and Orionids, but never has been proved observationally for the Delta Aquarids.

Radiant-points of Delta Aquarid Meteors

No.	Date (G.C.T.)	Radiant R.A.	Radiant Dec.	Mets.	Ob.	Wt.	l	L	l–L	b	Δl	Δb
		°	°				°	°	°	°	°	°
1	1933 July 22·64	339·6	−19·0	6/7	G	1	334·0	29·6	304·4	− 9·6	3·4	1·5
2	,, ,, 23·47	340·0	−20·0	5	G	1	334·0	30·5	303·5	−11·2	2·5	3·1
3	,, ,, 26·58	341·7	−17·4	9	G	1	336·5	33·4	303·1	− 8·9	2·1	0·8
4	1928 ,, 26·67	341·6	−15·1	15	M	3	337·7	33·7	304·0	− 6·6	3·0	1·4
5	1929 ,, 26·67	339·6	−17·0	5	M	1	335·9	33·5	302·4	− 8·2	1·4	0·1
6	1933 ,, 26·68	342·0	−17·5	6	M	1	336·7	33·5	303·2	− 9·1	2·2	1·0
7	,, ,, 26·69	339·5	−20·0	4	By	1	334·4	33·5	300·9	−10·2	0·1	2·1
8	1928 ,, 27·63	340·0	−16·0	26	Ba	7	335·5	34·7	300·8	− 7·0	0·2	1·1
9	1932 ,, 28·55	340·0	−17·5	8	Ba	1	334·8	35·6	299·2	− 8·0	1·8	0·1
10	1933 ,, 28·60	342·3	−17·5	27	G	7	337·0	35·4	301·6	− 9·2	0·6	1·1
11	,, ,, 28·60	342·7	−17·2	1	G	1	337·5	35·4	302·1	− 9·1	1·1	1·0
12	1926 ,, 28·65	340·0	−17·0	5	M	1	335·1	34·6	301·0	− 7·9	0·0	0·2
13	1929 ,, 28·66	341·0	−16·5	8	M	1	336·2	35·5	300·7	− 7·8	0·3	0·3
14	1932 ,, 28·67	341·0	−16·5	17	M	3	336·2	35·5	300·7	− 7·8	0·3	0·3
15	1933 ,, 28·70	342·0	−18·0	10	M	1	336·5	35·5	301·0	− 9·6	0·0	1·5
16	1930 ,, 28·70	341·0	−17·0	26	M	7	336·0	35·7	300·3	− 8·3	0·7	0·2
17	1932 ,, 29·40	339·0	−17·8	5	G	1	333·9	36·4	297·4	− 8·3	3·6	0·2
18	,, ,, 29·51	341·0	−17·5	22	Ba	5	335·8	36·5	299·3	− 8·7	1·7	0·4
19	,, ,, 29·67	342·0	−17·0	14	M	2	336·9	36·5	300·4	− 8·7	0·6	0·6
20	1930 ,, 29·68	341·7	−15·7	21	M	5	336·3	36·7	299·6	− 7·0	1·4	1·1
21	1932 ,, 30·50	343·0	−17·0	14	G	2	337·8	37·5	300·4	− 9·0	0·6	0·9
22	1929 ,, 30·65	343·5	−15·5	12	M	2	338·9	37·4	301·5	− 7·8	0·5	0·3
23	1932 ,, 30·67	343·0	−16·5	14	M	2	338·0	37·5	301·5	− 8·6	0·5	0·5
24	1930 ,, 30·68	344·0	−15·5	14	M	2	339·3	37·7	301·6	− 8·0	0·6	0·1
25	1932 ,, 31·54	343·5	−16·0	13	G	2	338·7	38·5	300·2	− 8·3	0·8	0·2
26	1933 ,, 31·58	344·0	−16·0	14	G	2	339·1	38·4	300·7	− 8·5	0·3	0·4
27	1930 ,, 31·70	344·5	−15·0	22	M	5	339·9	38·7	301·2	− 7·8	0·2	0·3
28	1929 ,, 31·71	344·5	−15·0	9	M	1	339·9	38·4	301·5	− 7·8	0·5	0·3
29	,, Aug. 1·45	347·5	−14·0	6	Ba	1	343·0	39·2	303·8	− 8·0	2·8	0·1
30	1932 ,, 1·60	344·0	−16·0	22	G	5	339·1	39·5	299·6	− 8·5	1·4	0·4
31	1930 ,, 1·69	346·0	−14·0	11	M	2	341·5	39·5	302·0	− 7·1	1·0	1·0
32	1929 ,, 1·69	345·7	−14·5	19	M	4	341·2	39·4	301·8	− 7·7	0·8	0·4
33	1931 ,, 2·39	343·0	−16·0	3/4	G	1	338·2	39·5	298·7	− 8·1	2·3	0·0
34	1932 ,, 2·54	343·5	−15·5	6/7	G	1	338·8	40·4	298·4	− 7·9	2·6	0·2
35	1929 ,, 3·66	347·3	−13·7	17	M	3	343·0	41·3	301·7	− 7·6	0·7	0·5
36	1932 ,, 2–3	345·0	−15·0	6	G	1	340·6	40·9	299·5	− 7·3	1·5	0·8
37	1929 ,, 4·66	348·5	−13·3	10	M	1	344·2	42·2	302·0	− 7·7	1·0	0·4
38	1931 ,, 4·49	348·0	−15·0	9	G	1	343·1	41·6	301·5	− 9·1	0·5	1·0
39	,, ,, 5·44	350·0	−14·0	4/5	G	1	345·3	42·5	302·8	− 8·9	1·8	0·8
40	,, ,, 6·47	349·5	−14·0	10	G	1	344·8	43·5	301·3	− 8·7	0·3	0·6
41	1932 ,, 5–6	346·0	−13·0	5/6	G	1	342·1	43·8	298·3	− 6·5	2·7	1·6
42	1931 ,, 7·51	352·0	−12·5	12	G	2	347·7	44·5	303·2	− 8·3	2·2	0·1
43	1929 ,, 8·67	352·3	−11·5	8	M	1	348·1	46·1	302·0	− 7·7	1·0	0·4
44	1931 ,, 9·56	352·5	−12·0	10	G	1	348·1	46·5	301·6	− 8·2	0·6	0·1

No. 11 is based on one stationary meteor.
Nos. 36 and 41 are deduced from two days' observations combined.

From the mean position derived the equatorial co-ordinates for selected dates were calculated and those for intervening dates interpolated. The resulting ephemeris is given below.

Ephemeris of Radiant-point for 1934

1934	R.A.	Dec.	1934	R.A.	Dec.
	°	°		°	°
July 22·0	334·9	−19·2	August 1·0	344·3	−15·9
,, 23·0	335·8	18·8	,, 2·0	345·1	15·1
,, 24·0	336·8	18·4	,, 3·0	346·0	14·8
,, 25·0	337·7	18·1	,, 4·0	346·9	14·4
,, 26·0	338·6	17·7	,, 5·0	347·8	14·0
,, 27·0	339·6	17·4	,, 6·0	348·7	13·6
,, 28·0	340·5	17·0	,, 7·0	349·7	13·1
,, 29·0	341·4	16·6	,, 8·0	350·6	12·7
,, 30·0	342·4	16·3	,, 9·0	351·5	12·2
,, 31·0	343·3	15·9	,, 10·0	352·4	11·8

From the adopted mean position of the Aquarid radiant the following parabolic orbit was calculated for the maximum of the shower :—

$$
\begin{aligned}
i &\ 55{\cdot}8^\circ \\
\pi &\ 104{\cdot}3 \\
\Omega &\ 304{\cdot}7 \\
q &\ 0{\cdot}0393 \\
&1934 \text{ July } 28{\cdot}0.
\end{aligned}
$$

All computations for this paper have been performed to four places of logarithms, the final figures being rounded off to tenths of a degree.

Since beginning this paper I have found that a somewhat similar method of preparing an ephemeris has been used in a paper, "The Ephemeris of Perseid," by Miss N. Sytinskaja, *Publications of the Tashkent Observatory*, **1**, 87. In that paper the author adheres to the principle of taking the mean of each day's radiants, and she calculates latitude and the difference in longitude between the radiants and the Sun for these mean positions. Referring the radiant to the Sun is for all practical purposes equivalent to referring it to the meteoric apex, for although this method does not take into account the eccentricity of the Earth's orbit the variation from this cause during the period of activity of the average meteor shower is much smaller than the inherent errors of observation.

Private Observatory,
Epsom, Auckland, N.Z.:
1934 *March* 9.

OCCULTATIONS OF STARS BY THE MOON OBSERVED AT BIRMINGHAM UNIVERSITY DURING THE YEAR 1933.

James Young.

This report is in continuation of those published in previous years. The method adopted has been described in *M.N.*, **92**, 456, 1932, and need not be repeated here. The co-ordinates of the 7-inch Cooke equatorial with which all the observations were made are given in the current *Nautical Almanac.*

Table I gives particulars of the observations. The G.C.T.'s given are corrected for lag and the corrections are shown in the table under the appropriate heading. Nos. 71 and 72 have not been identified.

Table II gives the reductions. In making these a correction of $0^h.0025$ was added to the G.C.T.'s for the purpose of taking the Moon's right ascension, declination, and parallax from the *Nautical Almanac*, as suggested by Professor E. W. Brown.

TABLE I

No.	Star	Mag.	Phase	Date	G.C.T.	Corr.
				d	h m s	s
60	δ Pis	4·5	D	Jan. 03	16 43 43·8	−0·2
61	406 B Tau	5·6	D	Jan. 09	20 27 37·3	−0·2
62	B.D. +27° 887	7·7	D	Jan. 09	20 30 33·1	−0·4
63	κ Gem	3·6	D	Jan. 11	22 44 02·5	−0·2
64	κ Gem	3·6	R	Jan. 11	23 24 16·0	−0·5
65	W.Z.C. 176	6·7	D	Feb. 02	22 48 04·0	−0·2
66	B.D. +26° 1404	9·0	D	Mar. 06	19 52 16·9	−0·5
67	B.D. +26° 1427	8·5	D	Mar. 06	20 45 30·4	−0·4
68	B.D. +26° 1431	9·1	D	Mar. 06	20 58 53·9	−0·8
69	B.D. +26° 1440	9·1	D	Mar. 06	21 52 14·4	−0·5
70	B.D. +27° 857	9·1	D	Apr. 01	19 48 10·5	−0·3
71	Anon.	(9)	D	Apr. 01	19 58 13·2	−0·3
72	Anon.	(9)	D	Apr. 01	20 35 46·8	−0·9
73	B.D. +27° 866	8·0	D	Apr. 01	21 08 26·3	−0·3
74	B.D. +27° 880	7·3	D	Apr. 01	22 08 26·6	−0·3
75	B.D. +25° 1706	9·4	D	Apr. 03	20 18 13·9	−0·3
76	B.D. +25° 1709	8·0	D	Apr. 03	20 32 02·5	−0·3
77	B.D. +25° 1713	8·2	D	Apr. 03	21 09 49·1	−0·3
78	B.D. +25° 1716	8·6	D	Apr. 03	21 54 24·3	−0·3
79	α Leo	1·3	D	Apr. 06	20 53 23·6	−0·3
80	α Leo	1·3	R	Apr. 06	21 07 44·4	−0·4
81	79 Leo	5·5	D	May 05	20 55 25·7	−0·3
82	79 Leo	5·5	R	May 05	21 10 34·9	−2·0
83	17 Tau	3·8	R	Nov. 03	20 43 48·8	−0·5
84	16 Tau	5·4	R	Nov. 03	20 54 40·7	−0·5
85	q Tau	4·3	R	Nov. 03	21 06 03·5	−0·5
86	20 Tau	4·1	R	Nov. 03	21 27 44·2	−0·5
87	13 Pis	6·4	D	Nov. 25	21 28 50·8	−0·3
88	101 Pis	6·2	D	Dec. 25	19 14 37·3	−0·3

I am very much indebted to Mr. J. D. McNeile for independent reductions of these occultations.

Table III gives the positions of stars not in the *Nautical Almanac*. No. 65 is an Albany position passed on to me by Mr. McNeile. In the remaining cases the authority is the Greenwich 1910 Catalogue.

TABLE II

No.	$\sigma' - \sigma$	χ	ρ	$\chi - \rho$
	″	° ′	° ′	° ′
60	−1·8	61 05	62 43	− 01 38
61	−1·3	65 33	89 59	− 24 26
62	−0·8	135 41	90 00	+ 45 41
63	−0·4	164 38	103 09	+ 61 29
64	+0·1	225 31	103 19	+122 12
65	−1·2	84 00	71 31	+ 12 29
66	+1·2	159 03	98 09	+ 60 54
67	−3·2	111 37	98 39	+ 12 58
68	+0·4	101 37	98 42	+ 02 55
69	+0·6	55 33	98 56	− 43 23
70	−0·4	99 00	89 53	+ 09 07
73	−1·4	139 06	90 14	+ 48 52
74	−0·2	145 56	90 30	+ 55 26
75	−1·5	144 36	102 21	+ 42 15
76	−1·0	111 33	102 25	+ 09 08
77	+1·9	102 46	102 34	+ 00 12
78	−0·4	48 11	102 44	− 54 33
79	+0·0	45 27	115 28	− 70 01
80	+0·3	23 16	115 31	− 92 15
81	+2·4	205 05	118 00	+ 87 05
82	−0·4	229 19	118 00	+111 19
83	+0·9	216 38	76 58	+139 40
84	+0·8	257 09	77 01	−179 52
85	+1·8	291 22	77 03	−145 41
86	+0·8	254 46	77 08	+177 38
87	−0·8	91 30	62 22	+ 29 08
88	−0·4	17 16	66 21	− 49 05

TABLE III

No.	$\alpha_{1933\cdot0}$	$\Delta\alpha$	$\delta_{1933\cdot0}$	$\Delta\delta$
	h m s	s	° ′ ″	″
62	5 46 35·40	+1·99	+27 40 04·6	+ 9·3
65	2 55 02·29	+0·71	+21 21 03·3	+11·2
66	6 53 43·81	+1·94	+26 39 31·3	+ 7·6
67	6 57 26·80	+1·97	+26 40 10·1	+ 7·4
68	6 57 52·27	+1·97	+26 41 28·8	+ 7·3
69	6 59 09·99	+1·98	+26 47 47·9	+ 7·3
70	5 41 28·35	+0·98	+27 49 45·5	+10·8
73	5 43 32·54	+1·00	+27 36 45·6	+10·7
74	5 45 25·59	+1·01	+27 31 53·1	+10·6
75	7 29 59·50	+1·69	+25 01 32·3	+ 6·0
76	7 30 45·41	+1·70	+25 06 28·6	+ 5·9
77	7 31 50·92	+1·70	+25 03 19·8	+ 5·9
78	7 32 51·64	+1·71	+25 10 02·3	+ 5·9

Notes.—60 Through thin cloud. Certain.
68 Observed also by B. E. Atkins.
75 Not quite sudden. Very clear. Observed also by T. D. Smith.
76 Observed also by T. D. Smith.
77 Observed also by T. D. Smith.
79 Observed also by T. D. Smith.
81 Bright limb. Difficult.
82 Bright limb. Very difficult.
88 Through thin haze. Certain.

University of Birmingham Observatory,
Edgbaston, Birmingham :
1934 *March* 16.

Errata

Dr. A. G. Walker's paper :

P. 161, first footnote, *for* Milne *read* McCrea

P. 164, equation (27), *for* $\frac{d^2\psi}{ds^2}$ *read* $\frac{d^2\psi}{d\beta^2}$.

Dr. Chandrasekhar's paper :

P. 449, in the equations (44) and (45), the factor $\frac{3}{4}$ in front of the integral $\int_0^\tau \sin^2\theta_r d\tau$ should *read* $\frac{3}{2}$.

P. 457, equation (107), *for* $\frac{1}{2}e^{-\tau}$ *read* $\frac{1}{2}e^{-\tau_1}$.